QEX

$7

July/August 2017

www.arrl.org

A Forum for Communications Experimenters

Issue No. 303

PY2EAJ integrates all the hardware of an RF power meter in a compact package.

ARRL The national association for AMATEUR RADIO™
225 Main Street
Newington, CT USA 06111-1494

New

APRS® / D-STAR®

TH-D74A 144/220/430 MHz Tribander

Introducing the TH-D74A for the ultimate in APRS and D-STAR performance. KENWOOD has already garnered an enviable reputation with the TH-D72A handheld APRS amateur radio transceiver. And now it has raised the bar even further with the new TH-D74A, adding support for D-STAR, the digital voice & data protocol developed by the JARL, and enabling simultaneous APRS and D-STAR operation – an industry first.

- APRS compliance using packet communication to exchange real-time GPS position information and messages
- Compliant with digital/voice mode D-STAR digital amateur radio networks
- Built-in high performance GPS unit with Auto Clock Setting
- Wide-band and multi-mode reception
- 1.74" (240 x 180 pixel) Transflective color TFT display
- IF Filtering for improved SSB/CW/AM reception
- High performance DSP-based audio processing & voice recording
- Compliant with Bluetooth, microSD & Micro-USB standards
- External Decode function (PC Decode 12kHz IF Output, BW:15 kHz)
- Free software for Memory and Frequency Control Program
- Data Import / Export (Digital Repeater List, Call sign, Memory Channel)
- Four TX Power selections (5/2/0.5/0.05 W)
- Dust and Water resistant IP54/55 standards

APRS (The Automatic Packet Reporting System) is a registered American trademark of WB4APR (Mr. Bob Bruninga).
D-Star is a digital radio protocol developed by JARL (Japan Amateur Radio League).

Customer Support/Distribution Customer Support:
(310) 639-4200 Fax: (310) 537-8235

www.kenwood.com/usa

July/August 2017

QEX (ISSN: 0886-8093) is published bimonthly in January, March, May, July, September, and November by the American Radio Relay League, 225 Main Street, Newington, CT 06111-1494. Periodicals postage paid at Hartford, CT and at additional mailing offices.

POSTMASTER: Send address changes to: QEX, 225 Main St, Newington, CT 06111-1494
Issue No 303

Offices

225 Main St, Newington, CT 06111-1494 USA
Telephone: 860-594-0200
Fax: 860-594-0259 (24 hour direct line)
e-mail: **qex@arrl.org**

Subscription rate for 6 issues:

In the US: $29;

US by First Class Mail: $40;

International and Canada by Airmail: $35

Members are asked to include their membership control number or a label from their QST when applying.

In order to ensure prompt delivery, we ask that you periodically check the address information on your mailing label. If you find any inaccuracies, please contact the Circulation Department immediately. Thank you for your assistance.

About the Cover

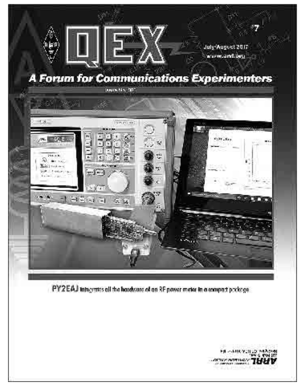

Euclides Lourenço Chuma, PY2EAJ, designed a low cost precision power meter integrated in a single compact piece of equipment that is connected directly to a computer via a USB connection. Measurements are possible from -70 dBm to +10 dBm at frequencies ranging up to 2.5 GHz, with a precision of 0.1 dBm.

In This Issue

Features

Index of Advertisers

Kazimierz "Kai" Siwiak, KE4PT

Perspectives

Moving On

By the time this issue appears in your mail box the Dayton Hamvention® will have moved from Trotwood to Xenia, Ohio. Times change, we move on, but at the new venue you can still find your basic bargain teen-aged transceivers that can be easily upgraded to modern capabilities. Amateur Radio moves on as well, sometimes subtly.

How many of you, Dear Readers, have logged two-way contacts using a Software Defined Radio (SDR) system? I believe, *a greater number than you might think*. A basic SDR system comprises some form of RF front end, followed by conversion between the analog and digital realms, along with a general purpose personal computer (PC). The PC operates software producing a wide range of different communications protocols, or "waveforms". More simply, it is a ham transceiver (that bargain find at the hamfest) connected via a sound card to a PC running digital protocol software — a protocol or waveform that is not native to the transceiver. Surprised? In this scheme the transceiver's SSB "audio" is just the last IF that is centered near 1500 Hz. The PC software implements the protocols, including software filters as narrow as a few hertz, and presents the operator with a suitable graphical user interface. Teen-aged radio, in fact any modern transceiver: meet SDR capability. You point and click your way into a modern-day contact — not otherwise possible with just the bare-bones transceiver — using protocols that were not even in existence when that transceiver was manufactured!

The point is that much innovation has occurred in the design of digital waveforms and digital protocols — the software of this basic SDR — that greatly extends the communications capability of Amateur Radio, and it has happened subtly. More comprehensive SDRs have pushed the digitization closer and closer to the antenna in both transmitting and receiving, and closer to the PC, sometimes avoiding the sound card altogether. But they all thrive on the same digital protocols and waveforms available to the basic SDR. That's progress, embrace the new world. We move on, but watch this space for more new modulation waveforms, and for further SDR evolution.

In This Issue

Our *QEX* authors touch upon wide variety of Amateur Radio topics. These are at the top of the queue.

Riccardo Gionetti, IØFDH, describes an automatic tracking filter for a DDS generator.

Euclides Lourenço Chuma, PY2EAJ, describes a modern RF power meter with accuracy that rivals the best commercial RF power meters.

Charles Preston, K7TAA, uses *WSPR* (Weak Signal Propagation Reporter) software to facilitate reliable and accurate comparison of two HF transmitting antennas.

Marcus C. Walden reports findings in a 5 MHz experiment on HF near vertical incidence skywave propagation.

Scott Roleson, KC7CJ, describes a high-dynamic range broadband amplifier that enhances the usability of an SDR or any HF receiver.

Keep the full-length *QEX* articles flowing in, but if a full length article is not your aspiration, share a brief **Technical Note** that is perhaps several hundred words long plus a figure or two. Expand on another author's work and add to the Amateur Radio *institutional memory* with your technical observation. Let us know that your submission is intended as a **Note**.

QEX is edited by Kazimierz "Kai" Siwiak, KE4PT, (**ksiwiak@arrl.org**) and is published bimonthly. *QEX* is a forum for the free exchange of ideas among communications experimenters. The content is driven by you, the reader and prospective author. The subscription rate (6 issues per year in the United States is $29. First Class delivery in the US is available at an annual rate of $40. For international subscribers, including those in Canada and Mexico, *QEX* can be delivered by airmail for $35 annually. Subscribe today at **www.arrl.org/qex**.

Would you like to write for *QEX*? We pay $50 per published page. Get more information and an Author Guide at **www.arrl.org/qex-author-guide**. If you prefer postal mail, send a business-size self-addressed, stamped (US postage) envelope to: *QEX* Author Guide, c/o Maty Weinberg, ARRL, 225 Main St, Newington, CT 06111.

73,

Kazimierz "Kai" Siwiak, KE4PT

Euclides Lourenço Chuma, PY2EAJ

Rua Cel Manuel de Moraes 204, Campinas, SP 13073-022, Brazil: **codigocerto@yahoo.com.br**

A High Performance 1 MHz to 2.5 GHz USB Power Meter

This modern power meter uses a PC with USB connection to display information, rivaling the best commercial RF power meters.

An RF power meter is one of the most useful pieces of equipment on the workbench of any professional or experimenter who works with RF circuits. It is useful for accurately measuring RF power and making many checks, such as measuring the power input and output in RF amplifier stages, or in a mixer.

Not long ago measuring RF power required the use power meters with power sensors. Currently, power meters and power sensors are integrated into a single compact unit that is directly connected to a computer by a USB port or an Ethernet LAN port. The measured RF power is displayed by software installed on the computer. Many settings are possibilities.

This project follows the same principle as do modern power meters. All of the hardware is integrated in a single compact piece of equipment that is connected directly to a computer via a USB connection. Measurements are possible from -70 dBm to +10 dBm at frequencies ranging from low frequencies up to 2.5 GHz, with a precision better than 0.1 dBm. Figure 1 shows the power meter in operation.

The Project

Figure 2 illustrates a block diagram of the power meter. A MAX2016 logarithmic detector is followed by an LTC2400 analog-digital converter (ADC), and an Arduino Nano module via a serial peripheral interface (SPI), with software installed on a computer. A precision voltage reference source, ADR421, provides a reference voltage to the ADC.

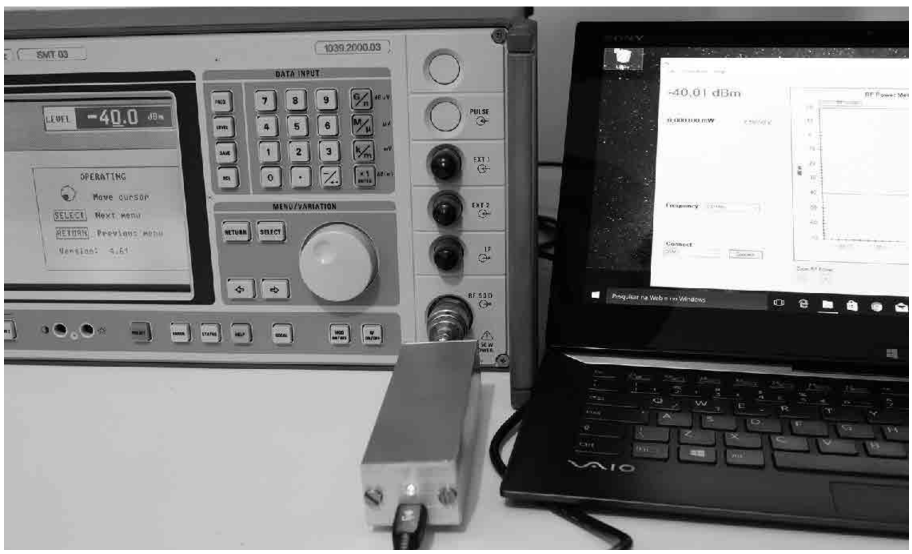

Figure 1 — Power meter in operation, connected to a signal generator.

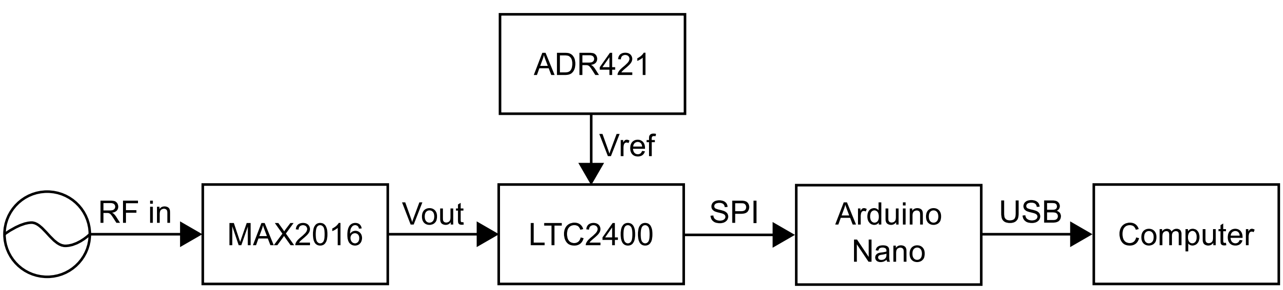

Figure 2 — Block diagram of the power meter.

Figure 3 — Screen presentation of the user interface for the software.

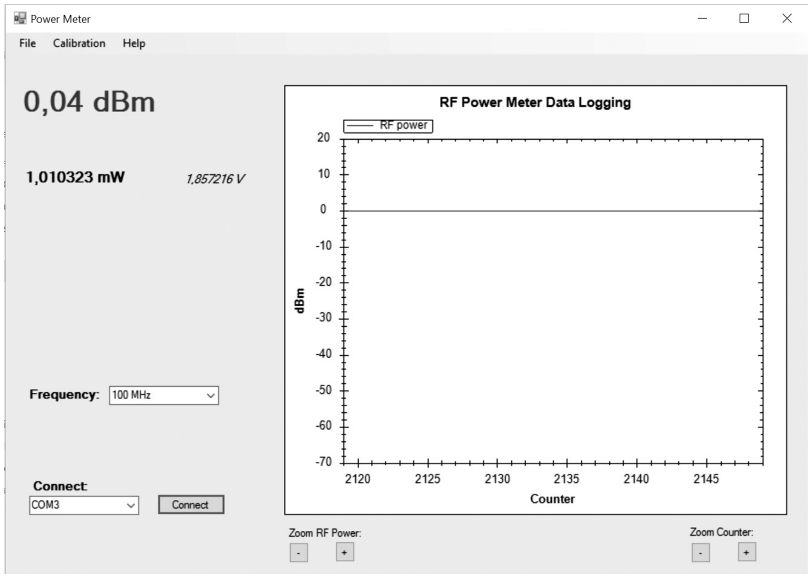

Figure 4 — Schematic diagram of the power meter.
Arduino Nano, https://www.arduino.cc/en/Main/arduinoBoardNano
C1 – C4 — 680 pF ceramic capacitor, Johanson Technology R15S S-Series NP0
C5, C7, C9, C11 — 33 pF ceramic capacitor, Johanson Technology R15S S-Series NP0
C6, C8, C10, C12 – C14, C16, C17, C23 — 100 nF ceramic capacitor, Johanson Technology R15S S-Series NP0
C15, C20 — 1 µF, 10 V capacitor
C18, C19, C21 — 22 µF, 10 V capacitor
C22 — 10 µF, 10 V capacitor
D1 — LED
J1, J2 — SMA bulkhead 50 Ω jack, Amphenol part 132289 (see text)
R1 – R4 — 0 Ω resistor (jumper)
R5 — 1 kΩ resistor
U1 — Maxim MAX2016ETI
U2 — Linear Technology LTC2400
U3 — STMicroelectronics LD1117S33TR
U4 — Analog Devices ADR421ARZ.

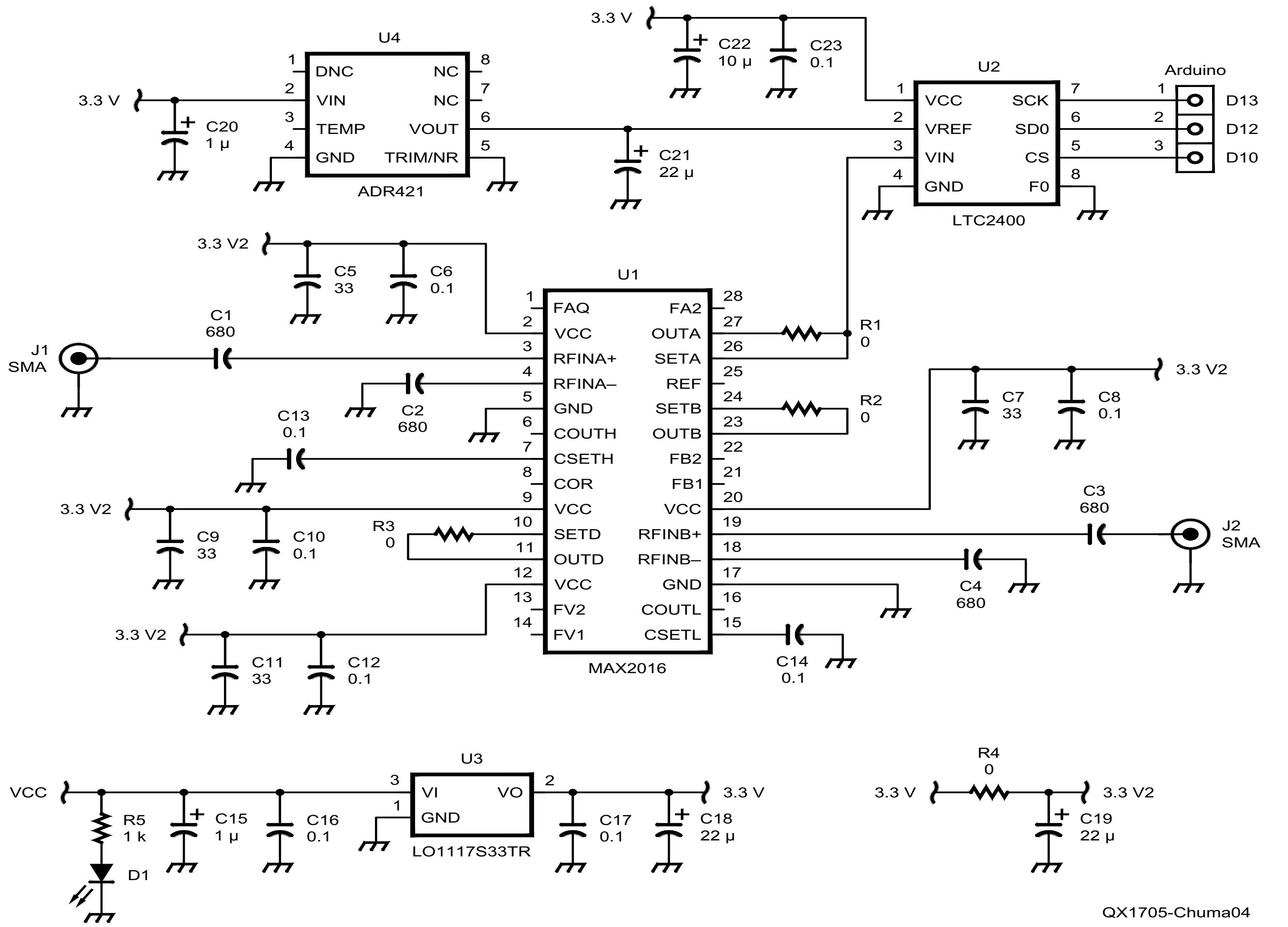

The RF signal at the input is converted to an output voltage that is linear in decibels, using a Maxim MAX2016 DS logarithmic detector.[1] This detector has an 80 dB dynamic range and can measure signals between -70 dBm and +10 dBm over the frequency range from low frequencies to 2.5 GHz. We note, however, that the dynamic range of the MAX2016 is reduced at the low and high limits of the frequency range. In the circuit of this project it operates satisfactorily between 3 MHz and 2.5 GHz. The MAX2016 has two RF input ports and therefore can be configured to measure return loss (and hence SWR). In this project I used one port (J2 is not used in this project) since the project goal was the construction of a power meter that was to be as compact as possible.

The output voltage of the MAX2016 is proportional to the logarithm of the RF input signal. This voltage is digitized in the LTC2400 ADC from Linear Technology.[2] The 24-bit resolution of this ADC allows monitoring of small voltage variations at the output of MAX2016 that correspond to small variations in the RF power signal being measured. A good voltage reference is needed for the LTC2400 to achieve good accuracy in the conversion of the analog signal to a digital signal. For this purpose I used the Analog Devices ADR421ARZ.[3] This unit provides a voltage reference of 2.50 V with an initial accuracy of 0.12% and a temperature coefficient of 10 ppm/°C.

The software for the Arduino Nano[4] module was programmed in the Arduino language, and converts the data on the SPI coming from LTC2400 to a string that is sent to the computer by USB communication using the *CmdMessenger* library.[5] The software used on the computer was programmed in the C# language in the Microsoft Visual Studio. Figure 3 shows a screen image of the user interface.

In the computer software, the power in dBm is calculated from the voltage measured by the power meter and compared with values obtained by a previous calibration. The MAX2016 is a logarithmic detector that provides a linear output voltage, *V*, proportional to the logarithm of the input level. See for example the V_{OUTA} vs. P_{RFINA} graph of the MAX2016 data sheet. Thus, is possible calculate the straight line from two points of voltage and then find the power in dBm at any point in this straight line.

The software first determines in which interval between two calibration points the measured voltage lies, then calculates the slope of the straight line passing by two points,

$$a = \left(y_2 - y_1\right) / \left(x_2 - x_1\right).$$

From this slope it is possible can calculate the power value, y_{dBm}, in dBm from the measured voltage, x_{Vin},

$$y_{dBm} = \left(a\, x_{Vin}\right) - \left(a\, x_1\right) + y_1 \quad .$$

Building the Power Meter

The schematic diagram can be seen in Figure 4. For good operation of the circuit it is always important to pay attention to details and to the quality of the selected components. I used Johanson Technology R15S S-Series NP0 ceramic capacitors. I also used an Amphenol SMA bulkhead 50 Ω jack.

The MAX2016, which is the heart of the power meter circuit, is in a QFN-28 package that provides a bit of a challenge for soldering into the circuit. With good vision and some patience, you can use solder paste and apply hot air. The other components are standard SMD, that (with some experience) can be easily soldered.

The Arduino Nano was purchased already assembled, and has a default operating voltage of 5 V. The LTC2400 operates with a 3.3 V voltage supply, so it is necessary to adjust the voltage of the Arduino Nano to 3.3 V. This is easily done by changing the voltage regulator from a 5 V to a 3.3 V device. An Internet search reveals many conversions of the Arduino Nano to operate from 3.3 V. The power meter has its own 3.3 V voltage regulator, therefore the +5 V USB VCC is used to supply the power meter circuit.

The PCB is designed in *KiCad* and was made from FR-4 material with double-sided copper and with 1.6 mm of thickness. The final PCB dimensions were made to fit in aluminum shield (Figure 5). The aluminum shielding is desirable for RF circuits. The completed PCB including all components and the Arduino Nano is shown in Figure 6.

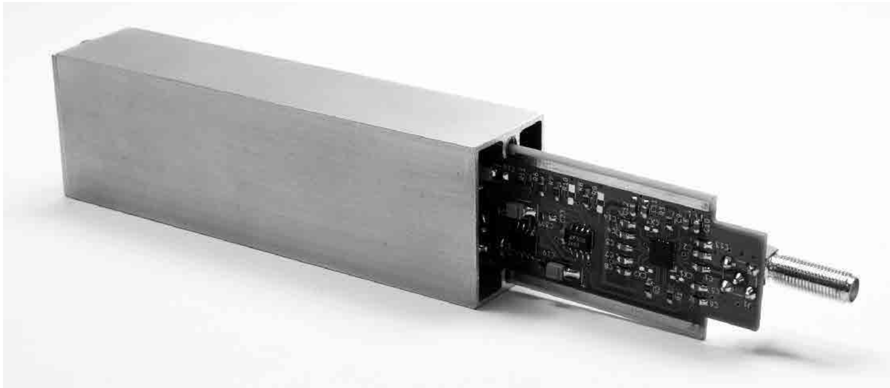

Figure 5 — Power meter PCB mounted inside aluminum an case.

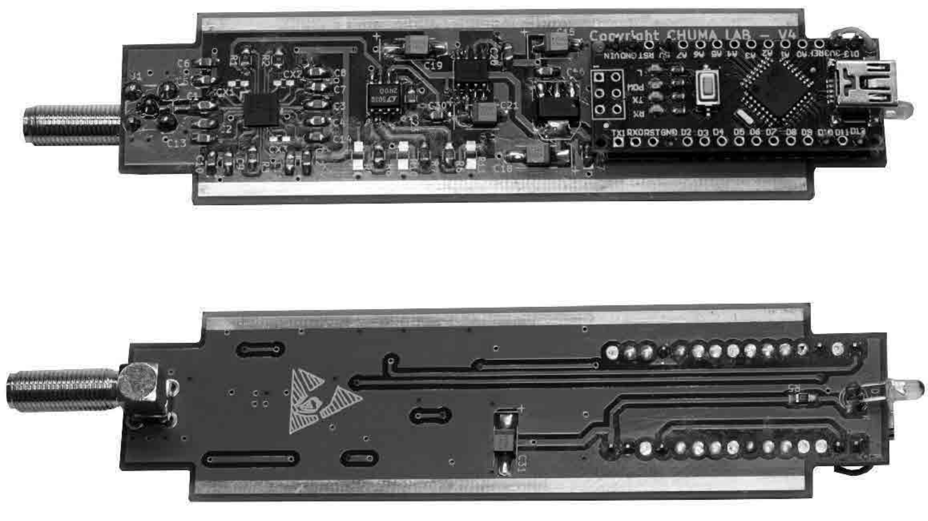

Figure 6 — PCB top and bottom views.

Results

The power meter should be calibrated. This consists in applying an RF signal at

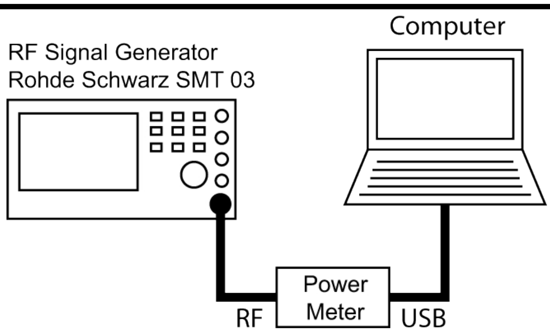

Figure 7 — Block diagram for calibration process.

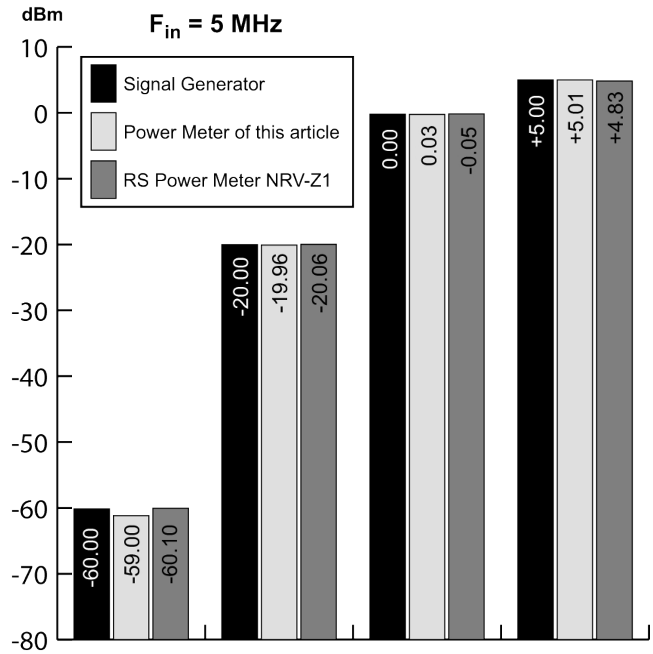

Figure 8 — A comparison at 5 MHz of power meter of this article with Rohde Schwarz signal generator, and NRVS power meter with NRV-Z1 power sensor.

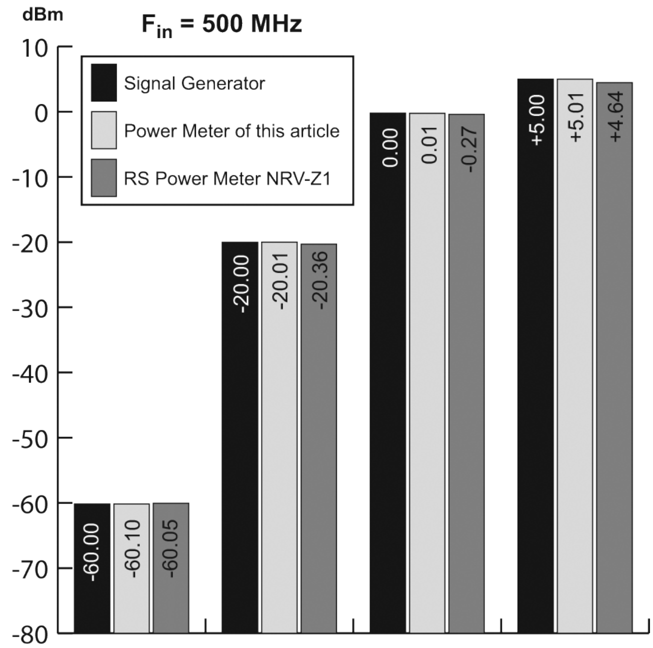

Figure 10 — A comparison at 500 MHz of power meter of this article with Rohde Schwarz signal generator, and NRVS power meter with NRV-Z1 power sensor.

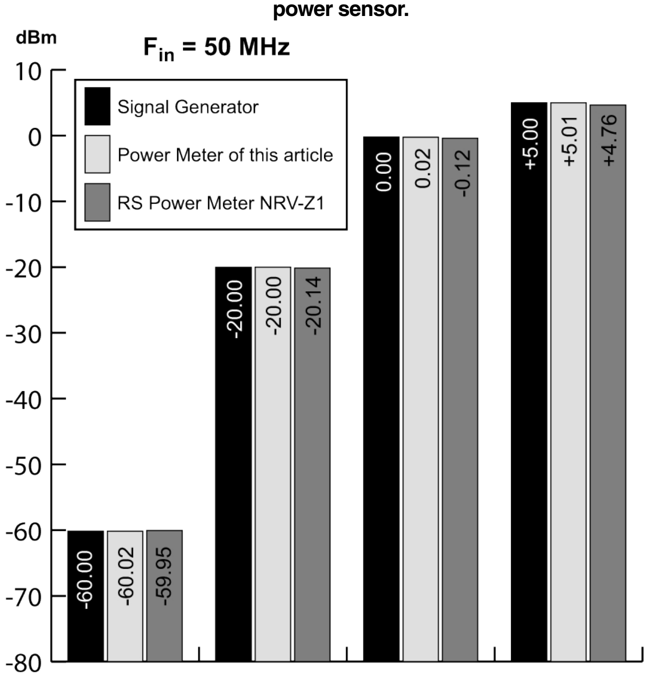

Figure 9 — A comparison at 50 MHz of power meter of this article with Rohde Schwarz signal generator, and NRVS power meter with NRV-Z1 power sensor.

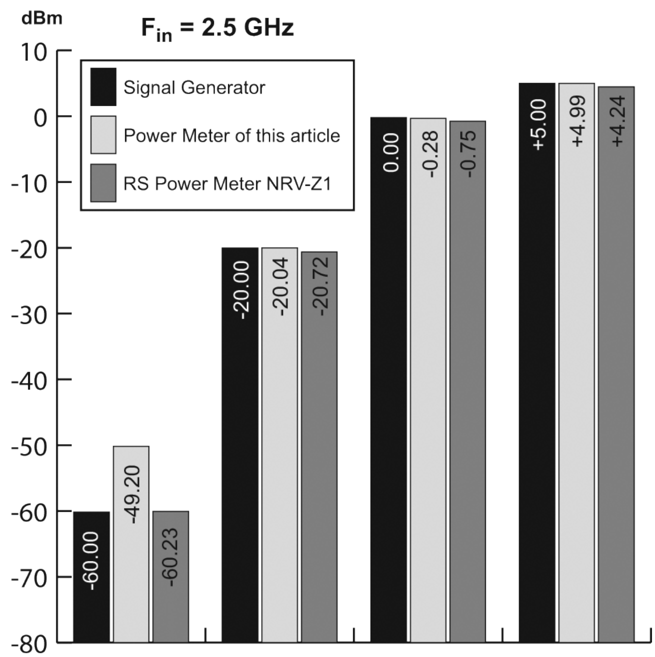

Figure 11 — A comparison at 2.5 GHz of power meter of this article with Rohde Schwarz signal generator, and NRVS power meter with NRV-Z1 power sensor.

well-known frequencies and amplitudes to the input of the power meter and measuring the voltage generated, as can be seen in the test setup of Figure 7, also pictured in Figure 1.

The input impedance of the MAX2016 changes with frequency, so the voltage at the output of the MAX2016 changes with the frequency as well, but remains proportional on the logarithmic scale. I found it necessary to perform separate calibrations for each operating frequency range and store the measured values in XML files for each frequency range. Each XML file contains information about the RF power in dBm, the corresponding measured voltage and frequency. The advantage of using XML files is that they can be easily changed using any text editor.

As can be seen in Figures 8 for 5 MHz, Figure 9 for 50 MHz, Figure 10 for 500 MHz and Figure 11 for 2.5 GHz, the power meter of this project provides very good results when compared to expensive professional equipment. At the lowest frequencies the power measurement range is reduced, and at 2.5 GHz the minimum power measured with precision is -40 dBm. This power meter is a great choice for anyone needing a low cost precision power meter. Software and circuit board files are available from the author.[6] The software files are also available on the *QEX*-files web page.[7]

I gratefully acknowledge the assistance of my friend Adinei Brochi, PY2ADN, in this and other projects.

Euclides Lourenço Chuma, PY2EAJ earned a degree in Mathematics from UNICAMP and a graduate degree in Network and Telecommunications Systems in the INATEL. Currently he is MSc Candidate in Electrical Engineering at UNICAMP, SP-Brazil. Euclides works as a software engineer in the private sector. His research interests are antennas, wireless power transfer, software defined radio and cognitive radio.

Notes

[1]Maxim MAX2016 DS datasheet, **https://datasheets.maximintegrated.com/en/ds/MAX2016.pdf**.

[2]Linear Technology LTC2400 datasheet **cds.linear.com/docs/en/datasheet/2400fa.pdf**.

[3]Analog Devices ADR421 datasheet **www.analog.com/media/en/technical-documentation/data-sheets/ADR420_421_423_425.pdf**.

[4]Arduino Nano, **https://www.arduino.cc/en/Main/ArduinoBoardNano**.

[5]CmdMessenger software from, **playground.arduino.cc/Code/CmdMessenger**.

[6]**www.chumalab.com.br/power-meter/**.

[7]**www.arrl.org/qexfiles**.

Charles Preston, K7TAA

608 Scott Street, PO Box 113, Troy, ID 83871; **charles.preston@hushmail.com**

Antenna Comparisons Using Simultaneous WSPR Measurements

WSPR (Weak Signal Propagation Reporter) software facilitates reliable and accurate comparison of two HF transmitting antennas.

.

You can use near vertical incidence skywave (NVIS) ionospheric propagation with a single receiving location or with many auto-reporting receiving locations, or point to point propagation with two transmitting antennas and one receiving location. The two transmitter measurement method requires two licensed operators (US FCC rules) and two transmitters capable of exactly the same power output, usually 0.5-5W, transmitting simultaneously. Antenna efficiency or antenna gain can be compared within an accuracy of 0.5 dB. If two antennas don't have the same pattern, their suitability for a particular use such as DX from a particular location, or reliable emergency communications with a particular set of ARES or other stations can still be determined more efficiently and accurately than by other methods.

Several years ago I wanted to find out how well small portable antennas could work compared with full size wire antennas, especially for near vertical incidence skywave (NVIS) propagation in a 300 to 400 mile radius for wide-area disaster communications. I started testing short wire antennas used with an automatic antenna tuner. Automatic tuners can tune fast and they can be uncomplicated for a band-switching operator in an emergency communications support scenario, but determining how much loss they have under field conditions is difficult.

Because ionospheric propagation conditions often change in seconds, and fading can amount to more than 10 dB (about 2 S units) and at more than 10 fades per minute, making accurate A/B comparisons of HF antenna signals is very difficult. Often the more serious experiments require some form of automatic switching and hundreds of comparisons to arrive at an accurate final value. Jack Belrose, VE2CV, describes[1] the experimental gain comparisons of terminated dipoles and other dipoles over an NVIS path. He described the difficulty of getting accurate results when the upper and lower quartile values of sets of field intensity measurements differed by more than 1 dB.

Many people were willing to say that small and highly portable antennas radiated less signal than a half-wave dipole on 40 and 80 meters, but nobody was able to quantify the difference. Different matching methods were known to have more loss than a resonant half-wave dipole, but nobody could say how much loss. With respect to NVIS transmissions, some operators were convinced that an 80 meter dipole 2 to 6 feet above ground was not only as good as 16 to 20 feet up, but better, despite evidence to the contrary.

WSPR Measurements are Better

Each WSPR transmission[2] is just 6 Hz wide, and designed for HF conditions, minimizing effects from ionospheric distortion, with a 2 minute transmission cycle. Measurements with two antennas can be performed using less than 30 Hz of the HF spectrum. With rare exceptions, two simultaneous WSPR transmissions, one from each tested antenna, are being received on the same receiver, in the same passband, on the same antenna, and undergo the same ionospheric disturbances or path disturbances, and the same man-made or atmospheric noise, second by second. The measurement of each signal is automated and logged, eliminating clerical errors. Second-by-second propagation path disturbances, always a factor in measuring RF signals, are greatly reduced as a source of error over the almost 2-minute transmission. The long transmission period is tolerant of short duration interfering signals or noise. Measuring signal to noise ratio (SNR), and using the same passband noise, still yields the difference in amplitude between two signals. Due to the sensitivity of the WSPR protocol and signal processing, measurements can be done using very low power, often less than 1 W, reducing any interference potential while transmitting measurement signals. The need for calibrated receivers or S meters or antenna factors are avoided by using signal to noise measurements.

With WSPR comparisons, you know exactly what each antenna can do, as far as reception at particular locations. Since the received SNR at a particular power level input to the feed line has been shown to be linear by WSPR design and these experiments, the relative performance of the measured antenna with 10, 100, or 1000 W is also known.

My First Simultaneous WSPR Antenna Experiments

In 2009 I compared a Buddipole dipole and a 300 foot horizontal loop located on the same city lot. On that particular day, for DXing on the 30 meter band, the Buddipole dipole was about as effective as the loop.[3] Other experiments[4], indicated that a particular brand and type of end-fed transmitting antenna was much less efficient than another end-fed antenna.

Current experiments

When Richard, G3CWI, read the two reports, he pointed out that I didn't have any proof that using WSPR to compare antennas was reliable and accurate, and that I could do some better experiments, starting with identical antennas and then varying the power to one by a known level. I believe the experiments reported in this article, from 2016, demonstrate that WSPR comparative measurements can be reliable and accurate.

The 2016 experiments reported here used 40 meters, 20 meters, and 10 meters, and both ionospheric and non-ionospheric propagation paths.

Common elements for experiments in 2016

The following conditions were met for each of the transmitting experiments reported here.

(1) – Each pair of antennas was at least one wavelength apart with a similar ground surface.

(2) – The antennas were erected end to end and aligned in the same direction within 1 to 2 degrees.

(3) – No significant above-ground metal was within one wavelength of either antenna.

(4) – "Identical" Elecraft KX3 transceivers were used to generate the signal on each antenna. These were purchased at the same time, with close serial numbers and the same circuit board revision versions.

(5) – Elecraft W2 power meters were used to measure the power level delivered to each antenna feed line or attenuator, and checked to see that each showed the same power at 1 W nominal transmitter output. Attenuation was checked for each feed line and each common mode choke.

(6) – Power levels to each feed line were monitored during each 2 minute simultaneous transmission.

(7) – Each 50 foot RG-8X coaxial feed line on the ground was at right angles to the antenna wire.

(8) – Each feed line was new at the start of the experiments.

(9) – Antenna hardware was identical and new at the start of the experiments.

(10) – Each antenna was a resonant half wave dipole showing similar VSWR while transmitting.

(11) – A common mode isolation choke was at the antenna feed point and at the output of the power meter or attenuator.

(12) – Paired simultaneous WSPR signal reports greater than 0 dB SNR were discarded as potentially unreliable, as were those under -28 dB SNR, based on written comments from Joe Taylor, K1JT, the originator of the WSPR protocol.

(13) – The digital interfaces between the control computers, the computers, and the software used to generate the WSPR transmissions were also identical.

(14) – The WSPR sessions or received "spots" not listed or referenced in this article are those where technical issues made it either certain or likely that equal power was not being delivered to each antenna and / or attenuator/antenna, and the data would be misleading, rather than contribute to a fair test of this measurement method. In other words, the results listed do not use intentionally "cherry picked" data designed to produce a particular outcome.

Experimental Method and Equipment

Two identical transmitting antennas were used for each experiment session (except see Remark 4 below). This includes the same supporting fiberglass center masts, the same center connection point hardware, the same #14 AWG insulated wire elements, the same element ends, and the same lengths of cord terminating in ground stakes so the slope of the elements of each antenna of the pair was the same. A MyAntennas CMC-130-3K common mode choke was at the feed point at the end of a 50 foot section of RG-8X coaxial cable. A Pelican equipment case was placed on the (sometimes wet) ground, and held an Elecraft KX3, an Elecraft W2, a MyAntennas CMC-130-3K common

Figure 1 — Half-wave transmitting dipoles were set up end to end, with one wavelength between the wire element ends, as a dipole with drooping elements but not as a narrow angle inverted V.

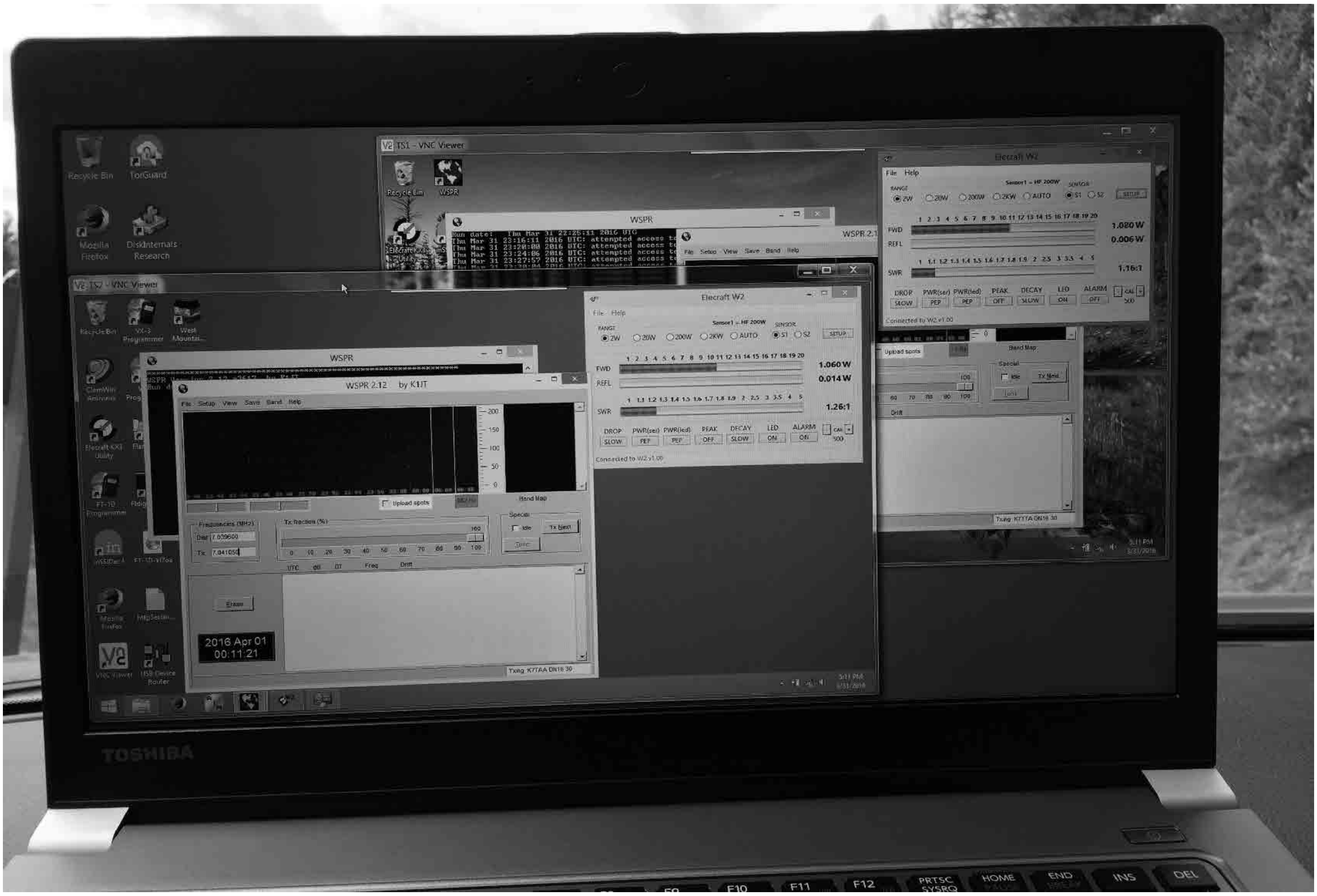

Figure 2 — The computers in the field were controlled using an IEEE 802.11n Wireless Local Area Network, operating at 2.4 GHz, using RealVNC. The RealVNC screens from both computers could be viewed simultaneously to track WSPR transmissions and power output levels. Operators were Charles Preston, K7TAA, and Karin Preston, K7TTA.

mode choke, a RigRunner dc distribution block, and usually, one or two Buddipole 4S2P LiFePO4 battery packs, along with a microHAM USB III digital interface, and a Toshiba laptop computer running Windows 8.1 and WSPR 2.12_r3617. A 12 V dc 4" fan was used to move air past the KX3 heat sinks, since the black cases were in full sunlight part of the time, and some WSPR transmissions were almost continuous for some periods of time. The location for most of the transmitting sessions was a large flat field adjacent to the US Forest Service Little Boulder Campground near Helmer, ID. We operated under a Special Use Permit for Recreation Events. This area is part of the Nez Perce-Clearwater National Forests.[5] The half-wave resonant transmitting dipoles, see Figure 1, were set up end to end, with one wavelength between the wire element ends, as a dipole with drooping elements but not as a narrow angle inverted V.

Because this field is below the average terrain in the direction of Troy, ID, a geographical elevation profile and transmitting experiments showed that NVIS propagation could be used, with the receiving site in Troy about 13 miles away but with no line of sight propagation.

The receiving station for the local transmissions was an Elecraft KX3, West Mountain Radio RIGblaster Advantage, and 40 meter dipole. By driving about 1.2 miles from the Little Boulder transmitting site, a cellular data Internet connection allowed GoToMyPC remote control of the receiving site computer. This was running WSPR software and the Win4K3Suite software so that the receiving KX3 attenuator or preamp could be used to keep the received SNR between -28 dB and 0 dB, where the WSPR SNR response is linear. Figure 2 shows the computer used in the field to control the transmissions.

A written log of power readings from each remotely controlled W2 was created for each simultaneous WSPR transmission from the two KX3s, with the power output noted once during each minute. The WSPR software was set to transmit simultaneously on each KX3, with one as K7TAA and the other as K7TTA. The frequencies were usually set 20 Hz apart in the WSPR passband, with the idea that would be far enough to avoid mutual interference in the receiver and avoid as much ionospheric selective fading as possible.

Some of the experimental transmitting sessions were shorter than planned, since antenna, WLAN, and computer setup took hours for each day's session.

The plan was to use identical power levels on identical antennas, and once a baseline was established, to introduce change by adding an HP attenuator to one of the transmitters. This was carried out, along with a couple of sessions where the power output setting on one KX3 was reduced by a known amount, and checked with the W2 power meter.

Results – Point to point propagation, May 6, 2016, 10 meters

Two identical 10 meter antennas were set up in a field at the Spring Valley Reservoir[6], about 3.6 air miles from Troy, ID. The receiving site was in Troy. Because antenna VSWR was higher than 1.5:1, the ATU in each KX3 was used, to avoid any fold back in RF power output from the KX3s. This is from the ALL_WSPR.txt file captured in Troy during the 10 meter point to point testing over a 3.6 mile path that is not line of sight. Identical antennas and power levels produced WSPR SNR reports that average 0 dB difference, see Figure 3. A standard deviation calculation of the variance does not seem appropriate for WSPR SNR values. The SNR is reported in minimum 1 dB steps, even if the actual difference between a -4 dB report and a -5 dB report could be caused by a signal difference of 0.1 dB or less.

Inspecting the reports from 0034 and 0038 from the log of Figure 3, at 0034 K7TAA is weaker by 1 dB, and at 0038 K7TAA is stronger by 1 dB. Any consistent difference in signal strength should be immediately obvious from the mean of the difference between K7TAA and K7TTA. Using the mean would be misleading if the relative positions of K7TAA and K7TTA were changing, since a frequently stronger K7TAA would sometimes get subtracted from a weaker K7TTA, and sometimes the reverse, causing the -1 dB and +1 dB to be averaged to 0, and hiding the actual received signal difference.

Using the mean to average value, several or many signal reports should be a way to minimize random path effects such as movement near the antenna, small antenna movements due to wind, and changes in the RF path characteristics during the measurement period. Time gaps in the transmissions are due to traveling from the transmitter site to the receiver site and back again to make sure received SNR levels were within the linear range of -28 dB to 0 dB, since there was no Internet connection, and therefore, no remote control of the receiver from the Spring Valley transmitting site.

While the number of simultaneous transmissions (12) shown in Figure 3 may seem like a small number of comparisons, bear in mind that it represents almost 24 minutes of continuous RF signal measurement. For contrast, anyone watching a high frequency RF signal with a spectrum analyzer from even 50 yards away for 1 minute will see very frequent amplitude changes under what seem like stable conditions. Figure 4 shows WSPR received signals, matching antennas and with 6 dB reduced power output on one antenna. An HP 8491A 6 dB attenuator was inserted between the Elecraft W2 power meter output and the common mode choke on the K7TAA transmitting unit.

Using the attenuator is an exception to the experimental design of avoiding the need for calibration, by using comparisons. The comparison method of measurement used in these experiments reduces the need to have NIST traceable calibration of instruments, since I'm not measuring absolute field strength from antennas, but using a well-characterized design (half wave dipole) as a reference. I'm not measuring absolute amplitude of power delivered to feed lines with the Elecraft W2 power meters, but only determining that each W2 reads the same value from the same power source. I'm not depending (for most measurements) on the W2 being linear over a certain power range as I reduce the power, but I'm using a fixed attenuator to reduce power after matching and monitoring the power output between the two KX3 transmitters.

Date	Time		SNR	DT	Freq	XMTR	GridSq	Pwr	Drift	DC	TT	Diff
160506	2230	26	-5	-1.2	28.127052	K7TAA	DN16	30	0	1	0	
160506	2230	26	-4	-1.6	28.127069	K7TTA	DN16	30	0	1	0	-1
160506	2236	26	-5	-1.7	28.127053	K7TAA	DN16	30	0	1	0	
160506	2236	26	-5	-2	28.127069	K7TTA	DN16	30	0	1	0	0
160506	2240	27	-5	-1.6	28.127053	K7TAA	DN16	30	0	1	0	
160506	2240	25	-4	-1.8	28.127069	K7TTA	DN16	30	0	1	0	-1
160507	0020	26	-5	-0.9	28.127052	K7TAA	DN16	30	-1	1	0	
160507	0020	25	-5	-0.8	28.127068	K7TTA	DN16	30	0	1	0	0
160507	0026	25	-4	-0.8	28.127044	K7TAA	DN16	30	-1	1	0	
160507	0026	25	-4	-0.7	28.127069	K7TTA	DN16	30	1	1	0	0
160507	0028	27	-4	-1	28.127044	K7TAA	DN16	30	0	1	0	
160507	0028	26	-4	-0.7	28.127070	K7TTA	DN16	30	0	1	0	0
160507	0030	27	-4	-1	28.127044	K7TAA	DN16	30	0	1	0	
160507	0030	25	-4	-0.8	28.127069	K7TTA	DN16	30	0	1	0	0
160507	0032	27	-4	-1	28.127044	K7TAA	DN16	30	0	1	0	
160507	0032	27	-5	-0.7	28.127069	K7TTA	DN16	30	0	1	0	1
160507	0034	27	-5	-0.9	28.127044	K7TAA	DN16	30	0	1	0	
160507	0034	25	-4	-0.7	28.127069	K7TTA	DN16	30	1	1	0	-1
160507	0036	27	-4	-0.9	28.127044	K7TAA	DN16	30	0	1	0	
160507	0036	25	-4	-0.5	28.127069	K7TTA	DN16	30	0	1	0	0
160507	0038	27	-4	-0.8	28.127045	K7TAA	DN16	30	0	1	0	
160507	0038	27	-5	-0.5	28.127069	K7TTA	DN16	30	0	1	0	1
160507	0040	27	-4	-0.7	28.127044	K7TAA	DN16	30	0	1	0	
160507	0040	27	-5	-0.7	28.127069	K7TTA	DN16	30	0	1	0	1
												0 Mean
												0 Median
												0 Mode

Figure 3 — WSPR received signals from matching antennas and power levels.

Date	Time		SNR	DT	Freq	XMTR	GridSq	Pwr	Drift	DC	TT	Diff
160507	0106	20	-10	-0.5	28.127052	K7TAA	DN16	30	0	1	0	
160507	0106	26	-4	-0.2	28.127067	K7TTA	DN16	30	0	1	0	-6
160507	0108	21	-10	-0.6	28.127052	K7TAA	DN16	30	0	1	0	
160507	0108	27	-4	-0.3	28.127069	K7TTA	DN16	30	0	1	0	-6
160507	0110	21	-10	-0.6	28.127052	K7TAA	DN16	30	0	1	0	
160507	0110	27	-4	-0.4	28.127069	K7TTA	DN16	30	0	1	0	-6
160507	0112	21	-10	-0.5	28.127053	K7TAA	DN16	30	0	1	0	
160507	0112	25	-4	-0.3	28.127069	K7TTA	DN16	30	1	1	0	-6
160507	0114	21	-10	-0.7	28.127053	K7TAA	DN16	30	0	1	0	
160507	0114	26	-4	-0.6	28.127069	K7TTA	DN16	30	0	1	0	-6
160507	0116	22	-10	-0.6	28.127052	K7TAA	DN16	30	0	1	0	
160507	0116	25	-3	-0.3	28.127069	K7TTA	DN16	30	0	1	0	-7
160507	0118	20	-10	-0.7	28.127052	K7TAA	DN16	30	-1	1	0	
160507	0118	25	-4	-0.4	28.127069	K7TTA	DN16	30	0	1	0	-6
160507	0120	20	-10	-0.5	28.127052	K7TAA	DN16	30	-1	1	0	
160507	0120	25	-4	-0.4	28.127069	K7TTA	DN16	30	0	1	0	-6
160507	0122	20	-10	-0.7	28.127053	K7TAA	DN16	30	0	1	0	
160507	0122	26	-5	-0.4	28.127068	K7TTA	DN16	30	-1	1	0	-5
160507	0124	21	-10	-0.6	28.127053	K7TAA	DN16	30	0	1	0	
160507	0124	26	-4	-0.3	28.127068	K7TTA	DN16	30	0	1	0	-6
160507	0126	22	-10	-0.7	28.127052	K7TAA	DN16	30	0	1	0	
160507	0126	27	-4	-0.5	28.127069	K7TTA	DN16	30	0	1	0	-6
												-6 Mean
												-6 Median
												-6 Mode

Figure 4 — WSPR received signals with matching antennas and 6 dB reduced power on one antenna.

An HP 8491B 10 dB attenuator was inserted between the Elecraft W2 power meter output and the common mode choke on the K7TAA transmitting unit. Figure 5 shows WSPR received signals with matching antennas and with 10 dB reduced power output on one antenna.

Transmitted power levels set in WSPR software during these experiments do not necessarily reflect the power output to the feed line, since not all power levels used can be specified or sent as part of the WSPR message. The ALL_WSPR.txt logged reports shown in the experiment spreadsheets, including these examples, should not be used to match transmitted power with received SNR differences. The same is true of the logged reports in the WSPRnet database. An example transmitting site log of the monitored power outputs from each KX3, and any attenuators used, is shown below, for the 10 meter measurement sessions shown here.

Measurements of the attenuators used in these experiments were made before and after their use to collect the transmission data. As of June 6, 2016, the measurements were, HP 8491A 3 dB was measured as 2.87 dB; the HP 8491A 6 dB was measured as 5.82; and the HP 8491B 10 dB was measured as 9.71. Additional measurement results are shown in Table 1.

Remarks in the measurements

Remark 1 — After the initial Internet remote receiver check for reception, when simultaneous transmissions were being received successfully, approximately 30 more transmissions were made, but one KX3 was off frequency for the remainder, and no additional measurements were captured.

Remark 2 — A number of short range transmission measurements were excluded because the WSPR SNR was greater than 0 dB. K1JT, Joe Taylor, wrote that he suspected those WSPR measurements might not be linear. Based on these experiments, the SNR range of 0-10 dB appears to be linear, but was excluded as a precaution.

Remark 3 — The KX3 power level for K7TTA was set at 1.0 W output, and the power level for K7TAA was set at 0.8 W output (1 dB lower)

Remark 4 — The center of the K7TAA antenna was approximately 20 inches lower than the K7TTA antenna. One section of the K7TAA telescoping mast was not fully extended, and this was discovered when it was being taken down. This antenna difference can be seen in the -1 dB measurements on 4-26-16 with no difference in the power supplied to each antenna.

Remark 5 — The center of the K7TAA dipole was approximately 20 inches lower than for K7TTA, and the receive measurements close to -7 dB show the effect of both the 6 dB HP attenuator and the difference between antennas. See Remark 4.

Remark 6 — The output power on the K7TTA KX3 was set to 2 W, and the power on the K7TAA KX3 was set to 0.5 W, (nominal 6 dB difference). The received signal measurements show the effect of both lower power input to the K7TAA antenna, and lower antenna position. Power

Date	Time		SNR	DT	Freq	XMTR	GridSq	Pwr	Drift	DC	TT	Diff	
160507	0136	15	-14	-0.4	28.127052	K7TAA	DN16	30	0	1	0		
160507	0136	27	-5	-0.3	28.127068	K7TTA	DN16	30	0	1	0	-9	
160507	0138	16	-14	-0.6	28.127052	K7TAA	DN16	30	1	1	0		
160507	0138	23	-4	-0.5	28.127069	K7TTA	DN16	30	1	1	0	-10	
160507	0140	16	-14	-0.7	28.127053	K7TAA	DN16	30	0	1	0		
160507	0140	25	-4	-0.5	28.127069	K7TTA	DN16	30	1	1	0	-10	
160507	0142	15	-13	-0.5	28.127052	K7TAA	DN16	30	0	1	0		
160507	0142	25	-4	-0.4	28.127069	K7TTA	DN16	30	0	1	0	-9	
160507	0144	16	-14	-0.4	28.127052	K7TAA	DN16	30	0	1	0		
160507	0144	26	-4	-0.3	28.127069	K7TTA	DN16	30	0	1	0	-10	
160507	0146	14	-14	-0.5	28.127053	K7TAA	DN16	30	0	1	0		
160507	0146	25	-4	-0.3	28.127069	K7TTA	DN16	30	-1	1	0	-10	
160507	0148	15	-14	-0.5	28.127053	K7TAA	DN16	30	0	1	0		
160507	0148	25	-4	-0.5	28.127069	K7TTA	DN16	30	0	1	0	-10	
160507	0150	16	-14	-0.5	28.127054	K7TAA	DN16	30	0	1	0		
160507	0150	27	-5	-0.3	28.127069	K7TTA	DN16	30	0	1	0	-9	
160507	0152	17	-14	-0.6	28.127054	K7TAA	DN16	30	0	1	0		
160507	0152	28	-4	-0.3	28.127069	K7TTA	DN16	30	0	1	0	-10	
160507	0154	17	-14	-0.5	28.127055	K7TAA	DN16	30	0	1	0		
160507	0154	27	-4	-0.3	28.127069	K7TTA	DN16	30	0	1	0	-10	
160507	0156	17	-14	-0.6	28.127054	K7TAA	DN16	30	0	1	0		
160507	0156	26	-4	-0.5	28.127069	K7TTA	DN16	30	0	1	0	-10	
160507	0158	17	-14	-0.5	28.127053	K7TAA	DN16	30	0	1	0		
160507	0158	26	-5	-0.2	28.127069	K7TTA	DN16	30	0	1	0	-9	
160507	0200	18	-14	-0.6	28.127054	K7TAA	DN16	30	0	1	0		
160507	0200	27	-4	-0.3	28.127069	K7TTA	DN16	30	0	1	0	-10	
												-9.69	Mean
												-10	Median
												-10	Mode

Figure 5 — WSPR received signals with matching antenna and 10 dB reduced power on one antenna.

measurements with the W2 power meters showed an average of 2.1 W from K7TTA, and -0.6 W from K7TAA, for a 5.44 dB difference. This closely matches the reported mean of -6.48 dB relative to the K7TTA transmissions plus antenna effect. See Remark 4.

Figure 6 shows a portion of one of the comparison spreadsheets compiled from the WSPRnet database after a simultaneous transmission on 20 meters.

Conclusion

Hundreds of WSPR measurements have been made, on different days during three different months, on three different frequency bands, under different propagation conditions, and using both point to point and ionospheric propagation. Three different sets of antennas were used, and these were set up multiple times in slightly different or very different locations. The averaged measurements differed less than 0.5 dB from the known comparative power levels delivered to the antennas, and indicate that this method of measurement of antenna performance is suitable to measure some characteristics of HF antennas without a formal antenna range.

Long transmitting sessions with two transmitters are not usually necessary with multiple reporting stations automatically sending their "spots" to the WSPRnet database. Pulling those database entries into a spreadsheet and matching the transmissions isn't hard or complicated. For data sets of around 100 simultaneous WSPR SNR measurements, accuracy in these experiments approached 0.1 dB when the measured values of the fixed HP attenuators are used, rather than their nominal values of 3 dB, 6 dB, or 10 dB.

Charles Preston, K7TAA, has an Amateur Extra Class license. He earned his first license at age 13. He has a B.A. in psychology. Charles retired from a career in law enforcement to provide cyber security training and consulting,

20160426 K7TAA 20" lower antenna center, 6 dB HP 2 W attenuator, correctly shows 7 dB due to both attenuator and antenna effect

									Diff
04/26/2016 22:30:00	K7TAA	-19	AI4RY		04/26/2016 22:30:00	K7TTA	-11	AI4RY	-8
04/26/2016 22:34:00	K7TAA	-23	AI4RY		04/26/2016 22:34:00	K7TTA	-16	AI4RY	-7
04/26/2016 22:46:00	K7TAA	-22	AI4RY		04/26/2016 22:46:00	K7TTA	-15	AI4RY	-7
04/26/2016 22:50:00	K7TAA	-25	AI4RY		04/26/2016 22:50:00	K7TTA	-17	AI4RY	-8
04/26/2016 22:54:00	K7TAA	-23	AI4RY		04/26/2016 22:54:00	K7TTA	-16	AI4RY	-7
04/26/2016 23:36:00	K7TAA	-26	AI4RY		04/26/2016 23:36:00	K7TTA	-19	AI4RY	-7
04/26/2016 23:44:00	K7TAA	-26	AI4RY		04/26/2016 23:44:00	K7TTA	-19	AI4RY	-7
04/26/2016 22:28:00	K7TAA	-20	K4COD		04/26/2016 22:28:00	K7TTA	-12	K4COD	-8
04/26/2016 22:34:00	K7TAA	-17	K4COD		04/26/2016 22:34:00	K7TTA	-10	K4COD	-7
04/26/2016 22:44:00	K7TAA	-21	K4COD		04/26/2016 22:44:00	K7TTA	-15	K4COD	-6
04/26/2016 22:46:00	K7TAA	-24	K4COD		04/26/2016 22:46:00	K7TTA	-17	K4COD	-7
04/26/2016 22:54:00	K7TAA	-20	K4COD		04/26/2016 22:54:00	K7TTA	-13	K4COD	-7
04/26/2016 22:58:00	K7TAA	-17	K4COD		04/26/2016 22:58:00	K7TTA	-10	K4COD	-7
04/26/2016 23:00:00	K7TAA	-16	K4COD		04/26/2016 23:00:00	K7TTA	-9	K4COD	-7
04/26/2016 23:08:00	K7TAA	-24	K4COD		04/26/2016 23:08:00	K7TTA	-17	K4COD	-7
04/26/2016 23:18:00	K7TAA	-24	K4COD		04/26/2016 23:18:00	K7TTA	-17	K4COD	-7
04/26/2016 23:28:00	K7TAA	-19	K4COD		04/26/2016 23:28:00	K7TTA	-12	K4COD	-7
04/26/2016 23:36:00	K7TAA	-16	K4COD		04/26/2016 23:36:00	K7TTA	-9	K4COD	-7
04/26/2016 23:44:00	K7TAA	-16	K4COD		04/26/2016 23:44:00	K7TTA	-8	K4COD	-8

Figure 6 — A portion of one of the comparison spreadsheets compiled from the WSPRnet database after a simultaneous transmission on 20 meters.

Table – 1
Additional results.

Date	*Band*	*Propagation type*	*Actual difference in power to each feed line*	*Number of simultaneous transmissions received*	*Mean rcvd sig. diff; Median; Mode; Max. Diff. variance K7TAA-K7TTA*
3-31-16	40	NVIS short range, 1 rcvr site	0 dB	3 [remark 1]	-0.33 dB; 0; 0; -1
4-1-16	40	NVIS short range, 1 rcvr site	0 dB	33 [remark 2]	0.06 dB; 0; 0; +2/-2
4-18-16	20	Ionospheric, long range, multiple rcvr sites	0 dB	115	0.04 dB; 0; 0;+3/-2
4-18-16	20	Ionospheric, long range, multiple rcvr sites	-6 dB K7TAA HP attenuator	42	-5.38 dB; -5.50; -6.00; -4/-8 (+2/-2 diff)
4-19-16	20	Ionospheric, long range, multiple rcvr sites	0 dB	131	-0.10 dB; 0; 0; +3/-3
4-19-16	20	Ionospheric, long range, multiple rcvr sites	-3 dB K7TAA HP attenuator	73	-2.89 dB; -3.0; -3.0; -5/0 (+3/-2 diff)
4-19-16	20	Ionospheric, long range, multiple rcvr sites	0 dB (2nd 0 dB session following 3 dB atten.)	49	0.18 dB 0; 0; +2/-3
4-19-16	20	Ionospheric, long range, multiple rcvr sites	-1 dB K7TAA Remark 3	147	-0.96 dB; -1; -1; -4/+2 (+3/-3 diff)
4-26-16	20	Ionospheric, long range, multiple rcvr sites	0 dB atten. but lower antenna Remark 4	140	-0.98 dB; -1; -1 ; -5/0 (-4/+1 diff)
4-26-16	20	Ionospheric, long range, multiple rcvr sites	-6 dB K7TAA plus lower antenna Remark 5	132	-6.89 dB; 7; 7; -10: -3 (+4/-3 diff)
4-27-16	20	Ionospheric, long range, multiple rcvr sites	-5.44 dB K7TAA plus lower antenna Remarks 4 & 6	82	-6.48 dB; 7; 7; -4/-8 (+3/-1 diff)

and performing security assessments including network penetration testing. He is the author and co-author of published articles in the field and digital forensics. Charles has also provided technical eavesdropping countermeasure services and propagation designs for wireless networks in large and complex buildings.

Notes

[1]John S. Belrose, VE2CV, "A Brief Overview of the Performance of Wire Aerials in their Operating Environments" in *International Antenna Collection Volume 1*, Edited by Dr. George Brown, M5ACN, ARRL item number 9156, available from your ARRL dealer, or from the ARRL Store, Telephone toll-free in the US 888-277-5289, or 860-594-0355, fax 860-594-0303; **www.arrl.org/shop/; pubsales@arrl.org**.

[2]WSPR 2.0 User's Guide, **physics.princeton.edu/pulsar/K1JT/wspr.html**.

[3]**www.charlespreston.net/antenna/WSPR-Antenna-Prop-Exp-PR.pdf**.

[4]**www.charlespreston.net/antenna/Compare-EndFedz-EF-30.pdf**.

[5]Select "Campground Camping" at **https://www.fs.usda.gov/activity/nezperceclearwater/recreation/camping-cabins**.

[6]Spring Valley Reservoir, **https://www.google.com/maps/place/Spring+Valley+Reservoir/@46.78,-116.75**.

Riccardo Gionetti, IØFDH

Via S. Bernadette 61, 00167 Roma RM, Italy: **rgionetti@virgilio.it**

Automatic Tracking Filter for DDS Generator

Reduce spurious responses from a digital synthesizer with this filter.

The design of a receiver local oscillator has several levels of difficulties, especially over an extended frequency range. In a VLF – HF receiver (0.01 to 30 MHz), with a 10.7 MHz IF, the range of the frequency of the local oscillator would be between 10.71 and 40.7 MHz. With DDS technology it is now possible to have a particularly stable oscillator covering that range of frequencies.

The DDS AD9851, by Analog Devices, allows for very good performance. It exhibits frequency stability, low phase noise and a wide range frequency from the low frequencies to 60 MHz, so it is very well suited for this application. There is, however, a down side. The spectrum of the signal generated by this wide range DDS is not particularly clean, and the several spurious responses in the receiver mixing process produce many birdies. Although the spurs are weak (equivalent to a 0.5 µV

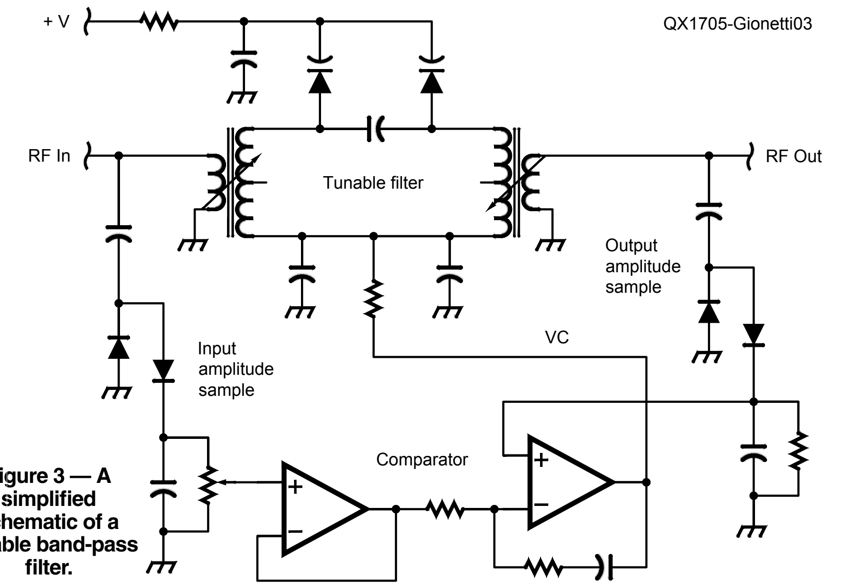

Figure 3 — A simplified schematic of a tunable band-pass filter.

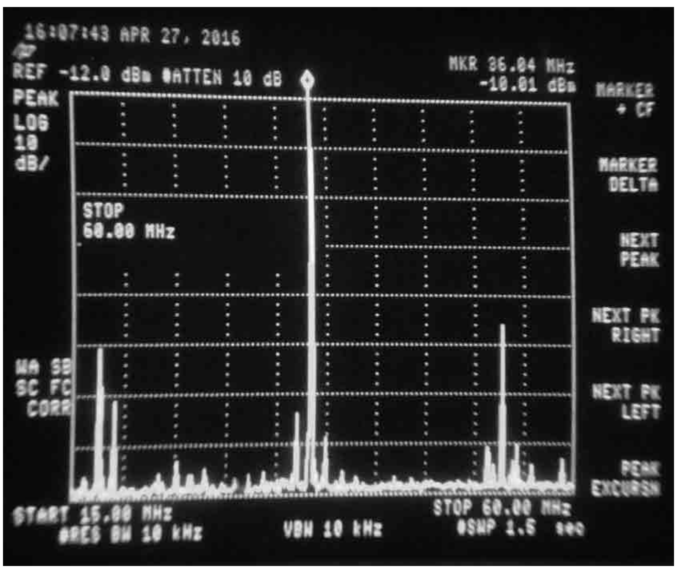

Figure 1 — A DDS Carrier 36 MHz, with unfiltered "birdies" above and below the carrier.

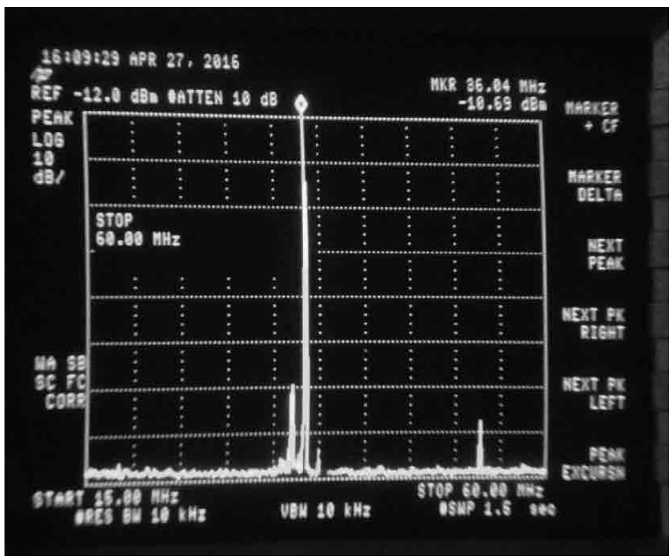

Figure 2 — A DDS Carrier 36 MHz, with "birdies" reduced by the band-pass filter.

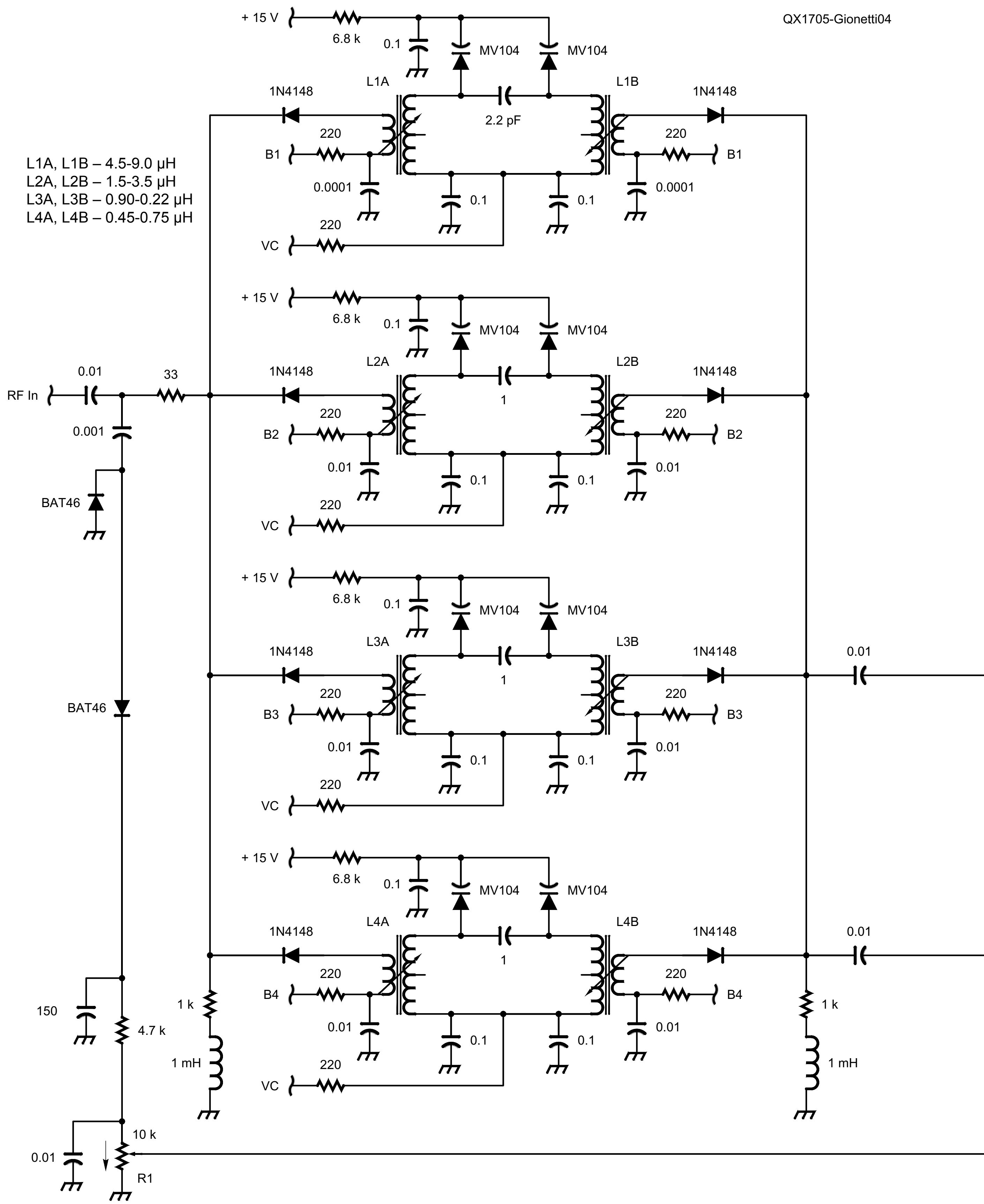

Except as indicated, decimal values of capacitance are in microfarads (μF);
others are in picofarads (pF); resistances are in ohms; k = 1,000, M = 1,000,000.

Figure 4 — Schematic diagram of multiple band-pass filters.

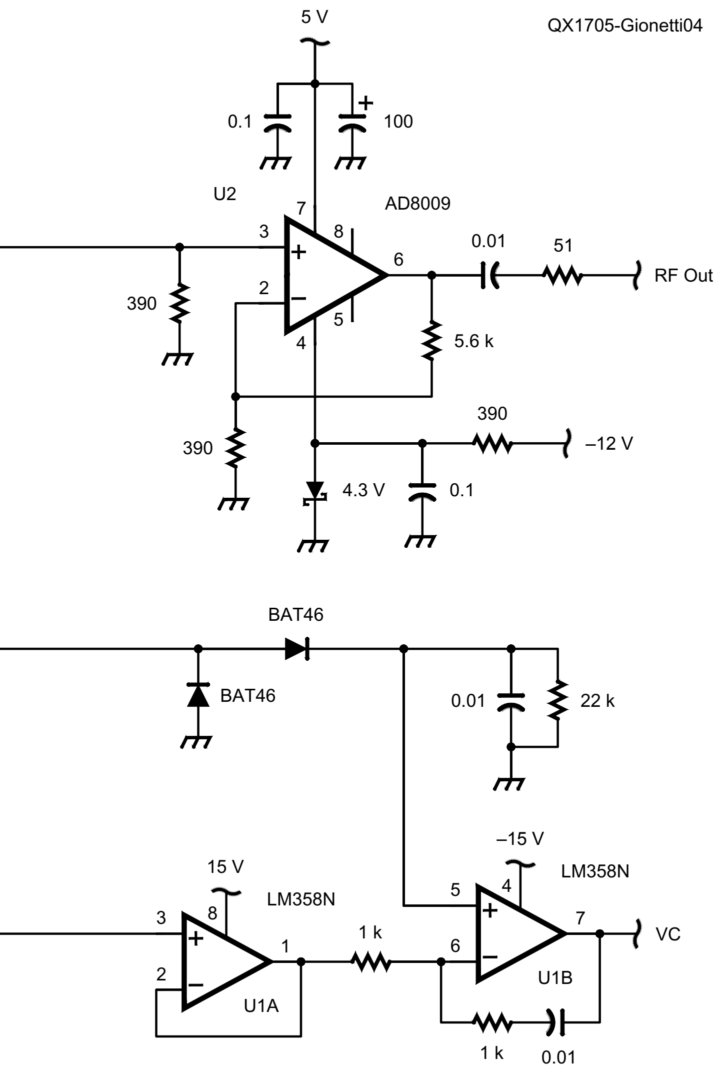

signal), they are very annoying.

A Technical Solution

Strong attenuation of the spurious signals can be achieved by placing a band-pass filter tuned to the DDS frequency between the output of DDS and the mixer Local Oscillator (LO) port. Figure 1 shows the measured spectrum of the DDS generating a carrier at 36 MHz without a filter. Figure 2 shows the same spectrum with the 36 MHz carrier, now filtered by a band-pass filter.

When changing the DDS frequency, the band-pass filter center frequency should be tuned to the new frequency to maintain effectiveness. This tuning operation should automatically follow changes in the DDS frequency.

After several attempts I implemented the following solution. Compare the level of the input signal with the signal level at the output of the filter, then tune the filter to maximize the output. If we use varicap diodes to tune the filter, the tuning is done by means of a dc voltage that can be obtained by an op-amp that compares the rectified input and output RF signals. So with a relatively simple circuit it is possible to implement an Automatic Tracking Filter.

Figure 3 shows a simplified diagram of the circuit. The filter maintains its resonance even when the frequency is changed quickly. Tracking, however, can be lost when the bandwidth limits are exceeded. The next filter in the filter bank then must be changed to re-establish the tracking.

We want the DDS to cover a receiving range from 0.01 to 30 MHz, so the band-pass filter must be able to track over the 30 MHz from 10.7 to 40.7 MHz. To do this we require a filter bank of at least four filters (Figure 4) having some overlap between them, to cover the entire frequency range. The first band-pass filter tunes between 10 and 16 MHz and uses a band select control voltage at B1 from the control circuit of Figure 5. The second tunes between 15 and 23 MHz, and is controlled by band select voltage on line B2. Figures 6 and 7 show no filtering and filtering respectively for a 16 MHz carrier. The third tunes between 21 and 30 MHz with the band select voltage on line B3. Figures 8 and 9 show no filtering and filtering respectively for a 26 MHz carrier. Finally, the fourth filter tunes between 28 and 42 MHz and is selected by the B4 control voltage.

Automatic Switching

The automatic switching of the several band-pass filters in the filter bank is done with a comparator U3 in Figure 5. The comparator controls the maximum and

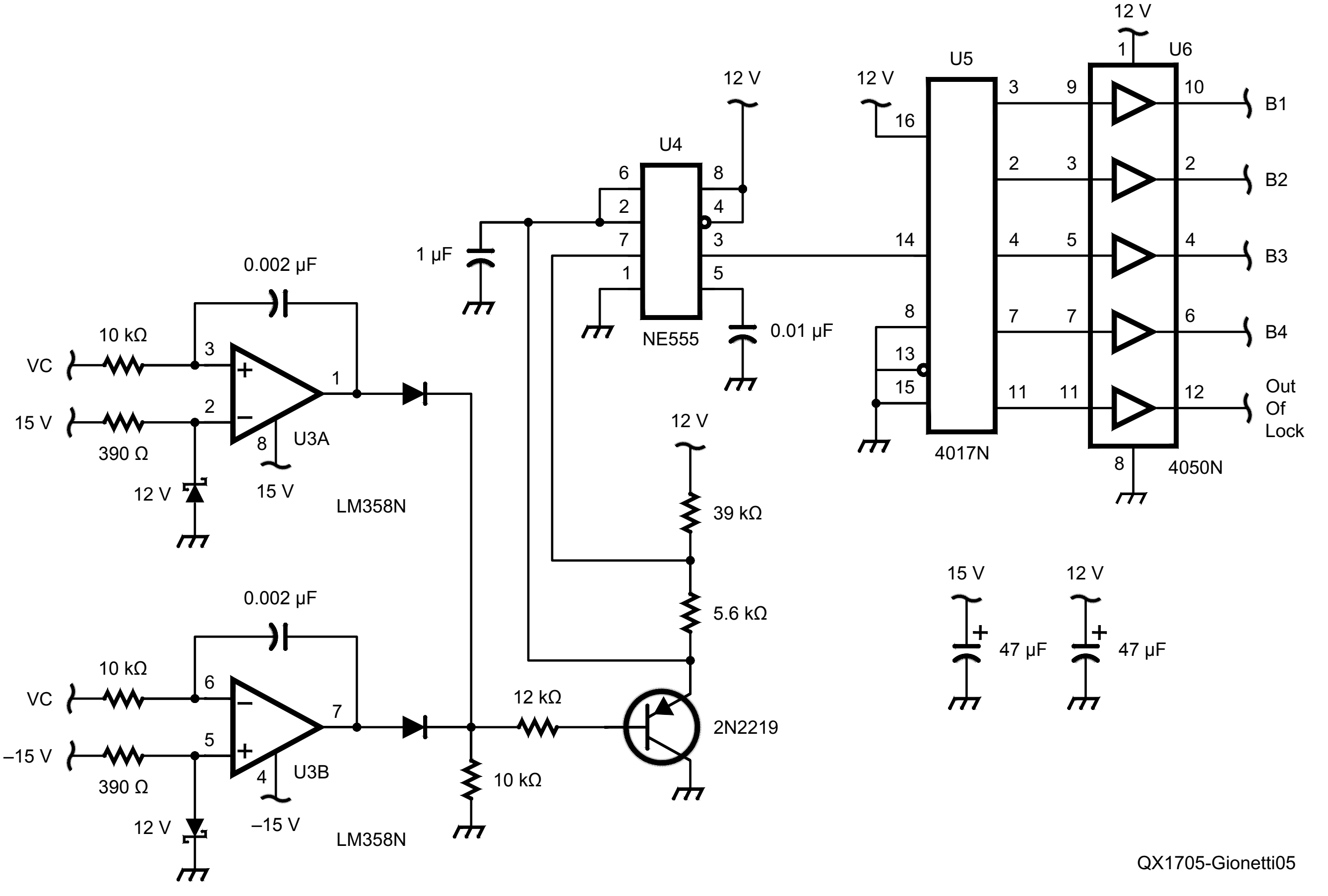

Figure 5 — Schematic diagram of the control circuitry.

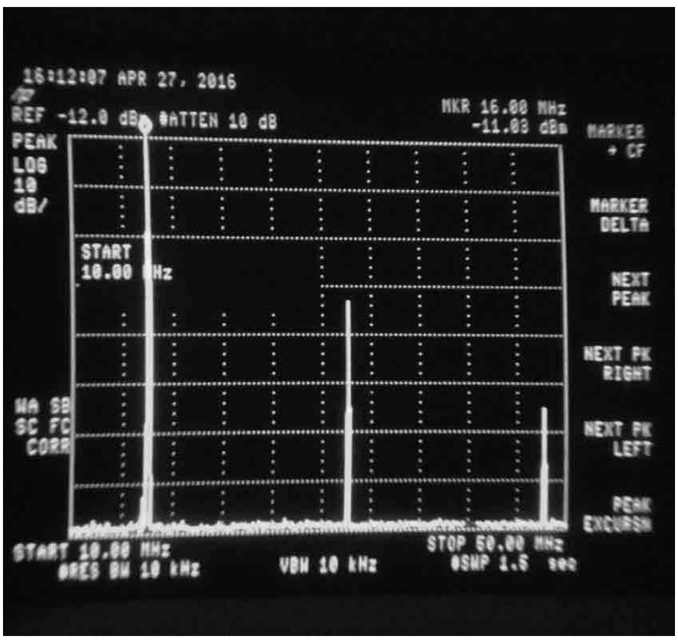

Figure 6 — DDS carrier at 16 MHz without filtering.

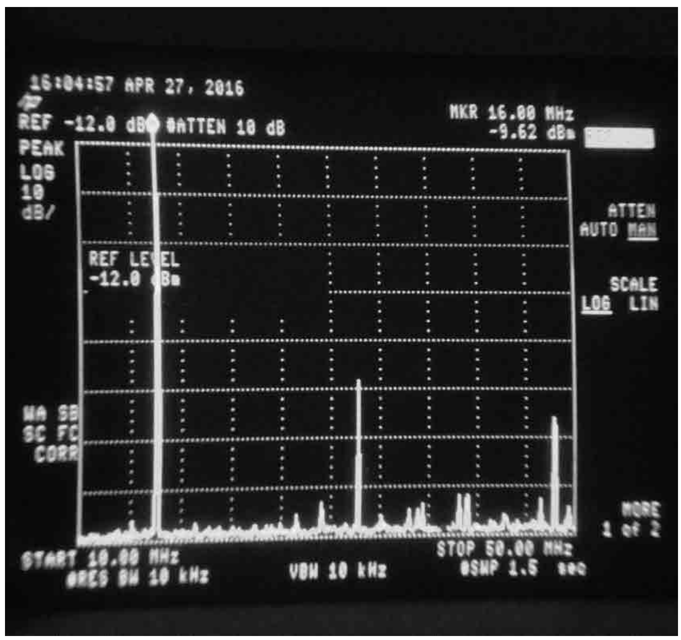

Figure 7 — DDS carrier at 16 MHz with band-pass filtering.

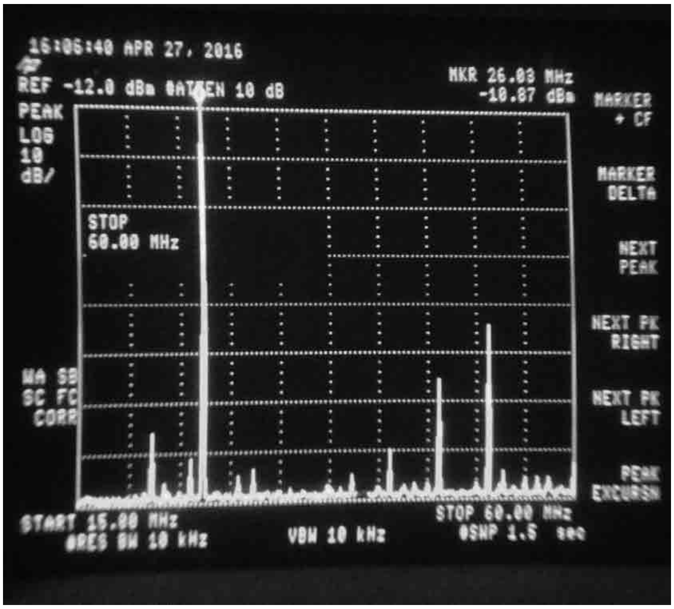

Figure 8 — DDS carrier at 26 MHz without filtering.

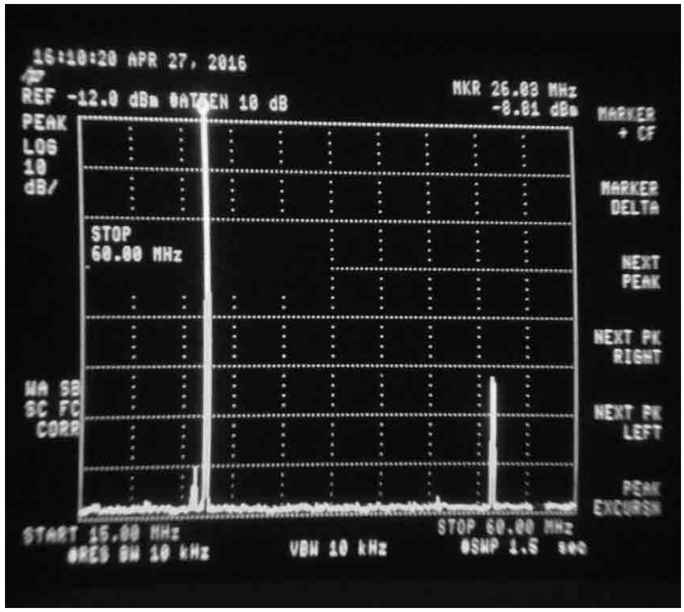

Figure 9 — DDS carrier at 26 MHz with band-pass filtering.

minimum voltages that the varicap diodes can reach, If these limits are exceeded, the output voltage of the comparator becomes positive and transistor Q1 is switched off. As soon as Q1 is off, U4 starts to oscillate and sends pulses to the input of a decimal counter U5. The counter outputs sequentially change with each counter output pulse.

The switching diodes of each band-pass filter are connected to an output of the counter U5 via a buffers U6. The filter is switched when the output of its buffer becomes positive. As soon as the filter is switched, the tracking is again acquired, at this point the comparator output goes low and Q1 short circuits the capacitor C1 across the collector-emitter pins, blocking operation of U4, and counter U5. This leaves a logic high at the output to which the filter is connected. This cycle is repeated at each change of frequency that corresponds to a loss of tracking.

Following the filter, an AD8009 amplifier stage U2 (Figure 4), compensates for the filter and switching diode losses, and matches the output impedance to 50 ohms.

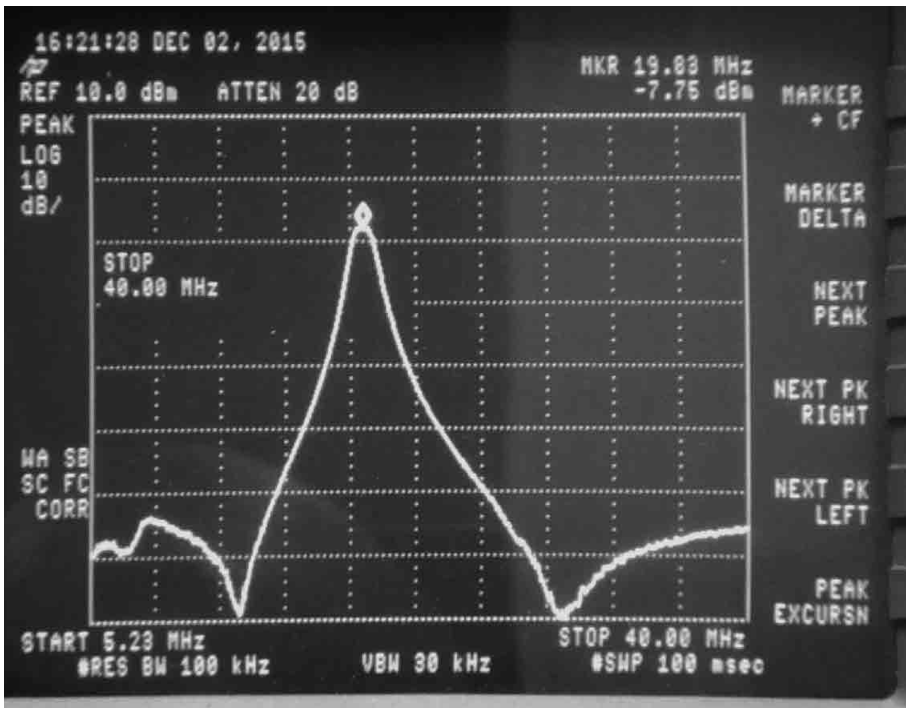

Figure 10 — Response of the band-pass filter tuned to 20 MHz.

Calibration and Results

Calibration is quick and you should not have any critical issues. The first step is the calibration of filters. Remove U1 and U6, which are mounted in sockets. Then,

[1] — Connect a +12 V source to the B1 (pin 10 of U6) output to select the first band-pass filter.

[2] — Connect +10 V to the VC line to bias the varicap tuning diodes.

[3] — Connect a sweep generator to the input of the band-pass filters, adjust the cores of input and output coils L1A and L1B to have a symmetrical response curve at 10 MHz, as seen in Figure 10.

[4] — Connect -12 V to the VC line and verify that the filter is tuned at 16 MHz.

Repeat this procedure for the other three band-pass filters at 15 and 23 MHz, 21 and 30 MHz, 28 and 42 MHz.

After completing the filter calibrations, reinsert the two ICs U1 and U6, and connect the DDS generator. With the trimmer R1, set the level of comparator reference voltage on the U1B. Starting from the highest frequency, adjust potentiometer R1 until tracking begins. This can be monitored with a voltmeter on the VC line.

Including the Automatic Tuning Filter between the DDS and the receiver mixer has reduced birdies by more than 80%.

Figure 11 shows an internal view of the tracking filter.

Additional Applications

Automatic Tuning Filter can also be used to automatically tune HF transmitter driver filters. The B1 – B4 control outputs can be used to automatically switch the band filters of a HF receiver.

Riccardo Gionetti, IØFDH was first licensed in 1974. He studied at University of Rome "La Sapienza - E. Fermi Institute" and received a degree in physics, specializing in cybernetics and electronics. He also attended additional technical courses in radar technology, microwave measurements, EMC, IR sensors, and electronic warfare. Riccardo worked for 10 years in a telecommunications company and for 30 years has held several positions in the Italian defense industry. In the last 10 years he was responsible for Applied Research and Technology for radar sensors and missile subsystems.

Riccardo has published over 50 technical articles and papers in professional and Amateur Radio venues, and is co-author of a handbook "HF Power Linear Amplifier Design", (in Italian) and is author of a course on "Tactical Radio Communications". He is now in retirement enjoying experimenting and building his own equipment. Riccardo's main interests are VLF, HF, VHF receivers and transceivers, RF power amplifiers, instrumentation and the restoring of old radios.

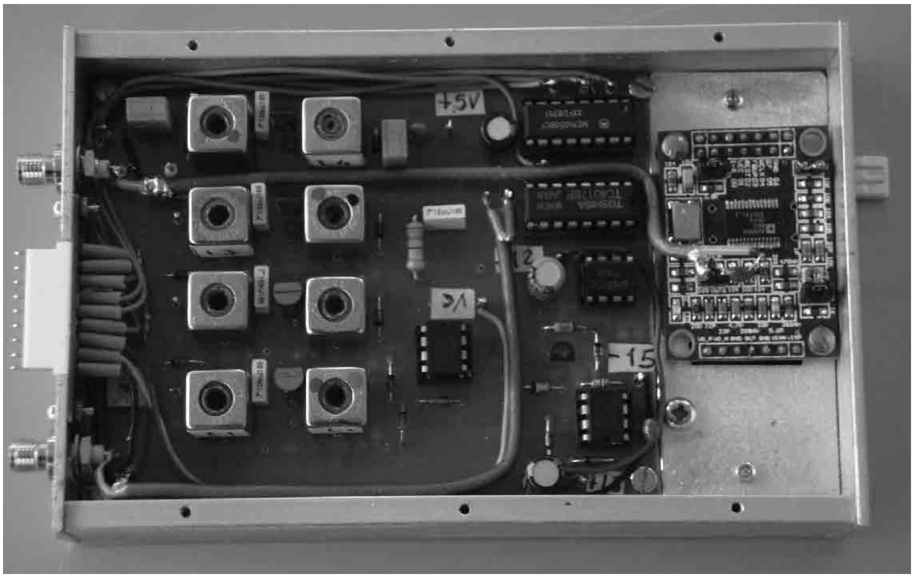

Figure 11 — Internal view of the tracking filter.

Marcus C. Walden

High-Frequency Near Vertical Incidence Skywave Propagation

Findings associated with the 5 MHz Experiment.

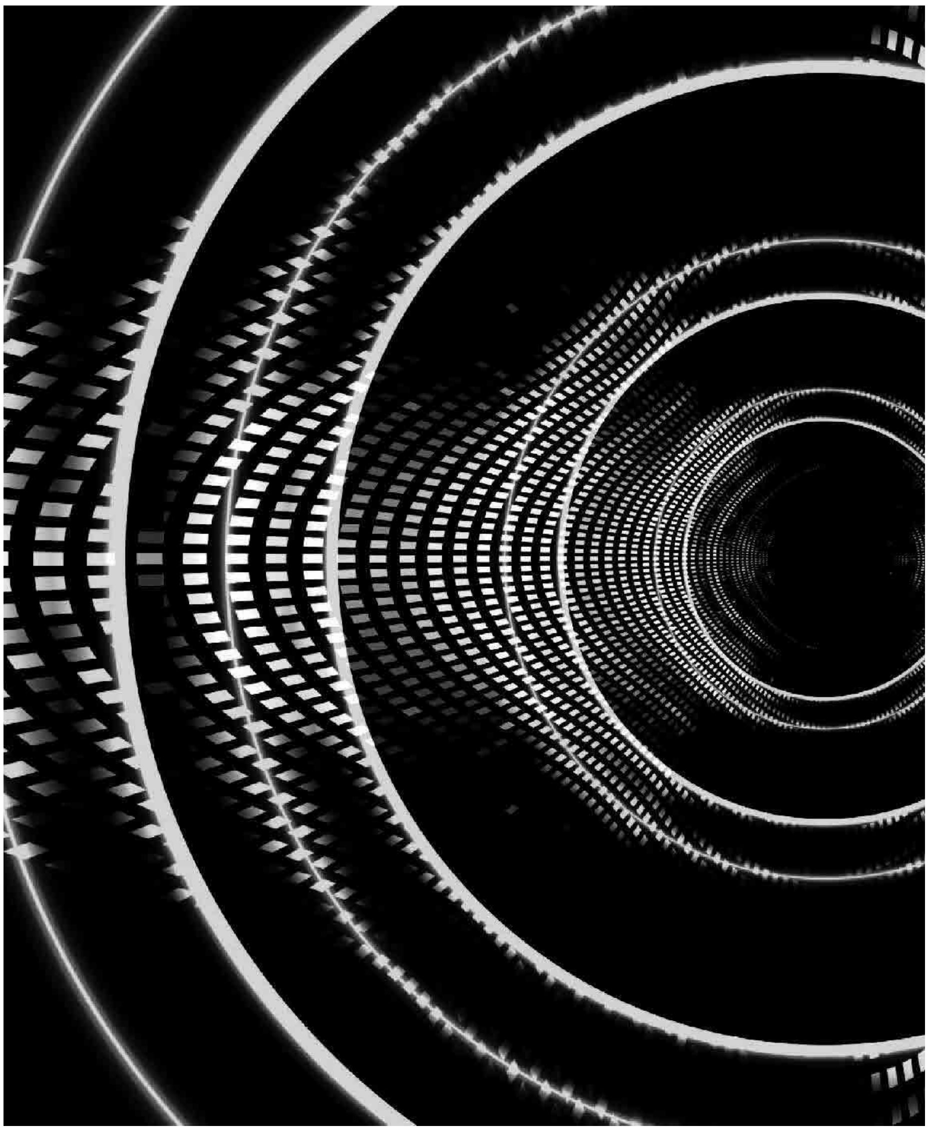

This article collates the findings from the 5 MHz Experiment, a U.K.-based amateur radio project involving a network of beacon transmitters and monitoring stations operating at 5.290 MHz. An analysis of the calibrated received signal-power measurements, together with ionosonde frequency measurements and high-frequency (HF) signal and frequency predictions, led to a number of important results relevant to near vertical incidence skywave (NVIS) communications. The emphasis of this article is on practical aspects of this technique for both professional and amateur users of the HF spectrum.

INTRODUCTION

NVIS propagation allows HF ionospheric communication over relatively short distances, typically up to 400–500 km, using frequencies generally in the range of 2–10 MHz. This technique is important for military and humanitarian organizations as well as amateur radio operators, particularly during emergency situations when the normal power and communications infrastructure may have failed [1]. There can, at times, be substantial overlap between these seemingly disparate NVIS user groups. For example, the Military Auxiliary Radio System in the United

Digital Object Identifier 10.1109/MAP.2016.2609798
Date of publication: 20 October 2016

States consists primarily of civilian radio amateurs supporting military communications [2]. Additionally, the Amateur Radio Emergency Service in the United States and the Radio Amateurs' Emergency Network in the United Kingdom provide volunteer communications for disaster situations as well as community radio services during normal times [3], [4].

This ionospheric-propagation technique primarily makes use of waves transmitted at high angles from the ground such that terrain obstructions (e.g., mountains) have little or no influence on signal strengths. Furthermore, direction finding on waves arriving from high angles is more difficult because bearing errors increase dramatically with decreasing range to the transmitter [5]. Bearing errors arise as a consequence of horizontal gradients in electron density or tilts in the ionosphere [6]. These characteristics make NVIS propagation an important tactical-communications technique at HF, although real-time ray tracing through a tilted ionosphere can lead to more reliable determination of transmitter locations on short-range links [7].

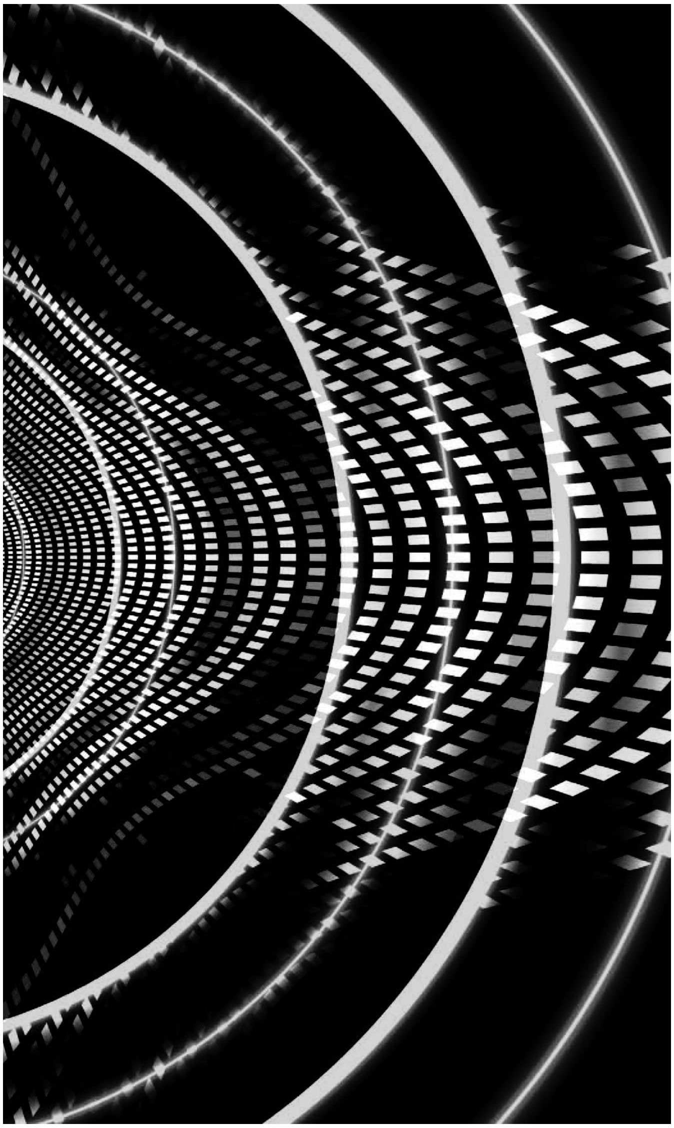

NVIS propagation is predominantly single hop via the F2 region of the ionosphere; therefore, an appropriate choice of operating frequency is important for effective NVIS communications. Additionally, the antenna system needs to be designed to maximize radiation at high elevation angles [1].

The focus of this article is on frequency and signal-level predictions and measurements for NVIS links. Although the regional emphasis is on the United Kingdom, the findings are, in general, relevant to midlatitude locations, which are defined as ~30–60° geomagnetic latitudes, north or south. Discussions on NVIS propagation expand this coverage to a global context.

The details of the 5 MHz Experiment and the associated beacon network that operates at 5 MHz in the United Kingdom are presented. This is an important frequency for midlatitude NVIS communications during daylight hours, particularly at low points in the sunspot cycle when there is insufficient ionization to support propagation at higher frequencies and lower frequencies incur substantial D-region absorption. The importance of 5 MHz for NVIS communications was emphasized by the substantial spectrum negotiations, culminating in a modest secondary allocation at 5 MHz to the amateur service, during the recent World Radiocommunication Conference [8]. Although an amateur radio project, the analysis of calibrated measurements obtained through this experiment resulted in a number of important findings related to NVIS propagation that are of practical relevance to the HF user community, both professional and amateur.

THE 5 MHz EXPERIMENT

OVERVIEW

In 2002, the U.K. Ministry of Defence and the U.K. communications regulator (Ofcom) allowed radio amateurs access to five 3-kHz-wide channels at 5 MHz under a notice of variation to their licenses. Over the subsequent years, further channels have been made available. The Radio Society of Great Britain, which is the national society promoting the hobby, launched the 5 MHz Experiment to encourage antenna and propagation experimentation at this frequency.

TRANSMITTING AND RECEIVING STATIONS

As part of this project, a network of beacon transmitters was established [9], [10]. A number of radio amateurs established receiving stations for long-term monitoring of the beacon transmitters. I analyzed data from five stations [60].

The call sign, location, and geographic coordinates of the transmitting and receiving stations are listed in Table 1, and Table 2 presents the geographic great-circle range and bearing from each transmitter to each receiving station. In total, there were nine NVIS links (i.e., ground range of <500 km).

Direct-conversion [or zero intermediate-frequency (IF)] receivers were used with the audio output sampled by a computer sound card. Each receiver was calibrated for signal power by its owner. Transmitting antennas are inverted-vee dipoles. Receiving antennas also included inverted-vee dipoles as well as a nonresonant, asymmetric dipole and two electrically small active loops (one tuned and the other broadband). These

TABLE 1. THE CALL SIGN, LOCATION, AND GEOGRAPHIC COORDINATES OF THE BEACON TRANSMITTING AND RECEIVING STATIONS.

Station Type	Call Sign	Location	Geographic Coordinates
Transmitting	GB3RAL	Oxfordshire, United Kingdom	51.56° N, 1.29° W
	GB3WES	Cumbria, United Kingdom	54.56° N, 2.63° W
	GB3ORK	Orkney Isles, United Kingdom	59.02° N, 3.16° W
Receiving	G3SET	Lincolnshire, United Kingdom	53.39° N, 0.57° W
	G3WKL	Buckinghamshire, United Kingdom	52.10° N, 0.71° W
	G4ZFQ	Isle of Wight, United Kingdom	50.73° N, 1.29° W
	G8IMR	Hampshire, United Kingdom	50.91° N, 1.29° W
	GM4SLV	Shetland Isles, United Kingdom	60.29° N, 1.43° W

TABLE 2. THE GEOGRAPHIC GREAT-CIRCLE RANGE (BEARING) FROM THE BEACON TRANSMITTERS TO THE RECEIVING STATIONS [60].

Station	G3SET	G3WKL	G4ZFQ	G8IMR	GM4SLV
GB3RAL	210 km (14°)	70 km (33°)	92 km (181°)	74 km (180°)	968 km (0°)
GB3WES	189 km (133°)	302 km (154°)	435 km (168°)	418 km (167°)	639 km (6°)
GB3ORK	646 km (164°)	785 km (167°)	929 km (172°)	911 km (171°)	170 km (34°)

antennas were modeled using Numerical Electromagnetics Code-2 antenna simulation software with appropriate ground electrical characteristics as input [11]. Simulated dipole gains were consistent with previously published measurements of field-deployed antennas [12]. Similarly, simulated loop-antenna gains agreed well with expectations for electrically small loops (e.g., [13]). The effective isotropic radiated power was ~8–23 W depending on the simulated transmitting-antenna gain and the assumed conducted power level [60].

MAXIMUM FREQUENCY SUPPORTED BY THE IONOSPHERE FOR NVIS PROPAGATION

TRADITIONAL NVIS MAXIMUM FREQUENCY DOCTRINE

Literature describing the practical use of NVIS-propagation techniques emphasizes that the maximum frequency supported by the ionosphere at vertical incidence is *foF2* (e.g., [1], [5], and [15]). Frequently, *foF2* is defined as the critical frequency of the ionosphere—as if there were only a single critical frequency—and that the optimum working frequency (OWF) is approximately 0.85 times *foF2*. This doctrine encourages operation at low frequencies, which can lead to spectrum congestion, particularly during sunspot minima when maximum operating frequencies are low in the first place.

This section shows that these traditional NVIS-frequency guidelines are incorrect and oversimplified by considering established ionospheric physics and the underlying theory associated with HF-propagation prediction software. Additionally, signal-to-noise ratio (SNR) measurements from the 5-MHz beacon network are used in support of the already established theory [16]. Finally, I present a reason behind the incorrect use of *foF2* as the maximum NVIS frequency.

THE IONOSPHERE, MAGNETOIONIC THEORY, AND CRITICAL FREQUENCIES

The ionosphere is a weakly ionized plasma formed in the earth's atmosphere through ionizing radiation—extreme ultraviolet and X-ray radiation—emitted by the sun. The chemical and physical processes associated with the ionosphere, and magnetoionic theory in general, are described in [17]–[19].

Two equations describe radio-wave propagation through the ionosphere: the Appleton equation and the magnetoionic polarization equation [17]. To paraphrase Hunsucker and Hargreaves [20], "it is virtually impossible for an ordinary mortal to make much sense" of these equations "in their full glory." Indeed, it could be argued that the HF user does not need to. However, some knowledge of the salient points could aid in the understanding of NVIS propagation at HF. Of most relevance to this discussion, the equations indicate that two characteristic waves propagate through the ionosphere: the ordinary wave (*O*-wave) and the extraordinary wave (*X*-wave).

These two waves follow different paths through the ionosphere, have orthogonal polarization, and experience different absorption. Additionally, the maximum frequency supported by the ionosphere—termed the *critical frequency*—differs for each characteristic wave, and each region within the ionosphere has critical frequencies associated with it. For example, the F2 region critical frequencies are *foF2* and *fxF2* for the *O*- and *X*-waves, respectively.

The value of *foF2* is directly related to the peak electron density of the F2 region, whereas *fxF2* is also influenced by the earth's magnetic field. The *O*- and *X*-wave critical frequencies for the F2 region are related through [17]

$$foF2^2 = fxF2^2 - fxF2\,f_H, \tag{1}$$

where f_H is the electron gyrofrequency, which depends on the earth's magnetic field strength, also varying with location. If both *foF2* and *fxF2* are much larger than f_H, then (1) reduces to the following approximation [17]:

$$fxF2 - foF2 \approx \frac{f_H}{2}. \tag{2}$$

IONOSONDES AND IONOGRAMS

An ionosonde measures the virtual reflection height of the ionosphere versus frequency. Figure 1 shows an ionogram taken at Chilton, United Kingdom (51.6° N, 1.3° W), using a Digisonde DPS-1 (Lowell Digisonde International, Lowell, Massachusetts) [21]. The red line represents the *O*-wave response, whereas the green line is that for the *X*-wave. The vertical asymptotes relate to their respective critical frequencies.

A model of the bottom-side ionosphere can be obtained through the analysis of the ionogram, usually obtained automatically. Digisonde uses automatic real-time ionogram scaler with true height (ARTIST) software with key parameters tabulated on the left of the ionogram [22]. It has been assumed that ARTIST interpretation errors occur infrequently, although it is noted an expert system for validating ionograms failed about one-third of the time [53]. ARTIST outputs *foF2* but not *fxF2*. A related parameter is *fxI*, which is the maximum recorded F region frequency and provides a measure of the degree of spread F associated with the overhead ionosphere [23]. Spread F is typically a low- or high-latitude phenomenon that gives rise to range or frequency

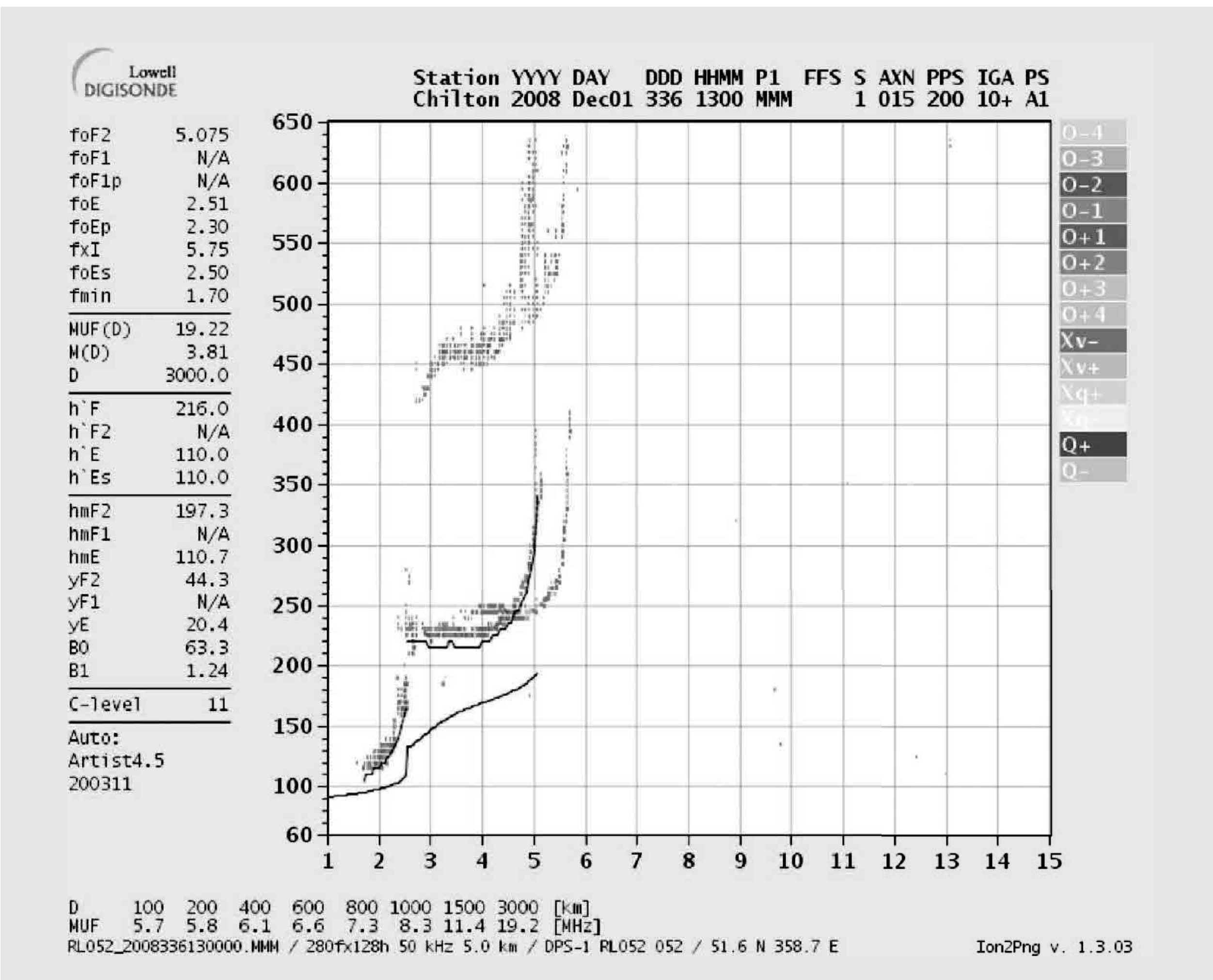

FIGURE 1. A Chilton ionogram at 1300 coordinated universal time (UTC) on 1 December 2008 [16].

spread on an ionogram [17]. When spread F is uncommon, the median fxI is equal to the median $fxF2$ [24]. On this assumption, fxI has been used in lieu of $fxF2$ for ionosonde data analysis in this article.

AMBIGUITY REGARDING THE MAXIMUM USABLE FREQUENCY

At first glance, it would appear that the term *maximum usable frequency* (*MUF*) is easily understood. However, its meaning is very much context dependent with regard to HF ionospheric propagation, which can lead to misinterpretation and misunderstanding. In one case, the MUF is the instantaneous value observed or measured for a given link at a given time and date. In the other, it refers to the monthly median value that is observed or measured. An alternative term for the instantaneous MUF, which I prefer, is the maximum observed frequency (MOF) [25].

The ionogram in Figure 1 also shows predicted MUF values for different length links (distances in kilometers) with Chilton as the midpoint of the link. These are instantaneous MUF, or MOF, values based on a single ionosonde measurement at a given time and date. Of relevance to this discussion is the predicted MUF (5.7 MHz) for a 100-km link (i.e., an NVIS link), which is comparable to the measured fxI (5.75 MHz). In other words, the ionosonde-measured fxI, a proxy for the X-wave critical frequency, is an indication of the instantaneous MUF/MOF for an NVIS link. By contrast, HF-propagation prediction routines attempt to predict the monthly median MOF, among other parameters.

PREDICTIONS OF THE MUF

During World War II, the use of HF for short- and medium-range operational purposes intensified, leading to the development of HF prediction methods within a number of organizations, including the Service de Prévision Ionosphérique Militaire in France, the Central Radio Propagation Laboratory of the National Bureau of Standards in the United States, and the Interservices Ionospheric Bureau in the United Kingdom. These methods considered the X-wave contribution to the MUF [26], [27].

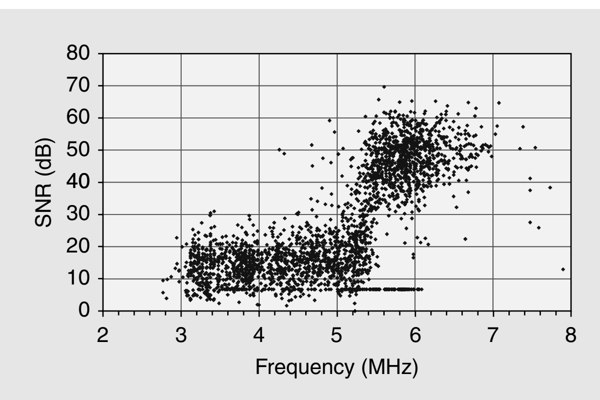

FIGURE 2. A measured GB3RAL SNR at G3WKL against Chilton $fxI\sec(\varphi)$ in September 2007 [16].

Over time, HF prediction methods became automated, which enabled the selection of optimum operating frequencies without the use of complicated charts and nomograms. Unfortunately, the automation of these prediction methods has hidden the role of the X-wave in MUF predictions from the HF user. Examples of modern HF prediction software include the Advanced Stand Alone Prediction System (ASAPS) [28], the Voice of America Coverage Analysis Program (VOACAP) [25], [29], and the software program associated with International Telecommunication Union Radiocommunication Sector (ITU-R) Recommendation P.533 (ITURHFPROP) [30], all of which can calculate the expected MUF—in this case, the monthly median MOF—for a given link at a given time.

For zero ground distance (i.e., vertical incidence), ASAPS, ITURHFPROP, and VOACAP revert to the same equation to calculate the F2 region MUF,

$$\mathrm{MUF} = foF2 + \tfrac{f_H}{2}, \tag{3}$$

which is, in effect, the approximation for the X-wave critical frequency in (2). The draft *IONCAP Theory Manual* [31] and ITU-R Recommendation P.533 [30] provide more detailed equations for calculating the F2 region MUF for nonzero ground distances that are used in VOACAP and ITURHFPROP (and, effectively, ASAPS).

SNR MEASUREMENTS USING THE 5-MHz BEACON NETWORK

Comparisons of signal strength and/or SNR measurements from the 5-MHz beacon network with ionosonde measurements clearly show agreement with (3) and that the O-wave critical frequency $foF2$ is not the maximum frequency supported by the ionosphere for NVIS links [16]. The latter fact is evident in Figure 2, which shows the peak signal-to-average-noise ratio for GB3RAL measured at G3WKL against the Chilton $fxI\sec(\varphi)$ in September 2007. In this case, fxI has been modified by the secant law because the ionosphere supports higher frequencies for waves at oblique incidence [17]. Although application of the secant law to the ionosonde $foF2$ and fxI measurements is technically correct, it is not entirely necessary for short NVIS links because $\sec(\varphi) \approx 1$ for short ground ranges and reflection from the F2 region.

A near-step increase in SNR occurs only when $fxI\sec(\varphi)$ exceeds the beacon operating frequency of 5.290 MHz, which is consistent with (3) and emphasizes the importance of the X-wave in NVIS propagation. By contrast, plotting the same beacon data against $foF2\sec(\varphi)$ (not shown here) would show a near-step increase in SNR at ~4.60 MHz, which contradicts traditional NVIS-frequency guidelines.

HAPPY HOUR

Recently, Dutch researchers have coined the term *Happy Hour* as the period of time when the ionospheric-propagation path is open with only the X-wave propagating [32]. The Happy Hour duration depends on the rate of change of electron density within the ionosphere, which is determined by the season and state of the sunspot cycle. For example, the Happy Hour might be only ~30 min during the winter, whereas it could be a few hours during the summer.

Figure 3 compares the Chilton *foF2* and *fxI* with the sound-card signal level for the GB3RAL beacon received at G4ZFQ in February 2010. The data points represent instantaneous measurements, and the solid lines represent the monthly median of the respective measurements. At ~0730 UTC, the monthly median signal level rises sharply as the monthly median *fxI* exceeds the beacon operating frequency, whereas it is another 30 min before the monthly median *foF2* exceeds the beacon frequency at ~0800 UTC.

During sunspot minima, when electron densities and, therefore, maximum frequencies supported by the ionosphere are low, it is possible that only the *X*-wave is supported at the operating frequency. For example, Figure 4 compares the Chilton *foF2* and *fxI* with the sound-card signal level for the GB3RAL beacon received at G3WKL in January 2009, and, for the majority of this month, the ionosphere supported only the *X*-wave at 5.290 MHz. In this example, the median duration of the Happy Hour is approximately 5.5 h. Again, these data illustrate the relevance of the *X*-wave for NVIS propagation.

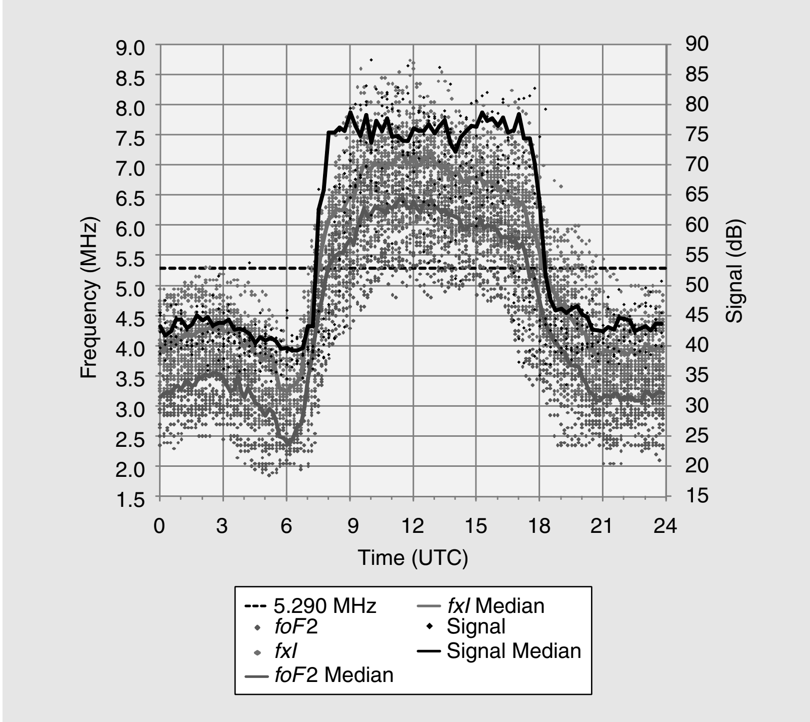

FIGURE 3. A comparison of Chilton *foF2* and *fxI* and the measured sound-card signal level for GB3RAL received at G4ZFQ in February 2010.

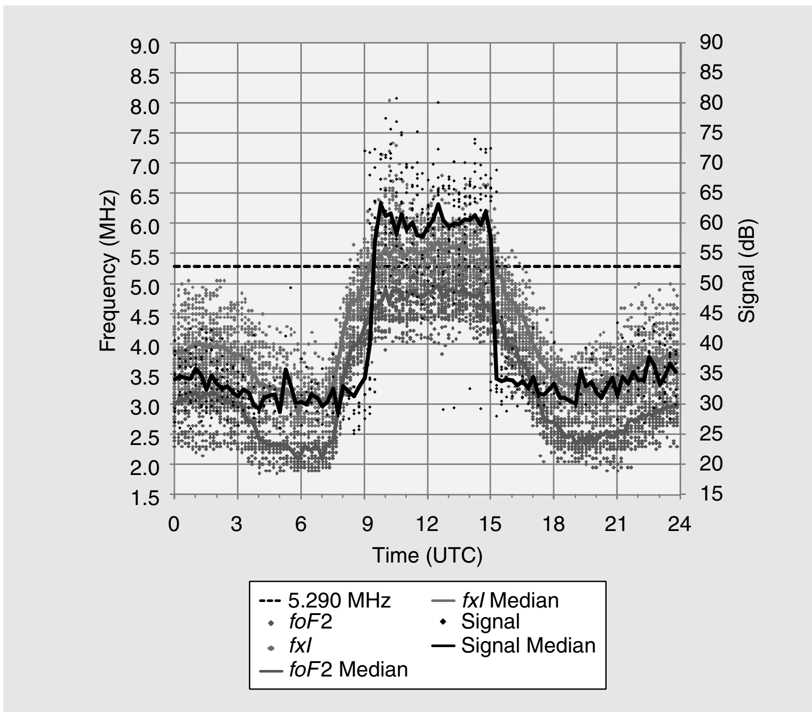

FIGURE 4. A comparison of Chilton *foF2* and *fxI* and the measured sound-card signal level for GB3RAL received at G3WKL in January 2009.

COMPLICATIONS ASSOCIATED WITH THE IONOSPHERE

IONOSPHERIC VARIABILITY

Median curves derived from measurements over a long period of time (e.g., one month) typically show smooth characteristics that mask any short-term variability. Median measurements show good long-term correlation with the smoothed sunspot number (SSN)—a useful and convenient solar index derived from monthly observed sunspot numbers averaged over a 12-month period—but the short-term correlation is poor because solar flux characteristics exhibit chaotic behavior [33]. The National Oceanic and Atmospheric Administration provides seven-day plots of *foF2*, in which general trends are obvious [34]. Typical Chilton measurements would show *foF2* as greatest around midday and lowest in the night during winter months, but there would also be an indication of the critical frequency variability that can arise over relatively short time periods (e.g., frequency changes of a few hundred kilohertz in <1 h).

ABSORPTION

Collisions among electrons, neutral molecules, and ionized particles within the ionosphere result in absorption of radio-wave energy. Ionospheric absorption can be defined as nondeviative and deviative. For nondeviative absorption, the *X*-wave experiences greater absorption than the *O*-wave, particularly at frequencies approaching the electron gyrofrequency [17]. This effect can be observed on daytime ionograms, where *X*-wave returns lower than ~4 MHz are not present owing to substantial D-region absorption (for example, see Figure 1). Deviative absorption occurs when the operating frequency at vertical incidence is close to the critical frequency, and its effect is shown in Figure 2 as a ramp-up in SNR rather than a step change once $fxI\sec(\varphi)$ exceeds the beacon transmit frequency. At lower frequencies, excessive absorption renders the *X*-wave ineffective, whereas absorption of the two waves is comparable above ~5–8 MHz [35].

The guideline that *foF2* is the maximum vertical-incidence frequency is location specific.

POLARIZATION

Wave polarization depends on geomagnetic latitudes and angles of incidence. A wave entering the ionosphere separates into the two characteristic waves. The region at the bottom of the ionosphere is the limiting region because the polarization of a downcoming wave no longer varies with height once it passes below, and the polarization acquired here is the limiting polarization [36]. Polarization is circular at a magnetic dip pole (i.e., ±90°), whereas the two characteristic waves are linearly polarized at the magnetic dip equator. In the latter case, an antenna aligned north–south excites only an *O*-wave, whereas it excites only the *X*-wave when aligned east–west [17]. At midlatitude locations, these waves are elliptically polarized with opposite senses of rotation; polarization becomes highly elliptical at medium frequencies, whereas it tends to circular polarization at higher frequencies [37].

The sense of rotation for circular polarization is described as either left- or right-hand circular polarization. Unfortunately, two definitions for the sense of rotation exist: a classical optics definition and the IEEE definition [38]. Budden [39] emphasized that care is required when interpreting work by other authors on wave polarization through the ionosphere.

Some classic ionospheric texts (e.g., [17] and [18]) describe the sense of rotation relative to the direction of the magnetic field, presumably to avoid any confusion about the polarization. Davies [17] provides a useful rule for remembering the sense of rotation: "When the thumb points in the direction of the magnetic field B_0, the rotation of the extraordinary-wave vectors is given by the fingers of the right hand; the rotation of the ordinary-wave vectors is given by the fingers of the left hand." It is evident that the polarization of the upward wave is opposite that of the downward wave at vertical incidence. Although not commonly described in HF literature, Witvliet [40] refers to this fact.

For a linearly polarized upward wave at vertical incidence at midlatitudes, the power is divided approximately evenly between each characteristic wave. At frequencies where absorption is similar for the *O*- and *X*-waves, received power levels will be comparable, which can result in polarization fading if these two waves recombine in the limiting region to form a linearly polarized wave. The resultant electric field rotates over time in a manner related to the total electron content of the path through the ionosphere. This effect is known as a *Faraday rotation* [17].

RADIO NOISE

External noise sources—atmospheric, galactic, and man-made—tend to limit HF-receiver sensitivity. Owing to the simultaneous presence of multiple strong signals, HF receivers do not, as a rule, have low noise figures but instead require good strong-signal-handling capabilities [41].

Generally, noise levels decrease as the operating frequency increases [42]. The existing frequency-of-optimum-traffic (FOT) guideline encourages operation at lower frequencies where noise levels might be higher. Operation at higher frequencies might yield an improved SNR, although the path loss is less at lower frequencies, which would offset the increased noise to some extent.

CONUNDRUM REGARDING EMPHASIS ON foF2

These results raise the question as to why traditional NVIS literature has placed the emphasis on the *O*-wave critical frequency *foF*2 as being the highest frequency supported by the ionosphere. An explanation is offered that, to the best of my knowledge, has not previously been presented.

Substantial work relating to NVIS propagation—specifically, quasi-transverse propagation—was carried out by U.S. researchers during the Vietnam War in the 1960s and 1970s (e.g., [43]–[45]). This part of Southeast Asia is very close to the magnetic dip equator, where the limiting polarization of the characteristic waves at vertical incidence is linear and where there would be a risk of polarization mismatch if linearly polarized NVIS antennas were oriented orthogonal to each other. Nacaskul [45] showed that excitation of the *O*-wave (i.e., north–south alignment) generally produced stronger signals than when the *X*-wave was excited (i.e., east–west alignment), which led to the primary recommendation that antennas should be aligned north–south. In the event that the *O*-wave is not supported on a particular frequency, then east–west alignment should be tried if diversity systems are available.

I believe that it is highly unlikely—not to mention impractical—that soldiers under difficult wartime conditions would experiment with antenna orientation. The simplest and lowest-risk approach would be to orientate antennas north–south for *O*-wave excitation alone. Consequently, the *O*-wave critical frequency *foF*2 would be the maximum frequency supported by the ionosphere under this antenna configuration. The guideline that *foF2* is the maximum vertical-incidence frequency is location specific. However, over time, this guideline has been applied in a global context, and its technical origins appear to have been forgotten.

To identify the MOF (or at least refine the MOF estimate), some form of real-time channel evaluation is required.

MAXIMUM NVIS-OPERATING-FREQUENCY GUIDELINES

A MOF-seeking approach should be adopted when selecting NVIS operating frequencies to maximize the received SNR with the additional benefit of reducing congestion at lower frequencies [5]. To identify the MOF (or at least refine the MOF estimate), some form of real-time channel evaluation is required. Ionosondes could be used for NVIS links, but automatic link establishment (ALE) systems, in which a bank of channels is sounded to identify the channel with the best link quality, have become the norm [46]. ALE systems have evolved over recent years to a third generation capable of supporting wide-band-HF-modulation schemes [47]. Lane [48] provided guidelines for selecting the range of suitable ALE frequencies based on HF-propagation prediction tools.

Owing to ionospheric variability as well as increased deviative absorption, it would be prudent not to operate too closely to the NVIS MOF in case of a rapid loss of signal. Additionally, wave polarization (which is frequency and location dependent) and antenna orientation need to be considered. Ultimately, the amount of frequency margin required will depend on consideration of these different parameters, how critical a given link is, and for how long a link outage could be tolerated before the link is reestablished.

COMPARISON OF IONOSONDE VERTICAL-INCIDENCE MEASUREMENTS WITH HF-PROPAGATION PREDICTIONS

BACKGROUND

In the design of an NVIS system, the selection of a good operating frequency is important. If the operating frequency is too high, then the radio waves simply penetrate the ionosphere, whereas if it is too low, absorption might be excessive. HF-prediction software facilitates the choice of frequencies. This section compares Chilton ionosonde frequency measurements with ASAPS and VOACAP frequency predictions [49], [54].

FREQUENCY DEFINITIONS RELATING TO MONTHLY MEDIAN VALUES

HF-propagation prediction software such as ASAPS and VOACAP attempt to predict the statistical spread of usable frequencies for a given link over a set time period (usually one month). ITU-R Recommendation P.373 provides definitions of maximum and minimum transmission frequencies relevant to HF-propagation predictions, including the MUF, which is a median value (i.e., monthly median MOF) [5], [50].

The OWF and the highest probable frequency (HPF) exceed the MUF in 90% and 10% of the specified period, respectively. In this context and assuming that one month has 30 days, the OWF is expected to be supported on 27 days of a month, whereas the HPF should be available on three days of the month. Consequently and potentially confusing, it is possible for operation at frequencies above the MUF (ATM).

The OWF is a misleading term because there is no indication as to the performance or quality of service [51]. In other words, system performance may not be optimum at the OWF. The merit of the OWF is perhaps best understood when considering frequency allocations from a licensing perspective. If only one frequency were to be made available and there was an expectation that the frequency must be supported on most days of the month (e.g., 90% of days), then the OWF would be the frequency of choice.

HF PREDICTIONS AND CHILTON IONOSONDE MEASUREMENTS

The ASAPS and VOACAP vertical-incidence-frequency predictions were compared with Chilton ionosonde measurements from 1996 to 2010 [49]. VOACAP method 9 predicts the MUF, HPF, and FOT (equivalent to the OWF) and uses the SSN as the solar index to drive predictions [25]. ASAPS predicts the MUF, OWF, and upper decile (UD; equivalent to the HPF) and uses the T index (an effective sunspot number based on global ionosonde *foF2* measurements) to drive its frequency predictions. [52]. The HF MUF predictions were compared with the monthly median *foF2* and *fxI* on a month-by-month basis. Likewise, the predicted OWF/FOT and UD/HPF were compared with the measured lower-decile (LD) and UD frequencies respectively.

COMPARISON RESULTS

ASAPS tended to predict the *X*-wave critical frequency, thereby showing consistency with (3), whereas VOACAP was more conservative in its prediction of the MUF (i.e., VOACAP predicted lower frequencies). The average differences between the measured and predicted MUF from 1996 to 2010 inclusive are presented in Table 3.

Both ASAPS and VOACAP (the latter more so) were conservative in their predictions of the LD frequencies. For the UD frequencies, ASAPS again showed consistency with (3), whereas VOACAP was again conservative in its frequency prediction.

ALE-frequency–planning guidelines recommend the use of frequencies from just below the lowest FOT/OWF up to the highest HPF/UD [48]. From this analysis, ASAPS appears to be a better choice than VOACAP for preparing ALE-frequency scan lists for U.K. NVIS links.

Statistics summarized in a single table fail to describe multiple facets observed over a complete solar cycle. For example, both the ASAPS- and VOACAP-predicted MUF tended toward *foF*2 lower than ~4 MHz during winter months, particularly around the sunspot minimum. These discrepancies could be due to Chilton autoscaled *foF*2 values exhibiting positive errors at low frequencies [54], [55]. Spread F might also contribute to the observed inconsistency with (3). Although spread F is typically a low- and high-latitude phenomenon, high-latitude spread F begins at ~40° geomagnetic latitude. Furthermore, high-latitude spread F occurs mostly during the night [37]. Nighttime vertical-incidence frequencies during the winter tend to be low (i.e., <4 MHz). A recent study presents the statistics of nighttime spread F observed at a midlatitude location over a full solar cycle [56].

From 1996 to 2010, ASAPS MUF predictions were within ~10% of *fxF*2, except at low or negative values of the T index. VOACAP was relatively consistent, albeit conservative, in its prediction of the MUF, except for high SSNs (i.e., more than ~100). VOACAP is likely to be inaccurate or overly pessimistic for MUF predictions on U.K. NVIS links when the difference between the T index and SSN (i.e., T – SSN) exceeds ~15, as illustrated in Figure 5.

Although the SSN can be useful for long-term forecasting of HF propagation, the sun's chaotic behavior makes short-term forecasting more difficult using daily sunspot numbers.

Although the SSN can be useful for long-term forecasting of HF propagation, the sun's chaotic behavior makes short-term forecasting more difficult using daily sunspot numbers. Predictions using ersatz indices (e.g., T index) are known to outperform predictions using direct indices such as the SSN. Furthermore, the sunspot number is only a circumstantial index with regard to predicting ionospheric propagation [5]. Goodman [33] suggested that taking a five-day average of effective sunspot numbers strikes a good balance.

TABLE 3. THE AVERAGE DIFFERENCES BETWEEN THE MEDIAN CHILTON MEASUREMENTS AND PREDICTIONS (1996–2010) [49].

Measurement (50%)	Prediction	Mean (MHz)	Standard Deviation (MHz)
fxI	ASAPS MUF	0.09	0.25
foF2		−0.65	0.25
fxI	VOACAP MUF	0.48	0.31
foF2		−0.25	0.30

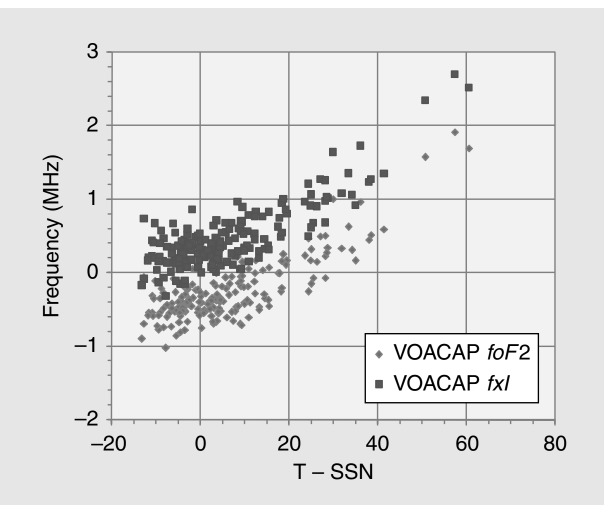

FIGURE 5. The monthly mean difference between Chilton measurements and the VOACAP MUF against T – SSN [49].

COMPARISON OF 5-MHz BEACON MEASUREMENTS WITH HF-PROPAGATION PREDICTIONS

OVERVIEW

Some limited work has compared SNR measurements with VOACAP predictions for NVIS links [57]. Another study compared median signal-power measurements, including a 490-km NVIS link, with ASAPS and VOACAP predictions over a ten-month period [58].

Since its inception, a large database of automatic beacon measurements has resulted from the 5 MHz Experiment. The early analysis of beacon data indicated that high-reliability (i.e., >90%) NVIS links could be achieved using narrow-band modes (e.g., below ~500 Hz) at typical man-pack power levels (e.g., 10–20 W) when received in low-noise environments [14]. It was also found that SNR measurements could be strongly affected by cochannel interference, even over one month. For example, SNR measurements for the GB3ORK-GM4SLV link in November 2009 showed a notch in the SNR between ~1200 and 1300 UTC, which was probably caused by regular cochannel interference. For this reason, signal-power levels were analyzed instead of the SNR. This section compares the measured signal-power levels against those predicted by ASAPS and VOACAP for nine NVIS links over a 23-month period from May 2009 to March 2011 during the last sunspot minimum [59], [60].

PREDICTIONS OF MEDIAN SIGNAL-POWER LEVELS

VOACAP predictions used method 20 (complete system performance) with Consultative Committee on International Radio coefficients and the SSN as input. The VOACAP sporadic E model was not enabled [25]. The ASAPS T index was negative for some months, meaning that the observed ionospheric conditions were worse than expected for the nonzero, positive SSN.

In view of the transmitting- and receiving-antenna types used, the ASAPS approximation algorithm was used to determine median signal levels [28]. The ASAPS and VOACAP hourly predictions were interpolated to 15-min intervals to coincide with the beacon transmit interval.

COMPARISON OF SIGNAL-LEVEL MEASUREMENTS AND PREDICTIONS

Figure 6 shows an example of signal measurements and the corresponding ASAPS and VOACAP median signal predictions observed for the GB3RAL-G3WKL link in March 2010. Differences tend to increase at the start and end of NVIS propagation, corresponding to a low ASAPS probability or VOACAP MUFday. Signal-level measurements show a small spread during the day. This particular example shows very good correlation between median measurements and predictions. However, some measurements for other months show less agreement. The statistics from all nine NVIS links were viewed together. If taken in isolation, measurements showing large differences from predictions could be viewed as being in error.

The root-mean-square (rms) difference between the median signal levels and predictions when VOACAP MUFday and ASAPS probability were >0.03 (i.e., ionospheric support for the primary mode is expected on at least one day in the month) appeared to show a cyclical trend, which was much more apparent when limiting the comparison to a smaller time window at approximately 1200 UTC, as shown in Figure 7 for VOACAP predictions. The rms differences were low in September, October, November, and March. By contrast, the rms differences were larger during the day in the summer months (April to August) and during the winter (December to February). ASAPS predictions showed greater rms differences than VOACAP during the summer but lower rms differences during the winter.

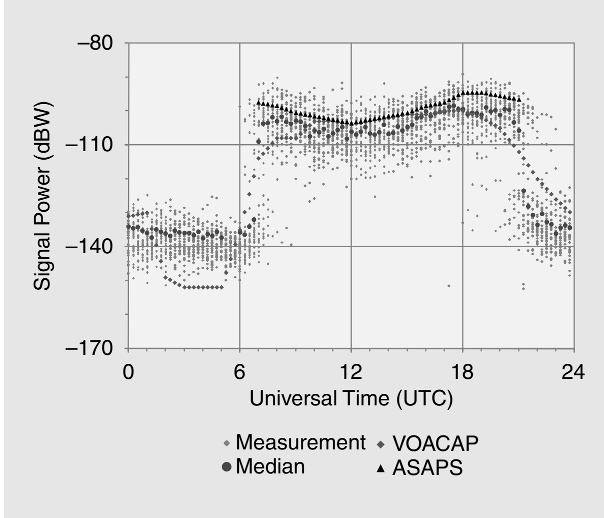

FIGURE 6. A comparison of measurements and predictions for GB3RAL received at G3WKL in March 2010 [60].

The summer differences could be related, in part, to the absorption effects (both deviative and nondeviative). The greater spread in signal levels during the summer daytime suggests the presence of multiple propagation modes, including sporadic E, which might have influenced the measurement statistics. The greater absorption observed in December, January, and February is consistent with the winter anomaly when there is anomalously high absorption.

Table 4 presents the range of mean differences and the overall rms differences. Both ASAPS and VOACAP appeared to overestimate the median signal level for the NVIS links at 5.290 MHz, based on the assumption that the prediction-input and antenna-modeling parameters were valid. On the whole, VOACAP showed slightly lower rms and mean differences between the measurements and predictions than ASAPS for

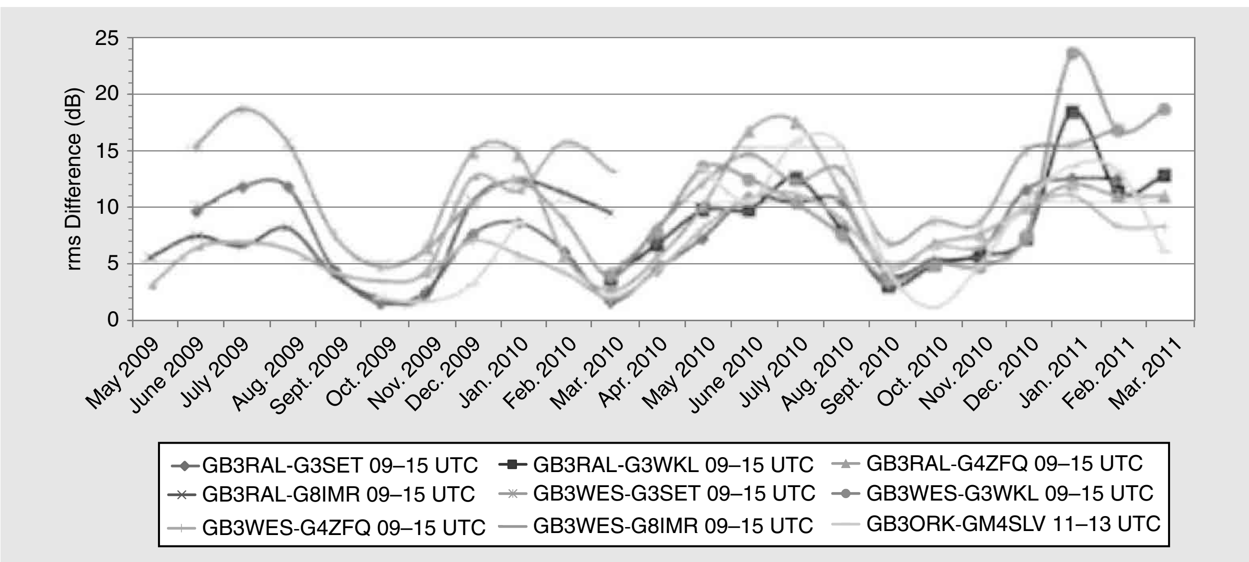

FIGURE 7. The rms difference between measurements and VOACAP predictions for a window at approximately 1200 UTC [60].

TABLE 4. THE RANGE OF MEAN DIFFERENCES BETWEEN THE MEASUREMENTS AND PREDICTIONS FOR ALL LINKS DURING THE MEASUREMENT PERIOD [60].

	VOACAP (MUFday > 0.03)	ASAPS (Probability > 0.03)	VOACAP (~1200 UTC)	ASAPS (~1200 UTC)
Mean (dB)	−4 to −12	−8 to −14	−6 to −11	−6 to −12
Overall rms (dB)	7–15	9–16	7–12	7–13

these NVIS links at 5.290 MHz over a 23-month period during the recent solar minimum.

ATM PROPAGATION

BACKGROUND

The beacon measurements frequently showed evidence of ATM propagation during the night when valid signal measurements were recorded. During this period, ASAPS probability and VOACAP MUFday predictions were zero (i.e., ionospheric support of the primary mode was not predicted). Measured critical frequencies at Chilton were below the operating frequency. The propagation mechanism was not NVIS but might have been a two-hop ground (or sea) side-scatter mode [61]. The median signal levels were generally 30–40 dB lower than the typical daytime levels. Therefore, these links might have been more effective at lower operating frequencies, where true NVIS propagation would actually have been supported by the ionosphere.

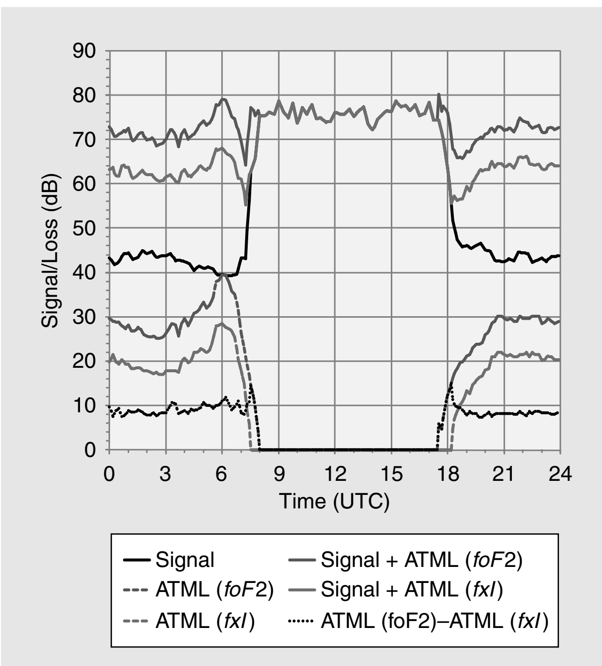

FIGURE 8. A comparison of the measured signal (black line), the predicted ATM loss (ATML; dashed red and blue lines), the measured signal adjusted for the predicted ATM loss (solid red and blue lines), and the difference between the predicted ATM losses (dotted black line) using the measured Chilton *foF2* and *fxI* for GB3RAL received at G4ZFQ in February 2010.

PREDICTION OF ATM LOSS

The ITU-R describes various propagation mechanisms that may give rise to propagation above the basic MUF (ABM) as well as a number of loss models, including the ITU-R Recommendation P.533 model [62]. Until recently, for F2 modes up to a range of 7,000 km, the ABM-loss model was given by [63]

$$L_m = 36\left[\left(\frac{f}{f_b}\right) - 1\right]^{\frac{1}{2}} \tag{4}$$

or 62 dB, whichever is smaller. The working frequency is given by f, and f_b is the basic MUF.

The latest version of ITU-R Recommendation P.533 at the time of writing this article predicts 5 dB of additional loss, although no information was provided regarding this change [30]:

$$L_m = 36\left[\left(\frac{f}{f_b}\right) - 1\right]^{\frac{1}{2}} + 5. \tag{5}$$

The purpose of predicting the ATM/ABM losses is less useful for SNR and reliability predictions on wanted links. Instead, the primary interest is for the prediction of interfering signal levels [64].

VOACAP incorporates an ATM-loss model, although the maximum ATM-loss limit is only 25 dB, which may be too low [65]. Related to this ATM-loss limit, it was found that VOACAP reliability predictions can be in error for short-range links at substantially ATM frequencies. Under these circumstances, users should carry out their own validation of the prediction data [66].

COMPARISON OF MEASURED BEACON-SIGNAL LEVELS AND PREDICTED ATM LOSS USING IONOSONDE FREQUENCY MEASUREMENTS

The ITU-R ABM loss was calculated using (4) with the Chilton median *foF2* and *fxI*—*fxI*, in lieu of *fxF2*—as the basic MUF values. The median beacon-signal level against time was then adjusted by the predicted ABM loss.

Figure 8 shows the median signal level for the GB3RAL beacon received at G4ZFQ (solid black line) as well the predicted ABM loss using the median *foF2* and *fxI* in February 2010. The ABM loss using *foF2* (dashed red line) was evidently greater than that using *fxI* (dashed blue line), which is to be expected considering (1) and (2). Modifying the beacon-signal level by the predicted ABM losses resulted in the solid red and blue lines using the *foF2* and *fxI* measurements, respectively, as the basic MUF in (4).

The solid red line in Figure 8 uses the median *foF2* value to predict the ABM loss. When ATM propagation occurs, the

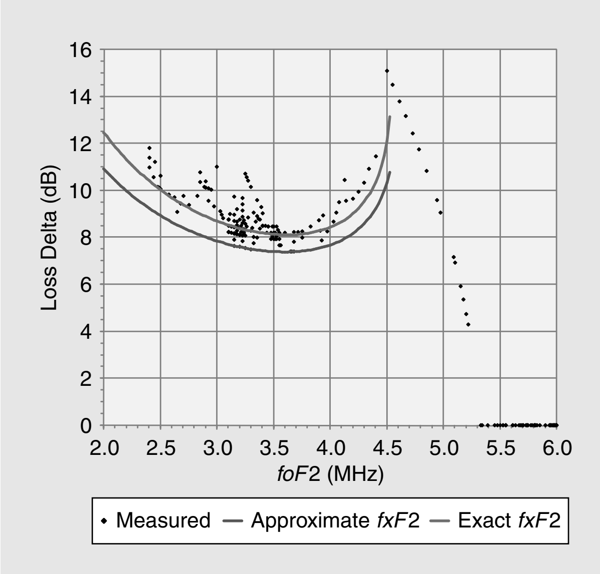

FIGURE 9. A comparison of the difference between the ATM losses calculated using Chilton *foF2* and *fxI* and the expected differences when using the approximate and exact expressions for *X*-wave critical frequency *fxF2* against Chilton *foF2* in February 2010.

adjusted beacon-signal level is comparable to the unadjusted signal level during the day (~0800–1700 UTC). Inspection of Figure 8 suggests that use of (5) might provide better agreement than (4). The dotted black line shows the difference between the predicted ABM losses using *foF2* and *fxI*. The latter data are plotted against the Chilton *foF2* in Figure 9. Also shown are the expected differences using the exact (blue line) and approximate (red line) expressions as given by (1) and (2), respectively. There is good agreement when the exact relationship given by (1) is used.

This analysis indicates that there is an inconsistency with the current ITU-R Recommendation P.533 with regard to the basic MUF term. The calculation of the basic MUF tends to the *X*-wave critical frequency *fxF2* for zero ground distance (i.e., NVIS links). However, the ABM-loss model appears to agree well with measurements when the *O*-wave critical frequency *foF2* is used as the basic MUF. Using *fxF2* (or *fxI*) as the basic MUF in (4) or (5) underpredicts the ATM/ABM loss by ~8–14 dB. This difference may be relevant for predictions of interference from nearby transmitters.

SUMMARY

This article presented numerous findings obtained through the analysis of beacon-signal-power measurements from the 5 MHz Experiment. These important findings relate to

1) maximum NVIS-operating-frequency definitions
2) U.K. NVIS-frequency predictions
3) U.K. NVIS-signal-power predictions
4) ITU-R above-the-loss models.

The findings are of practical relevance to professional and amateur users of NVIS-communications techniques.

ACKNOWLEDGMENTS

Numerous people have made substantial contributions to the 5 MHz Experiment, without which I would not have been able to carry out any data analysis. Those involved include Peter Martinez (G3PLX), Andrew Talbot (G4JNT/G8IMR), Michael Willis (G0MJW), John Linford (G3WGV), John Grieve (GM0HTH), David Aram (G3SET), John Gould (G3WKL), Alan Reeves (G4ZFQ), and John Pumford-Green (GM4SLV). The Radio Society of Great Britain coordinated the experimentation at 5 MHz and hosted the 5-MHz database. The U.K. Ministry of Defence and Ofcom allowed radio amateurs access to specific channels at 5 MHz.

AUTHOR INFORMATION

Marcus C. Walden (marcus.walden@plextek.com) received his B.Eng. (Hons) degree in electronic and electrical engineering in 1990 and his Ph.D. degree in microwave engineering in 1994 from the University of Leeds, United Kingdom. From 1995 to 1997, he was a radar engineer with the British Antarctic Survey, developing an airborne, very high-frequency (HF) radar system for measuring ice depth in the Antarctic. He is currently the technical lead of antennas and propagation with Plextek, Great Chesterford, United Kingdom. His research interests include antennas and propagation from HF to millimeter-wave frequencies. He is a Senior Member of the IEEE.

REFERENCES

[1] D. M. Fiedler and E. J. Farmer, *Near-Vertical Incidence Skywave Communications: Theory, Techniques and Validation*. Sacramento, CA: Worldradio Books, 1996.

[2] United States Army. Military Auxiliary Radio System. [Online]. Available: http://www.usarmymars.org/

[3] American Radio Relay League. Amateur Radio Emergency Service. [Online]. Available: http://www.arrl.org/ares

[4] Radio Amateurs' Emergency Network. [Online]. Available: http://www.raynet-uk.net/

[5] J. M. Goodman, *HF Communications: Science and Technology*. New York: Reinhold, 1992.

[6] L. F. McNamara, *The Ionosphere, Communications, Surveillance, and Direction Finding*. Melbourne, FL: Krieger, 1991.

[7] X. Huang and B. W. Reinisch, "Real-time HF ray tracing through a tilted ionosphere," *Radio Sci.*, vol. 41, no. 5, p. RS003378, Oct. 2006.

[8] International Amateur Radio Union (2015). Amateur radio: The greatest of all scientific hobbies. [Online]. Available: http://www.iaru-r1.org/index.php/3-news/newsflash/1492-new-band-at-5-mhz

[9] A. Talbot, "Design and construction of the 5 MHz beacons GB3RAL, GB3WES and GB3ORK—Part one," *RadCom*, vol. 81, no. 6, pp. 85–87, June 2005.

[10] A. Talbot, "Design and construction of the 5 MHz beacons GB3RAL, GB3WES and GB3ORK—Part two," *RadCom*, vol. 81, no. 7, pp. 88–89, July 2005.

[11] G. J. Burke and A. J. Poggio, "Numerical Electromagnetics Code (NEC)—Method of moments," Lawrence Livermore National Laboratory, Livermore, CA, Rep. UCID-18834, Jan. 1981.

[12] G. H. Hagn, "On the relative response and absolute gain toward the zenith of HF field-expedient antennas—Measured with an ionospheric sounder," *IEEE Trans. Antennas Propag.*, vol. 21, no. 4, pp. 571–574, July 1973.

[13] B. A. Austin, A. Boswell, and M. A. Perks, "Loss mechanisms in the electrically small loop antenna," *IEEE Antennas Propag. Mag.*, vol. 56, no. 4, pp. 142–147, Aug. 2014.

[14] M. C. Walden, "A comparison of measurements and propagation simulations for mid-latitude HF NVIS links at 5 MHz during sunspot minima," in *Proc. 9th Nordic HF Conf. HF 10*, Fårö, Sweden, 2010.

[15] N. Maslin, *HF Communications: A System Approach*. London: Sir Isaac Pitman, 1987.

[16] M. C. Walden, "The extraordinary wave mode: Neglected in current practical literature for HF NVIS communications," in *Proc. Inst. Engineering and Technology 11th Int. Conf. Ionospheric Radio Systems and Techniques*, Edinburgh, U.K., 2009, pp. 27–31.
[17] K. Davies, *Ionospheric Radio*. Stevenage, U.K.: Peregrinus, 1990.
[18] J. K. Hargreaves, *The Solar-Terrestrial Environment*. Cambridge, U.K.: Cambridge Univ. Press, 1995.
[19] J. A. Ratcliffe, *The Magneto-Ionic Theory and Its Applications to the Ionosphere*. Cambridge, U.K.: Cambridge Univ. Press, 1959.
[20] R. D. Hunsucker and J. K. Hargreaves, *The High-Latitude Ionosphere and Its Effects on Radio Propagation*. Cambridge, U.K.: Cambridge Univ. Press, 2002.
[21] Lowell Digisonde International. [Online]. Available: http://www.digisonde.com/index.html
[22] I. A. Galkin and B. W. Reinisch. (2008, Jan. 23). The new ARTIST 5 for all digisondes. *INAG Bull.* [Online]. *(24)*. Available: http://www.sws.bom.gov.au/IPSHosted/INAG/web-69/2008/artist5-inag.pdf
[23] Ionospheric Network Advisory Group. (1969, Sept.) Ionosphere station information bulletin. *INAG Bull.* [Online]. Available: http://www.sws.bom.gov.au/IPSHosted/INAG/pdf/inag01.pdf
[24] Ionospheric Network Advisory Group. (1971, Aug.) Ionosphere station information bulletin. *INAG Bull.* [Online]. Available: http://www.sws.bom.gov.au/IPSHosted/INAG/pdf/inag08.pdf
[25] G. Lane, *Signal-to-Noise Predictions Using VOACAP—A User's Guide*. Cedar Rapids, IA: Rockwell-Collins, 2001.
[26] K. Rawer, *The Ionosphere: Its Significance for Geophysics and Radio Communications*. New York: F. Ungar, 1956.
[27] K. W. Tremellen and J. W. Cox. "The influence of wave propagation on the planning of short-wave communication," *J. Inst. Electr. Eng.*, vol. 94, no. 11, pp. 200–219, Mar.–Apr. 1947.
[28] IPS Radio and Space Services. (2009). *ASAPS for Windows V5.3 tutorial*. [Online]. Available: http://www.sws.bom.gov.au/Category/Products%20and%20Services/Software/ASAPS/ASAPSVer5.3.pdf
[29] International Telecommunication Union. (2014). ITURHFPROP: A software method for the prediction of the performance of HF circuits based on Recommendation ITU-R P.533-12. [Online]. Available: https://www.itu.int/oth/R0A0400006F/en
[30] International Telecommunication Union, "Method for the prediction of the performance of HF circuits," Geneva, Switzerland, Recommendation ITU-R P.533-13, July 2015.
[31] J. L. Lloyd, G. W. Haydon, D. L. Lucas, and L. R. Teters. "Estimating the performance of telecommunication systems using the ionospheric transmission channel. Volume I: Techniques for analyzing ionospheric effects upon HF systems (draft)," U.S. Army Communications Engineering and Installation Agency, Fort Huachuca, AZ, Tech. Rep. EMEOPED-79-7, 1978.
[32] B. A. Witvliet, E. van Maanen, G. J. Petersen, A. J. Westenberg, M. J. Bentum, C. H. Slump, and R. Schiphorst, "Measuring the isolation of the circularly polarized characteristic waves in NVIS propagation," *IEEE Antennas Propag. Mag.*, vol. 57, no. 3, pp. 120–145, June 2015.
[33] J. M. Goodman, *Space Weather & Telecommunications*. New York: Springer, 2005.
[34] National Oceanic and Atmospheric Administration. (2015). [Online]. Available: http://www.ngdc.noaa.gov/stp/IONO/rt-iono/realtime/RL052_foF.png
[35] E. O. Olatunji, "Ionospheric absorption of the extraordinary wave," *Radio Sci.*, vol. 17, no. 5, pp. 1335–1342, Sept./Oct. 1982.
[36] P. A. Bradley, "Limiting polarisation of radio waves of medium and high frequency reflected from the ionosphere," *Proc. Inst. Electr. Eng.*, vol. 114, no. 12, pp. 1837–1841, Dec. 1967.
[37] K. Davies, *Ionospheric Radio Waves*. Waltham, MA: Blaisdell, 1969.
[38] J. D. Kraus, and R. J. Marhefka, *Antennas for All Applications*, 3rd Ed. New York: McGraw-Hill, 2002.
[39] K. G. Budden, *The Propagation of Radio Waves*. Cambridge, U.K.: Cambridge Univ. Press, 1985.
[40] B. A. Witvliet, "Near vertical incidence skywave: Interaction of antenna and propagation mechanism," Ph.D. dissertation, Univ. of Twente, Enschede, The Netherlands, 2015.
[41] G. K. Lott, W. R. Vincent, and S. Jauregui, "HF signal amplitude distributions and total spectrum power measurements," in *Proc. 6th Int. Conf. High Frequency Radio Systems and Techniques*, York, U.K., 1994, pp. 140–143.
[42] International Telecommunication Union, "Radio noise," Geneva, Switzerland, Recommendation ITU-R P.372-12, July 2015.
[43] G. H. Hagn and K. A. Posey, "Survey of literature pertaining to the equatorial ionosphere and tropical communication," Stanford Res. Inst., Menlo Park, CA, Special Tech. Rep. 12, Feb. 1966.
[44] G. H. Hagn, "Orientation of linearly polarized HF antennas for short-path communication via the ionosphere near the geomagnetic equator," Stanford Res. Inst., Menlo Park, CA, Research Memorandum 5 (revised), June 1964.
[45] P. Nacaskul, "Orientation measurements in Thailand with HF dipole antennas for tactical communication," Stanford Res. Inst., Menlo Park, CA, Special Tech. Rep. 31, June 1967.
[46] E. E. Johnson, S. Cook, R. I. Desourdis, G. Earle, and J. C. Ostergaard, *Advanced HF Radio Communications*. Norwood, MA: Artech House, 1997.
[47] E. E. Johnson, E. Koski, W. N. Furman, M. Jorgenson, and J. Nieto, *Third-Generation and Wideband HF Radio Communications*. Norwood, MA: Artech House, 2013.
[48] G. Lane, "Improved guidelines for automatic link establishment operations," in *Proc. Ionospheric Effects Symp. 2005*, Alexandria, VA, 2005, pp. 280–289.
[49] M. C. Walden, "Analysis of Chilton ionosonde critical frequency measurements during solar cycle 23 in the context of midlatitude HF NVIS frequency predictions," in *Proc. 12th Inst. of Engineering and Technology Int. Conf. Ionospheric Radio Systems and Techniques*, York, U.K., 2012.
[50] International Telecommunication Union, "Definitions of maximum and minimum transmission frequencies," Geneva, Switzerland, Recommendation ITU-R P.373-9, Sept. 2013.
[51] L. Barclay, "Outstanding problems for the probabilistic prediction of the performance of HF terrestrial services," in *Proc. 12th Inst. of Engineering and Technology Int. Conf. Ionospheric Radio Systems and Techniques*, York, U.K., 2012.
[52] J. A. Secan and P. J. Wilkinson, "Statistical studies of an effective sunspot number," *Radio Sci.*, vol. 32, no. 4, pp. 1717–1724, July/Aug. 1997.
[53] L. F. McNamara, "Quality figures and error bars for autoscaled digisonde vertical incidence ionograms," *Radio Sci.*, vol. 41, no. 4, p. RS4011, July 2006.
[54] M. C. Walden. Analysis of Chilton ionosonde critical frequency measurements during solar cycle 23 in the context of midlatitude HF NVIS frequency predictions (use of T-Index with VOACAP), in *Proc. High Frequency Industry Assoc. Meeting*, York, U.K., 2012. [Online]. Available: http://www.hfindustry.com/meetings_presentations/presentation_materials/2012_sept_hfia/presentations/10_Plextek_%20hfia2012_york_presentation_mcw_20120906.pdf
[55] R. A. Bamford, R. Stamper, and L. R. Cander, "A comparison between the hourly autoscaled and manually scaled characteristics from the Chilton ionosonde from 1996 to 2004," *Radio Sci.*, vol. 43, no. 1, p. RS1001, 2008.
[56] P. Bhaneja, G. D. Earle, R. L. Bishop, T. W. Bullett, J. Mabie, and R. Redmon, "A statistical study of midlatitude spread F at Wallops Island, Virginia," *J. Geophys. Res.*, vol. 114, no. A4, p. A04301, Apr. 2009.
[57] E. E. Johnson, "NVIS communications during the solar minimum," in *Proc. IEEE Military Communications Conf. 2007*, Orlando, FL, 2007.
[58] L. F. McNamara, R. J. Barton, and T. W. Bullett, "Analysis of HF signal power observations on two North American circuits," *Radio Sci.*, vol. 41, no. 5, p. RS5S38, Apr. 2006.
[59] M. C. Walden, "Comparison of propagation predictions and measurements for mid-latitude HF NVIS links at 5 MHz," in *Proc. 13th Int. Ionospheric Effects Symp.*, Alexandria, VA, 2011, pp. 304–311.
[60] M. C. Walden, "Comparison of propagation predictions and measurements for midlatitude HF near-vertical incidence sky wave links at 5 MHz," *Radio Sci.*, vol. 47, no. 4, p. RS0L09, Aug. 2012.
[61] L. F. McNamara, T. W. Bullett, E. Mishin, and Y. M. Yampolski, "Nighttime above-the-MUF HF propagation on a midlatitude circuit," *Radio Sci*., vol. 43, no. 2, p. RS2004, Mar. 2008.
[62] International Telecommunication Union, "Propagation at frequencies above the basic MUF," Geneva, Switzerland, Recommendation ITU-R P.2011-1, 1999.
[63] International Telecommunication Union, "Method for the prediction of the performance of HF circuits," Geneva, Switzerland, Recommendation ITU-R P.533-12, Sept. 2013.
[64] R. Hanbaba, "Performance prediction methods of HF radio systems," *Ann. Geofis.*, vol. 41, nos. 5–6, pp. 715–742, Nov.–Dec. 1998.
[65] G. Lane. (2016). Understanding above-the-MUF predictions. *VOACAP Quick Guide.* [Online]. Available: http://www.voacap.com/above-muf.html
[66] M. C. Walden. VOACAP reliability (REL) predictions: A sanity check for HF NVIS links, in *Proc. High Frequency Industry Assoc. Meeting*, Portsmouth, U.K., 2014. [Online]. Available: http://www.hfindustry.com/meetings_presentations/presentation_materials/2014_sept_hfia/presentations/1-VOCAP-Reliability.pdf

Scott Roleson, KC7CJ

14938 Amso Street, Poway, CA 92064; **kc7cj@arrl.net**

Experiments with a Broadband, High-Dynamic Range, Low Noise HF Receiver Preamplifier

This high-dynamic range broadband amplifier with bias stabilization should enhance the usability of an SDR or any HF receiver.

This article describes an effort to enhance an HF SDR project by adding a front-end preamplifier to help pull in weak signals. My goal was to have an amplifier that would not need continual tuning — just a simple on/off switch is enough — yet can handle strong signals that might also be within its passband. Oh yes, it should also have a low noise figure. Possibly this is a challenging goal.

Undeterred, I began searching through my stash of radio resources, including old *QST* and *Ham Radio* magazines and I searched on the web. I found ample references, including several in 1970-80s *Ham Radio* magazines by Joe Reisert (now W1JR). On a hunch, I dropped him a note, and he suggested I look at a circuit he published[1] in *Ham Radio* for November 1984 based on a design patented in 1975 by David Norton and Allen Podell[2]. Reisert wrote in the original article that this amplifier had about 9 dB of gain over 1.8 – 200 MHz, a +39 dB output intercept point, and noise figure of 2.5 – 3 dB with the 2N5109 transistor. It sounded ideal, but of course I couldn't help digging into this circuit's origins and look for opportunities to tweak the design.

Background – The Norton Lossless Feedback Amplifier

The Norton-Podell circuit uses a transformer with a single-turn primary winding in series with the input, and a tapped output winding, as shown in Figure 1. This is an RF equivalent circuit where dc biasing components are not shown. The objective of the patent was to provide gain with high dynamic range, low noise, good matching to input and output impedances, and in an economical design. Since feedback is provided by a transformer and not a resistor network, this amplifier is typically referred to as 'lossless' although in practice there is some loss in actual implementations of the transformer. Gain is a function of the transformer turns ratios. Specifically, with a single-turn primary, the according to the patent the secondary windings are related by,

$$n = m^2\left(\frac{R_S}{R_L}\right) - m - 1 \tag{1}$$

and net gain is,

$$G = m^2\left(\frac{R_S}{R_L}\right) \tag{2}$$

or, in decibels:

$$G_{dB} = 20\log\left[m^2\left(\frac{R_S}{R_L}\right)\right] \tag{3}$$

where integers n and m represent the transformer turns, and R_S and R_L are the source and load resistances, respectively. If amplifier is embedded in a system where R_S and R_L are identical (e.g., 50 Ω), then,

$$\frac{R_S}{R_L} = 1, \quad n = m^2 - m - 1,$$

and,

$$G_{dB} = 20\log(m^2)$$

Given that n and m are constrained as integers — no fractional-turn windings —

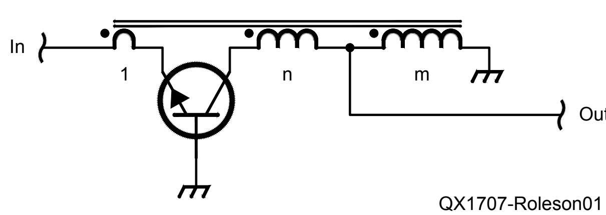

Figure 1 — Basic Norton lossless feedback amplifier (biasing not shown).

typical winding ratios and theoretical gains are shown in Table 1. One additional useful feature of this amplifier is its ability to transfer source and load impedances to the output and input impedances, respectively. From the patent, the input impedance is,

$$R_{in} = \left[\frac{m+n+1}{m^2}\right] R_L \tag{7}$$

and the output impedance is,

$$R_{out} = \frac{m^2}{m+n+1} R_s \tag{8}$$

Table 1.
Comparison between several published Norton lossless feedback amplifiers.

Wire turns 1:n:m	*Gain (dB)*
1:1:2	6.0
1:5:3	9.5
1:11:4	12.0
1:19:5	14.0

Using any of the prescribed 1:*n*:*m* wire turns ratios shown in Table 1, the term $[(m + n + 1) / m^2]$ or its inverse reduces to one. Consequently the input impedance is determined by the load, and the output impedance is determined by the source. To put it another way, everything matches up properly if you embed this amplifier in a 50 Ω system. If you were to embed it in a 75 Ω system instead, everything would still match without altering the circuit.

Table 2 compares several implementations of the original Norton lossless feedback amplifiers that I found in the literature. Curiously, most but not all reported that realized gain is 0.1 to1 dB lower than theoretical. For example, in his *Ham Radio* article Reisert reported 9 dB gain for his circuit with turns ratio 1:5:3, but Skelton[3] reported a gain of 10 dB ±1 dB from 1 to 100 MHz for a very similar circuit with the same turns ratio. This suggested to me that maybe the circuit is not entirely "lossless" and a small loss in the transformer may make the difference. For example, Reisert used relatively small FairRite 2843002402 binocular core, while Skelton's design used a much larger transformer made of four FT37-43 toroidal cores in a binocular arrangement. These two circuits also used different transistors operated at different bias points.

The prescribed turns ratios may not be "written in stone." Hicks et al.[4] described a 20 to 80 MHz radio telescope application of the Norton amplifier with a circuit very similar to that shown in the original patent, and to the one that Reisert used, except Hicks wrote that their transformer had a 1:*n*:*m* turns ratio of 1:4:3. Their application envisioned producing a large number of these amplifiers as modules, and their paper described what appears to be a custom modification of the Tele-Tech TX60-27 transformer[5] in an SMT package that employs a FairRite 2843002302 binocular ferrite core and #36 AWG wire. This core is similar to, but somewhat smaller than, the core that Reisert used, and Reisert used larger #32 AWG wire. Hicks reported a net gain of 8 dB, good linearity, and very low noise. What's not clear is if their 1 dB less gain than what Reisert saw was due to the different transformer turns ratio, or

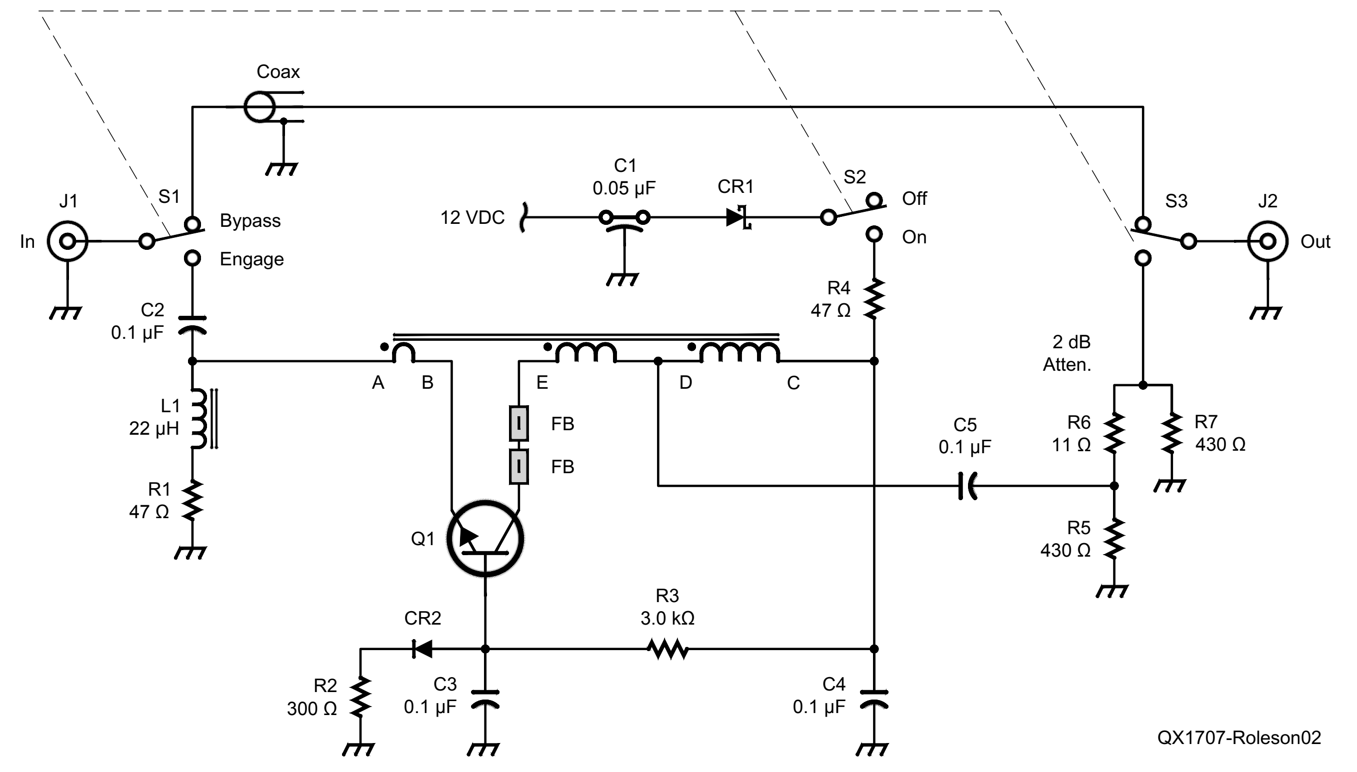

Figure 2 — Schematic of broadband, high-dynamic range RF amplifier. Diode CR2 and transistor Q1 are thermally bonded.

C1 — 0.05 µF feed thru capacitor, Tusonix 4400-041LF
C2 - C5 — 0.1 µF
CR1 — Schottky diode
J1, J2 — BNC female connector
L1 — Inductor, 22 µH, Bourns Series 78
Q1 — 2N5109 NPN RF transistor
R1, R4 — Resistor 47 Ω, 5%
R2 — Resistor 300 Ω, 5%
R3 — Resistor 3.0 kΩ, 5%
R5, R7 — Resistor 430 Ω, 5%
R6 — Resistor 11 Ω, 5%
S1- S3 — SPDT miniature toggle switch, C&K 7101
T1 — Transformer, custom (see text) on Fair Rite core 2843002402
8-pin DIP header — Aries #08-600-10, jameco.com.
Copper magnet wire — #34 AWG
DIP socket — Used by T1
Enclosure — Hammond 1590BS
Machine screws — 6-32 by 1/4 4
PCB — 4 by 2 inches.

possibly greater loss due to the smaller core and thinner wire.

Over the years, the basic Norton amplifier has lead others to devise clever derivative circuits. For example, a push-pull arrangement of two Norton amplifiers was described by Makhinson.[6] Several commercially available amplifiers using the Norton-Podell design are available from Clifton Laboratories[7] as described in their informative user manuals. Trask[8] described a method for "augmenting" the feedback to reduce distortion.

For my HF SDR RF preamp project application, I chose to stick with the simpler original configuration. I also envisioned possibly using this amplifier with filters to deal with strong broadcast signals, so the circuit's impedance characteristics were attractive. I also wanted to first build what was effectively a prototype that would allow me to experiment with biasing and the transformer design.

A Prototype Lossless Feedback Amplifier with Bias Stabilization

Figure 2 shows the amplifier circuit that I settled on, adapted from similar circuits described above. I chose the 2N5109 transistor, readily available and inexpensive (about $3 each from **mouser.com**). Most of the transistors used by others, see Table 2, are either obsolete or nearing obsolescence. The MRF586 used by Makhinson is still available, but much more expensive (about $11 each). Ferrite beads (FB) on the collector of Q1 are there to suppress any self-oscillation tendency. Feed-through capacitor C1 bypasses RF that might enter or exit via the dc power line, and Schottky diode CR1 provides protection from inadvertent dc polarity reversal.

The circuit includes a 2 dB pi-network resistive attenuator at the output port. I included this to help ensure that this amplifier was working into a 50 Ω system. I can always replace it later with a straight-through connection if I choose, or leave it in place if it seems to work better with broadcast signal rejecting filters. This attenuator also provides a means for selecting different overall gains than those set by the prescribed transformer turns ratios. I also observed that Makhinson used a similar attenuator in one of his circuit implementations to deal with load mismatch and to help preserve high-dynamic range performance.

I breadboarded the dc equivalent of the circuit — no RF components — to experiment with biasing and operating point, and settled on a dc emitter current, I_E, of about 18 mA. This seemed adequate and was very similar to what Reisert used for his well-performing amplifier. I was also concerned that a higher dc emitter current might compromise noise figure. As shown in Table 2, others chose widely different currents, but generally lower currents resulted in lower noise figures.

Setting I_E as I did resulted in a net power dissipation of just under 200 mW, well within the 1 W maximum dissipation allowed for the 2N5109 without a heat sink. Even so, the TO-39 can of the 2N5109 became noticeably warm. I measured I_E and noticed ~5.8% change over about 3 minutes after turn on. This was probably due to the well-known change in the base-emitter voltage V_{be} with temperature, typically given in textbooks as about -2 to -2.5 mV/°C. Using a small heat sink might have helped but would probably have only extended the time until the transistor temperature and I_E stabilized since the power dissipated was still the same. Addition of a diode in the transistor base circuit is a common method of compensating for this[9] but ideally this diode should be identical to the transistor and should be thermally bonded, that is, at the same temperature as the transistor. Connecting a second 2N5109 as a diode (shorting its base and collector) would be ideal except that thermal bonding becomes tricky since the 2N5109 collector is connected to the TO-39 can. After some experiments, I settled on using a small power diode similar to a 1N4005 that I had on hand. I thermally bonded this diode to the top of the 2N5109 with a small drop of cyanoacrylate adhesive taking care that the diode leads not touch the transistor can. Cyanoacrylate adhesive is commonly known by trade names like Superglue. Two-part thermal adhesive of the type sometimes used with heat sinks would probably work just as well. Better temperature compensation is sometimes achieved with two diodes in series, but perfection wasn't a design goal and the top of the transistor was crowded enough with one diode.

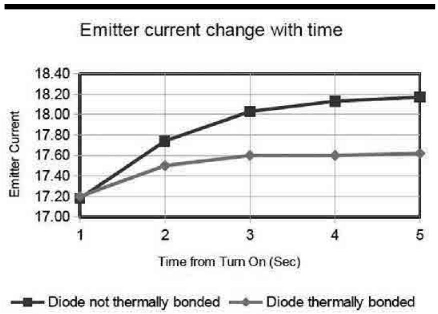

Figure 3 — Effect of diode thermal bonding to transistor on emitter current.

Thermal bonding is apparently more important than junction similarity. The change in I_E from turn-on dropped to about 2.4% and stabilized more quickly — in about 2 minutes. Figure 3 shows a graph of the change in I_E with the diode in the circuit but with and without thermal bonding. Figure 4 shows the final PCB assembly with the compensation diode glued to the 2N5109 can.

I mounted this PCB to the lid of a Hammond 1590BS die-cast aluminum enclosure, which I chose for its good shielding effectiveness. Mounting the PCB to the lid was simple and meant that no holes where needed in the main body of the enclosure. As shown in Figure 4, the PCB was held in place on the enclosure lid with two 3/8-inch long threaded stand-offs, and was also supported by small holes in the PCB that fit over the backs of the switches. Two SPDT toggle switches, one at the input and a second at the output, allowed for engaging or bypassing the circuit during testing.

Using two switches kept the input and output circuits better isolated than if I had tried to do this with a single DPDT switch. When S1 and S3 are switched to Bypass they connect to a short piece of coax with the shield soldered to the PCB ground plane. I used a small piece of semi-rigid 50 Ω coax that I had on hand, but flexible coax such as RG-174 or equivalent might have worked just as well.

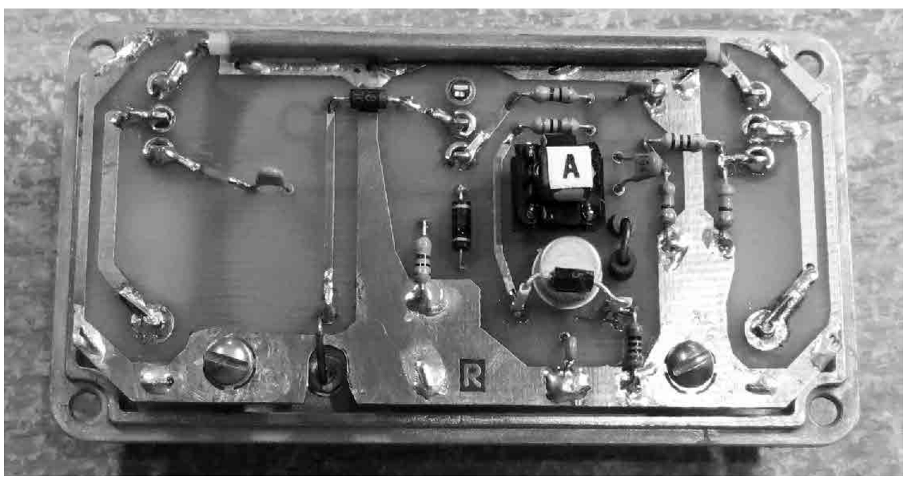

Figure 4 — PCB assembly is mounted on the enclosure lid. [Scott Roleson, KC7CJ, photo.]

Table 2.
Norton-Podell Amplifier Comparison.

Circuit Version	*Transformer Core*	*Transformer 1:n:m*	*Reported ~Gain (dB)*	*Reported bandwidth (MHz)*
Reisert circuit, See Note 10	FairRite 2843002402	1:5:3	9.0	1.8 – 200
U.S. Patent 3,891,934	Siemens D-62152-AD008-X030	1:5:3	8.0	5 – 350
Skelton – See Note 3	4 FT37-43 toroids as binocular	1:5:3	10.0	1 – 100+
Hicks LWA active balun – Notes 4, 5	FairRite 2843002302	1:4:3	8.0	20 – 80
Makhinson input amp – Note 6 (Mak. Fig 5)	2402	1:5:3	8.0	1 – 40
Makhinson post mixer amp– Note 6 (Mak. Fig 6)	2402	1:5:3	8.0	n/a

A third SPDT toggle switch controlled dc power. Conveniently, the back ends of the BNC jacks just fit within the intervening space, and connect directly to the PCB. The dc voltage fed through capacitor C1 wasn't quite long enough to reach the PCB, so I added a small wire to make this connection through a small notch cut in the edge of the PCB.

I mounted all three of these switches in-line and fashioned a linking bar that allows control of all three switches in tandem to facilitate testing and operation. This way, turning the two RF circuit switches to Engage also turns on the power to the amplifier. Figure 5 shows the completed amplifier exterior.

The two-sided PCB that I designed for this amplifier is shown in Figure 6A and 6B. The outside dimensions were 2.0 by4.0 inches, with corner notches as shown to fit within the corner screw attachment features of the aluminum enclosure. The letter "R" shown on the top side is a registration mark. It has no other significance. Since I was intending on building only one, I etched the PCB myself after using the laser printer toner transfer method to lay down photo resist on both sides of the blank PCB. I printed transferable images on clear plastic sheets then used a hot clothing iron to transfer the toner to the blank PCB. A flat piece of cotton cloth between the iron and the plastic sheets kept the iron from melting the plastic. The outside crosses shown in Figures 6A and 6B are registration marks to help orient the top and bottom layers prior to PCB transfer heating. More details of the PCB and parts layout are on the **www.arrl.org/QEXfiles** web page.

This method works well for one-off home-made PCBs, but does not provide for plated through holes. Consequently, I included several holes in the ground plane area and added short wires soldered to both layers to improve ground plane integrity.

Transformer Winding

To allow for transformer experimentation, I mounted an 8-pin DIP socket on the PCB and assembled several trial transformers on mating DIP headers. This is the component with the large "A" label in Figure 4. I used a modified Reisert method, that is, the transformer is wound as described by Reisert in his 1984 article (see Note 1) but with some "twists" of my own. I used a polyurethane / polyamide (nylon) coated solid copper magnet wire, which made later insulation removal and tinning easy. A hot soldering iron with a drop of solder effectively burned away the insulation, exposing and tinning the copper wire in one operation. If you haven't done this before, experiment on some scrap pieces first.

Figure 7 shows the transformer schematic and the DIP layout that I chose. The one-turn primary wires A and B, also shown in Figure 8A, are on one side of the FairRite 2843002402 binocular ferrite core and are wired to pins 1 and 4 respectfully of the DIP header. The tapped secondary wires are on the other side of the core and form the *n* and *m* windings, wired to pins 5, 7, and 8.

I built an assembly fixture from an alligator clip, heavy wire, and a 1 by 2 by 6.5 inch piece of pine, as shown in Figures 8A – 8D. There is nothing critical about this fixture — any fixture that holds the core reasonably steady a few inches above the work table without damaging the core should work. I found it helpful to add a small dab of paint to the core as shown to designate which way is 'front'. The one turn winding labeled A and B is added to the core first as shown in Figure 8A. Wire marking labels helped me remember which wire was which. Note that by convention a single turn consists of a wire routed through one of the two holes in the binocular core, then through the second hole in the opposite direction, and pulled firmly.

The wires for the tapped secondary start and come out of the other end of the binocular core. I found that starting with a length of wire about 60 to 65 cm long was about right. Start with the *m*-winding. Wind one turn from back hole to front, then add the label for wire C as shown in Figure 8B. Continue winding the total number of turns necessary for the *m*-winding as described above in the discussion of amplifier gain and required 1:*n*:*m* windings. That is, push the wire in the back hole where the C wire is coming out, right to left, then through front hole left to right. When complete, twist the end wire in a loop as shown in Figure 8B to form the autotransformer tap. This will become the D wire seen in Figure 8B and 8C. This twist must be done tightly. It is shown loose in the photo for better visibility.

Next, continue winding the wire in the same direction to wind the *n* winding, labeled

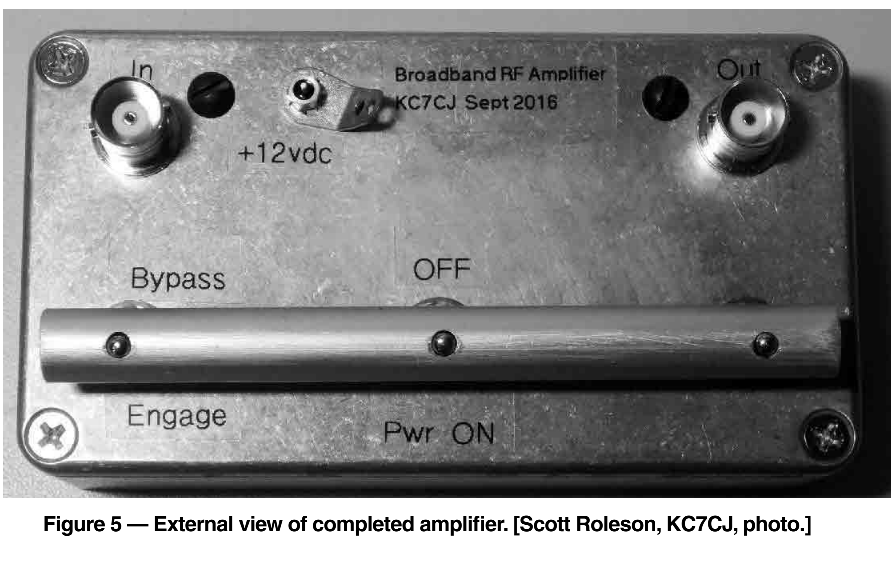

Figure 5 — External view of completed amplifier. [Scott Roleson, KC7CJ, photo.]

Reported noise figure (dB)	*Reported output IP3 (dBm)*	*Transistor*	*Bias point ~Ie (mA)*	*Remarks*
1.5 – 2	+39	NEC NE41632B	14-21, nominal 17	Mentions 2N5109 as substitute with 3 dB NF
1.2 – 1.5	n/a	NEC V-875	7.8	-
n/a	> +40	NEC 2SC1426	43	Mentions 2N5109 as substitute
–	+35	NEC NE461 MO2	~17	Bias circuit identical to Reisert – See Note 1
2.0	+48	MRF586	25 each	two circuits in push-pull
2.5	+42	MRF586	40 each	two circuits in push-pull

E, and wound in the same direction as the C to D winding. The completed transformer is shown in Figure 8C. Next, tin each of the wires for about a centimeter, no closer to the core than 1 or 2 mm, as shown in Figure 8D.

The core is too large to fit within the pins of the 8-pin DIP header, so I added a pedestal to the header made from a short piece of plastic rectangular stock. This pedestal lifts the transformer to just clear the forked header pins. There is also a small gap between the pedestal and the forked pins so that wires are more easily attached. I also found it helpful to dab a small amount of paint on the header indicating Pin 1. I again used cyanoacrylate adhesive to hold the pedestal in place and the transformer to the top of the pedestal, then soldered the wires to the appropriate pins, as in see Figure 7. The completed transformer is shown in Figure 9.

Transformer Experiments, Testing and Performance

I wound several transformers on identically sized cores with three different ferrite types to experiment with different turns ratios and ferrites. Table 3 shows these 7 transformers, labeled A to G, and their performance across the HF band. Amplifier gain, including the 2 dB attenuator shown in the schematic, is plotted in Figure 10, illustrating gain variation across HF.

Not having a well-equipped laboratory, I was compelled to improvise for these measurements. I used an old, rich-in-harmonics 4 MHz oscillator left over from another long-ago project along with a simple software defined radio — a DVB-T ‘dongle’ TV tuner — an HF converter and a copy of SDR-Sharp[10] software. This SDR arrangement provided a relative signal strength indication in dB, which I used to measure the change in gain when I switched the amplifier between Bypass and Engage.

Table 3 shows that the net gains of each configuration were slightly below theoretical values in all cases, with the greatest discrepancy at the highest gains. As noted earlier, this was generally consistent

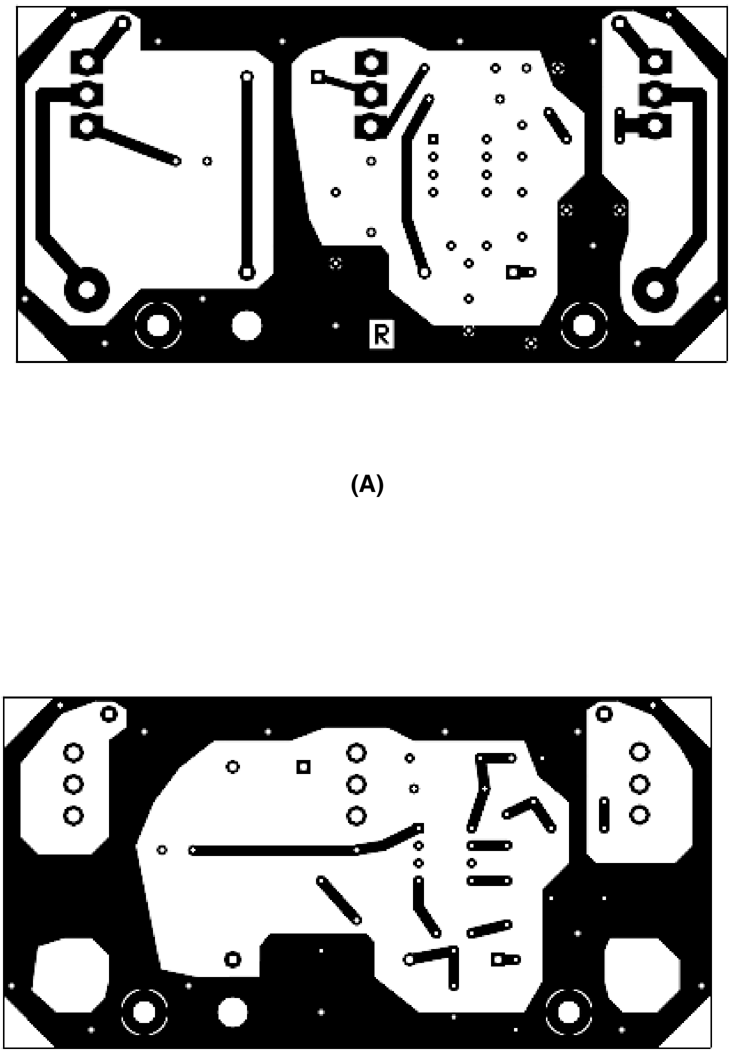

(A)

(B)

Figure 6 — (A) front, (B) back, PCB layout detail. [Scott Roleson, KC7CJ, photo.]

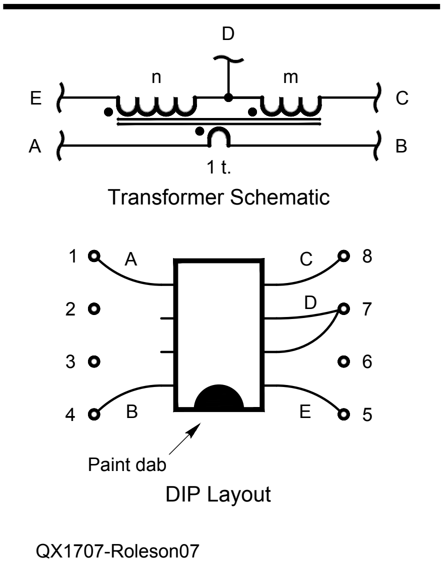

Figure 7 — Transformer windings and DIP layout

with the performance of this amplifier reported by others.

Type 43 ferrite cores generally produced the best results as shown in the flatness curves in Figure 10. The best overall was the 9 dB gain amplifier with 1:5:3 transformer-A turns ratio. The worst appeared to be transformer-F, the 12 dB amplifier with the 1:11:4 turns ratio on a type 67 core. However, transformers-B and -D (core types 43 and 73 with a 1:11:4 turns ratio) produced nearly identical performance. I relied on the supplier to designate the cores; they are all identical in appearance with no color coding or other differentiating markings.

Final Thoughts

There is an old saying, "There comes a time when you fire the engineer and ship the product!" It's been fun, but I must remember that my original goal was to find a front-end RF preamplifier for an SDR receiver project.

As a result of these experiments, I chose an amplifier with the transformer-B — having 1:11:4 turns ratio and #34 AWG wire on a Fair Rite 2843002402 core — followed by a 1 dB resistive attenuator for my SDR project. This should provide roughly 10 dB of gain across the HF band, be adequately low noise and adequately flat across the HF band, and provide some degree of impedance stabilization.

While good enough for Amateur Radio use, these experiments suggest that the design equations provided in the original patent should be viewed as approximations. I believe this because there was always about a 0.5 to 1 dB gain difference between theoretical and actual performance in my experiments and in most of the results reported by others. There is also the issue of mediocre gain flatness over the HF band.

For more discerning or precise applications, such as use in an RF instrument, a more detailed understanding of the underlying physics may be appropriate. I would start by characterizing the transformer

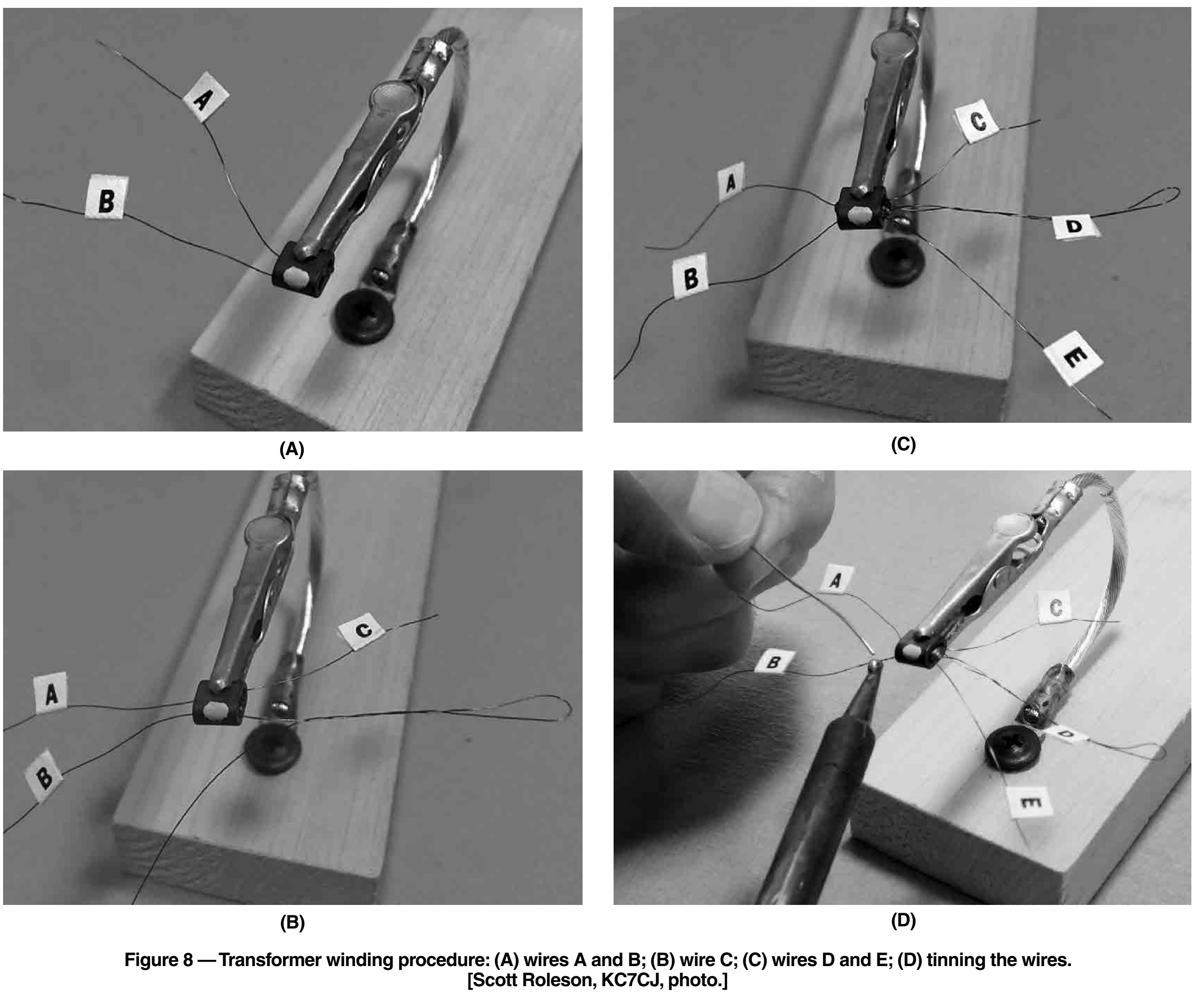

Figure 8 — Transformer winding procedure: (A) wires A and B; (B) wire C; (C) wires D and E; (D) tinning the wires. [Scott Roleson, KC7CJ, photo.]

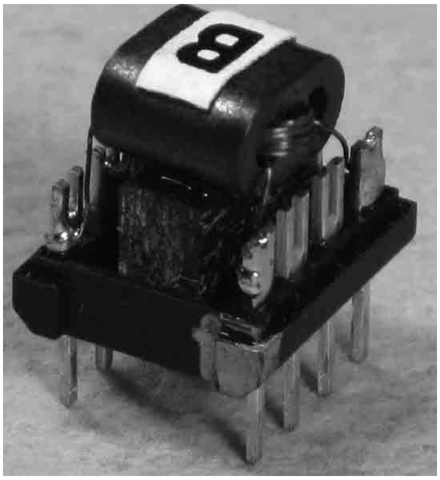

Figure 9 — Image of the completed transformer. [Scott Roleson, KC7CJ, photo.]

Table 3.
Transformers and experimental results. All cores were Fair Rite 28xx002402, where xx = ferrite type.

Transformer:

Parameter	*A*	*B*	*C*	*D*	*E*	*F*	*G*
Turns, 1:n:m	1:5:3	1:11:4	1:19:5	1:11:4	1:19:5	1:11:4	1:19:5
Ferrite type	43	43	43	73	73	67	67
Wire size	30	34	34	34	34	34	34
Theoretical gain (dB)	9.5	12.0	14.0	12.0	14.0	12.0	14.0

Measured Gain (dB):

Freq (MHz)	*A*	*B*	*C*	*D*	*E*	*F*	*G*
4	6.8	9.7	11.5	9.4	11.7	6.5	10.3
8	6.8	8.8	10.2	8.5	11.2	8.8	11.8
12	7.3	9.6	11.2	9.2	11.4	9.7	11.8
16	6.8	9.3	11.6	9.5	10.7	9.4	11.8
20	7.3	9.3	11.8	9.6	10.9	10.4	12.4
24	7.2	9.3	10.7	9.5	10.1	10.3	11.5
28	6.7	9.2	9.9	9.1	9.2	9.9	10.9
Averages:	**7.0**	**9.3**	**11.0**	**9.3**	**10.7**	**9.3**	**11.5**
Atten (dB)	**2.0**	**2.0**	**2.0**	**2.0**	**2.0**	**2.0**	**2.0**
Net gain (avg+atten)	**9.0**	**11.3**	**13.0**	**11.3**	**12.7**	**11.3**	**13.5**
Theoretical minus net gain (dB)	**-0.5**	**-0.7**	**-1.0**	**-0.7**	**-1.3**	**-0.7**	**-0.5**

for its mutual and self inductances, stray capacitance and resistance. Building a detailed analytical model around this better-understood transformer may then explain the real circuit gain differences and frequency response, and clarify ways to control performance better.

Scott Roleson, KC7CJ, was first licensed in 1964. He has a BSEE from Arizona State University, an MSEE from the University of Arizona. Scott is a licensed Professional Engineer in California, and a Life Senior Member of the IEEE. From 1993 to 1995 he was a Distinguished Lecturer of the IEEE EMC Society, and was the Distinguished Lecturer program chair 1995-1997. He retired after a 32-year career in electrical engineering where he worked on spectrum analyzer design, FAX machine testing, EMC and telecom regulatory engineering. Scott now gets to pick his own projects and maximize the 'fun return on investment.'

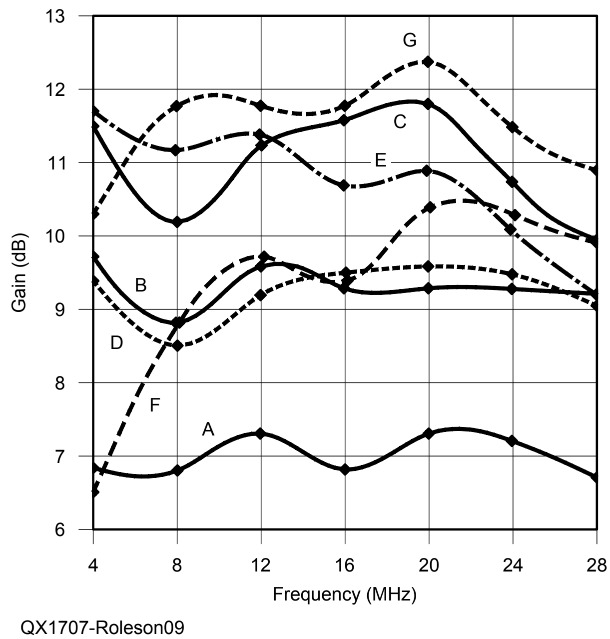

Figure 10 — Measured performance across HF of the transformers A – G described in Table 3.

Notes

[1]Joe Reisert,W1JR, "High Dynamic Range Receivers," Ham Radio Magazine, Nov. 1984, pp. 97-105. A nearly identical circuit also appears to have been used at the 20 – 70 MHz NRAO Green Bank Solar Radio Burst Spectrometer, see: **www.nrao.edu/astrores/gbsrbs/Pubs/lwa_2004_bradley.pdf**.

2 D. E. Norton, and A. F. Podell, "Transistor Amplifier with Impedance Matching Transformer," U.S. Patent 3,891,934, 24 June 1975.

[3]See Figure 6 in: Eamon Skelton, EI9GQ, "Homebrew – We start looking at high performance HF receivers," RADCOM (RSGB Journal), Jan. 2009, pp. 51-54.

[4]BrianvHicks, Nagini Paravastu, Richard Bradley, and Chaitali Parashare, "A Low Noise, High Linearity Lossless Feedback Amplifier for LWA Applications," Long Wavelength Array (LWA) Memo Series, document #71, 12 Dec. 2006; see: **www.faculty.ece.vt.edu/swe/lwa/**.

[5]Data sheet for Emhiser Tele-Tech TX60-27 transformer, see: **www.emhiser.com/images/datasheet/TX60%20SERIES.PDF**.

[6]Jacob Makhinson, N6NWP, "A High dynamic range MF/HF receiver front end," *QST*, Feb. 1993, pp. 23-28. See correction in "Feedback," *QST*, Jun. 1993, p. 73.

[7]Clifton Laboratories, **cliftonlaboratories.com/z10043a_norton_amplifier.htm**.

[8]ChrisTrask, "Distortion improvement of lossless feedback amplifiers using augmentation," Proceedings of the 1999 IEEE Midwest Symposium on Circuits and Systems, Las Cruces, NM, Aug. 1999, pp. 951-954.

[9]Temperature compensation using diode biasing, see: Donald Schilling and Charles Belove, *Electronic Circuits: Discrete and Integrated*, McGraw-Hill, 1979, pp. 187-192. See pp 179-180 for V_{be} change with temperature.

[10]SDR was similar to: James Forkin, WA3TFS, "All-Mode 1 kHz to 1.7 GHz SDR Receiver," QST, Jan. 2016, pp. 30-33.

Letters to the Editor

A Different Approach to Multi-Band Gain Antenna Design, (Jan/Feb 2017)

Dear Editor,

Somehow I forgot to mention in the article that this new design of parasitic elements can also be applied to director as well as reflector elements, of course with small adjustments to the inductor and capacitor values. — *Robert J Zavrel, W7SX*

An Improved Audio-Frequency Bandpass Filter for Morse Code Reception, (Mar/Apr 2017)

Dear Editor,

In Figures 4, 5 and 7 the labels "Transmission" and "Group Delay" were unfortunately swapped. — Jim Tonne, W4ENE

[We regret the error. In Figure 4, 5 and 7, the upper plots should be labeled "Transmission", and the lower plots should be labeled "Group Delay." The captions are correct. — *Ed.*]

Dear Editor,

I have been reading *QEX* for many years now and I still very much look forward to receiving the next edition. The articles are always interesting and show a great deal of original thought. Please pass on my congratulations to James Tonne for an excellent well written article. I have played with active and passive Morse filters on a number of occasions and I found his analysis and approach very insightful.

There is, however, one part of the article with which I beg to differ – the part where James speaks about an equivalent active filter. I feel he may be under a misconception here, unless I have misunderstood what he was trying to say.

My understanding of audio filters is that the shape of the filter response is set by the mathematics from which the filter design was derived. For example, if the filter is designed to have a particular Butterworth response, then it will have that same response, regardless of whether it is an active or a passive realization. Sure, the design process is different, as active and passive realizations do not use the same components, but the response will be the same, provided the design process has been carried out correctly for each type of realization.

On another aspect, I completely agree with his comments about the use of passive filters for such applications. They may be physically larger, but they use a lot less components and do not require a power supply. Once again, thank you James for a very interesting article. — *Cheers, George Georgevits, VK2KGG*

[The author replies]

I am pleased that Mr. Georgevits found the CW BPF article interesting. Allow me to clarify the low-pass to band-pass filter transformation process that was used. When done using the multiple feedback band-pass topology as shown in the first two stages in Figure 17, the response turns out to be symmetrical on a geometric basis. This yields the textbook low-pass to band-pass filter conversion, but that is not what we want for a CW band-pass filter. So we add the low-pass stages to warp the response making the overall response symmetrical on an arithmetic basis.

As a final item of interest, the wonderful traits of the passive version of this band-pass filter hold true only for a fourth-order design. — *James Tonne, W4ENE*

The Antenna Equivalent Radius: A Model for Non-Circular Conductors, (Mar/Apr 2017)

Dear Editor,

If there is any kind of award for paper of the year, I'd like to nominate the David Drumheller, K3WQ, article "The Antenna Equivalent Radius: A Model for Non-Circular Conductors". I sense that this is a very important paper. Thank you. — *James Lynes, KE4MIQ, jmlynesjr@gmail.com*.

The Polar Explorer (Mar/Apr 2017)

Dear Editor,

Regarding the Tony Brock-Fisher, K1KP, and Brian Machesney, K1LI, article, We've [the shortwave broadcast transmitter manufacturers — *Ed.*] been doing separate amplitude and phase amplification for 50 – 500 kW transmitters for the last 30 years. On HF broadcast transmitters for AM/PM service we see the necessity for precision neutralization. You can't really do active correction without perfect neutralization or you end up with the mismatched sidebands seen in Figure 7, where the upper and lower sideband levels don't match up. They will match if the amplifier is properly neutralized. Active correction isn't applied until after near-perfect neutralization is achieved.

Neutralization will become more important, and necessary, as linearization and active correction becomes more available. — *Cheers and 73, J. Fred Riley, W8OY*

Improve Performance of Your Octopus V/I Curve Tracer using a Single Voltage Transformer (May/Jun 2017)

In the Acknowledgement, Rene Stelmach should be identified as an electronics engineer. — *Correction submitted by Ed Wetherhold, W3NQN, ARRL Technical Advisor*

Send your *QEX* Letters to the Editor to, ARRL, 225 Main St., Newington, CT 06111, or by fax at 860-594-0259, or via e-mail to qex@arrl.org. We reserve the right to edit your letter for clarity, and to fit in the available page space. "Letters to the Editor" may also appear in other ARRL media. The publishers of *QEX* assume no responsibilities for statements made by correspondents.

Upcoming Conferences

SARA Annual Conference

July 23 – 26, 2017

NRAO Green Bank, WV

radio-astronomy.org

See website for details.

Central States VHF Society 2017 Conference

July 27 – 30, 2017

Albuquerque, NM

2017.csvhfs.org

On behalf of Rocky Mountain Ham Radio and the amateur radio community of New Mexico, we wish to welcome you to sunny Albuquerque, New Mexico for the 2017 Central States VHF Society Conference, to be held on July 27 – 30 at the Sheraton Albuquerque Airport Hotel, 2910 Yale Blvd SE, Albuquerque, NM 87106; (505) 843-7000. This year marks our Society's 51st Conference.

This year's event will feature many exciting activities, including state-of-the-art technical programs, noise figure measurements, antenna range, "Rover Row," "Dish Bowl," VHF 101 and 102 presentation tracks for newcomers of weak signal operation, luncheons, family activities and tours, prizes, evening socials/hospitality suites, guest speakers, a VHF/UHF/Microwave swapfest, the always much anticipated grand-finale banquet, and much more.

Bring the whole family! Albuquerque offers a wide variety of activities for everyone to enjoy, and the Conference will be offering a choice of trips and tours to entertain the whole family and showcase some of the jewels of the Land of Enchantment.

We hope you, your family, and ham friends will join us in Albuquerque this July.

See website for details.

36th Annual ARRL and TAPR Digital Communications Conference

September 15 – 17, 2017

Saint Louis, MO

www.tapr.org

Mark your calendar and start making plans to attend the premier technical conference of the year, the 36th Annual ARRL and TAPR Digital Communications Conference to be held September 15 – 17, 2017 in Saint Louis, MO.

Conference presentations, meetings, and seminars will be held at the Holiday Inn Airport West, 3400 Rider Trail South, Earth City, MO 63045, 314-291-6800.

The ARRL and TAPR Digital Communications Conference is an international forum for radio amateurs to meet, publish their work, and present new ideas and techniques. Presenters and attendees will have the opportunity to exchange ideas and learn about recent hardware and software advances, theories, experimental results, and practical applications.

Topics include, but are not limited to: Software Defined Radio (SDR), digital voice, digital satellite communications, Global Position System (GPS), precision timing, Automatic Packet Reporting System(tm)(APRS), short messaging (a mode of APRS), Digital Signal Processing (DSP), HF digital modes, Internet interoperability with Amateur Radio networks, spread spectrum, IEEE 802.11 and other Part 15 license-exempt systems adaptable for Amateur Radio, using TCP/IP networking over Amateur Radio, mesh and peer to peer wireless networking, emergency and Homeland Defense backup digital communications, using Linux in Amateur Radio, updates on AX.25 and other wireless networking protocols.

Call for Papers: Technical papers are solicited for presentation at the ARRL and TAPR Digital Communications Conference and publication in the Conference Proceedings. Annual conference proceedings are published by the ARRL. Presentation at the conference is not required for publication. Submission of papers are due by **July 31, 2017** and should be submitted to: Maty Weinberg, ARRL, 225 Main St., Newington, CT 06111, or by e-mail to **maty@arrl.org**.

Mid-Atlantic VHF Conference

October 6 – 8, 2017

Bensalem, PA

www.packratvhf.com/latest.htm#Anchor-49575

Sponsored by the Mt. Airy VHF Club (Pack Rats). Conference topics include VHF, UHF and microwave construction, operating, digital modes, EME, antennas, roving and more. Additional speakers and Proceedings papers sought. Contact **rick1ds@hotmail.com**.

The conference will be held at the Holiday Inn Bensalem-Philadelphia, 327 Street Rd. (Rt. 132), Bensalem, PA 19020, 215-639-9100.

See website for conference updates and registration details.

23rd Annual Pacific Northwest VHF-UHF-Microwave Conference

October 13 – 15, 2017

Moses Lake, WA

www.pnwvhfs.org

Join other weak-signal VHF, UHF and Microwave operators for the 23rd Annual PNW VHF Society Conference!

The conference will be held at Best Western Lake Front Hotel, 3000 Marina Dr., Moses Lake, WA 98837, 509-765-9211

Call for Papers: The Pacific Northwest VHF Society is looking for speakers and papers for our next conference.

Please send your abstract to Jim K7ND, **secretary@pnwvhfs.org**. Authors will be notified of acceptance by **September 14** for inclusion in the program and it will be posted on the website.

Abstracts are solicited on these VHF-UHF-Microwave topics and more: MSK441 and other digital modes; propagation; microwaves; EME Tools, tips and techniques; frequency stabilization; hilltopping, roving and portable operation; antenna theory and design; the world above 1000 MHz; operating with satellites; transverters and amplifiers; software defined radio; remote station operation; amateur television; contest equipment, techniques and strategy; lasers and other radiation sources; and other subjects related to VHF and up.

See website for details.